arXiv:2105.08811v1 [astro-ph.HE] 18 May 2021

The Photometric and Spectroscopic Evolution of Rapidly Evolving Extragalactic Transients in ZTF

Anna Y. Q. Ho,[1,2] Daniel A. Perley,[3] Avishay Gal-Yam,[4] Ragnhild Lunnan,[5] Jesper Sollerman,[5] Steve Schulze,[5] Kaustav K. Das,[6] Dougal Dobie,[7,8] Yuhan Yao,[6] Christoffer Fremling,[6] Scott Adams,[6] Shreya Anand,[9] Igor Andreoni,[6] Eric C. Bellm,[10] Rachel J. Bruch,[11] Kevin B. Burdge,[9] Alberto J. Castro-Tirado,[12] Aishwarya Dahiwale,[6] Kishalay De,[6] Richard Dekany,[13] Andrew J. Drake,[6] Dmitry A. Duev,[14] Matthew J. Graham,[6] George Helou,[15] David L. Kaplan,[16] Viraj Karambelkar,[6] Mansi M. Kasliwal,[6] Erik C. Kool,[5] S. R. Kulkarni,[6] Ashish A. Mahabal,[9,17] Michael S. Medford,[18,19] A. A. Miller,[20,21] Jakob Nordin,[22] Eran Ofek,[4] Glen Petitpas,[23] Reed Riddle,[13] Yashvi Sharma,[6] Roger Smith,[13] Adam J. Stewart,[24] Kirsty Taggart,[25] Leonardo Tartaglia,[26,27] Anastasios Tzanidakis,[6] and Jan Martin Winters[28]

[1]*Department of Astronomy, University of California, Berkeley, 501 Campbell Hall, Berkeley, CA, 94720, USA*
[2]*Miller Institute for Basic Research in Science, 468 Donner Lab, Berkeley, CA 94720, USA*
[3]*Astrophysics Research Institute, Liverpool John Moores University, IC2, Liverpool Science Park, 146 Brownlow Hill, Liverpool L3 5RF, UK*
[4]*Department of Particle Physics and Astrophysics, Weizmann Institute of Science, 234 Herzl St, 76100 Rehovot, Israel*
[5]*The Oskar Klein Centre, Department of Astronomy, Stockholm University, AlbaNova, SE-10691 Stockholm, Sweden*
[6]*Cahill Center for Astrophysics, California Institute of Technology, MC 249-17, 1200 E California Boulevard, Pasadena, CA, 91125, USA*
[7]*Centre for Astrophysics and Supercomputing, Swinburne University of Technology, Hawthorn, Victoria, Australia*
[8]*ARC Centre of Excellence for Gravitational Wave Discovery (OzGrav), Hawthorn, Victoria, Australia*
[9]*Division of Physics, Mathematics and Astronomy, California Institute of Technology, Pasadena, CA 91125, USA*
[10]*DIRAC Institute, Department of Astronomy, University of Washington, 3910 15th Avenue NE, Seattle, WA 98195, USA*
[11]*Department of Particle Physics and Astrophysics Weizmann Institute of Science 234 Herzl St. 76100 Rehovot, Israel*
[12]*Instituto de Astrofísica de Andalucía (IAA-CSIC) Glorieta de la Astronomia E18008, Granada, Spain*
[13]*Caltech Optical Observatories, California Institute of Technology, Pasadena, CA 91125*
[14]*Division of Physics, Mathematics, and Astronomy, California Institute of Technology, Pasadena, CA 91125, USA*
[15]*IPAC, California Institute of Technology, 1200 E. California Blvd, Pasadena, CA 91125, USA*
[16]*Center for Gravitation, Cosmology, and Astrophysics, Department of Physics, University of Wisconsin-Milwaukee, P.O. Box 413, Milwaukee, WI 53201, USA*
[17]*Center for Data Driven Discovery, California Institute of Technology, Pasadena, CA 91125, USA*
[18]*Department of Astronomy, University of California, Berkeley, Berkeley, CA 94720*
[19]*Lawrence Berkeley National Laboratory, 1 Cyclotron Rd., Berkeley, CA 94720*
[20]*Center for Interdisciplinary Exploration and Research in Astrophysics (CIERA) and Department of Physics and Astronomy, Northwestern University, 1800 Sherman Road, Evanston, IL 60201, USA*
[21]*The Adler Planetarium, Chicago, IL 60605, USA*
[22]*Institute of Physics, Humboldt-Universität zu Berlin, Newtonstr. 15, 12489 Berlin, Germany*
[23]*Harvard-Smithsonian Center for Astrophysics, 60 Garden Street, Cambridge, MA 02138, USA*
[24]*Sydney Institute for Astronomy, School of Physics, The University of Sydney, NSW 2006, Australia*
[25]*Department of Astronomy and Astrophysics, University of California, Santa Cruz, CA 95064, USA*
[26]*The Oskar Klein Centre, Department of Astronomy, AlbaNova, SE-106 91 Stockholm, Sweden*
[27]*INAF - Osservatorio Astronomico di Padova, Vicolo dell'Osservatorio 5, I-35122 Padova, Italy*
[28]*Institut de Radioastronomie Millimétrique (IRAM), 300 rue de la Piscine, F-38406 St. Martin d'Héres, France*

Submitted to ApJ

ABSTRACT

We present 42 rapidly evolving (time spent above half-maximum brightness $t_{1/2} \lesssim 12$ d) extragalactic transients from Phase I of the Zwicky Transient Facility (ZTF), of which 22 have spectroscopic classifications. This is one of the largest systematically selected samples of day-timescale transients to-date, and the first with spectroscopic classifications. Most can be classified as core-collapse supernovae (SNe), and we identify several predominant subtypes: (1) subluminous Type IIb or Type Ib SNe; (2) luminous Type Ibn or hybrid IIn/Ibn SNe; and (3) radio-loud, short-duration luminous events similar

to AT 2018cow. We conclude that rates quoted in the literature for rapidly evolving extragalactic transients are dominated by the subluminous events (mostly Type IIb SNe). From our spectroscopic classifications and radio, X-ray, and millimeter-band upper limits, we are motivated to consider the AT 2018cow-like objects a distinct class, and use ZTF's systematic classification experiments to calculate that their rate does not exceed 0.1% of the local core-collapse rate, in agreement with previous work. By contrast, most other events are simply the extreme of a continuum of established SN types extending to ordinary timescales. The light curves of our objects are very similar to those of unclassified events in the literature, illustrating how spectroscopically classified samples of low-redshift objects in shallow surveys like ZTF can be used to photometrically classify larger numbers of events at higher redshift.

1. INTRODUCTION

The vast majority of extragalactic transients detected by optical surveys to-date have a characteristic duration (often defined as the time spent above half-maximum brightness of the light curve) exceeding 10 d (Kashliwal 2012; Perley et al. 2020b). Events with shorter durations have garnered much attention in recent years, due to the significant increase in real-time discovery by wide-field optical surveys (Inserra 2019; Modjaz et al. 2019). Originally, a handful of events were discovered that were unusually rapidly evolving, such as the Type IIn supernova (SN) PTF 09uj (Ofek et al. 2010), the Type Ib SN 2002bj (Poznanski et al. 2010), and the .Iax candidate SN 2010X (Kashliwal et al. 2010).

Later, groups of unclassified objects were discovered in survey data. Drout et al. (2014) presented 14 events with a short duration ($\lesssim 12$ d) from the Panoramic Survey Telescope and Rapid Response System (Pan-STARRS, PS1; Chambers et al. 2016) Medium Deep Survey, of which 10 had a measured redshift. Arcavi et al. (2016) presented four luminous ($M \approx -20$ mag) fast-rising events from the Palomar Transient Factory (PTF; Law et al. 2009; Rau et al. 2009) and the Supernova Legacy Survey (SNLS; Astier et al. 2006), one of which (PTF10iam) was spectroscopically classified as a Type II SN. Pursiainen et al. (2018) identified 100 events from the Dark Energy Survey (DES), and Tampo et al. (2020) recently presented five events from Hyper Suprime-Cam. Rest et al. (2018) presented KSN2015K, a rapidly evolving transient in K2 Campaign 6 data of the extended Kepler mission (Howell et al. 2014).

A variety of mechanisms have been proposed to explain the light curves of rapidly evolving transients, including shock breakout or post-shock cooling emission from a dense wind or shell (Ofek et al. 2010; Drout et al. 2014; Arcavi et al. 2016; Rest et al. 2018; Moriya et al. 2020), magnetar spin-down (Kasen & Bildsten 2010; Woosley 2010; Arcavi et al. 2016; Whitesides et al. 2017), a low nickel yield (Kleiser et al. 2018), electron capture (Moriya & Eldridge 2016; Tolstov et al. 2019; Lyutikov & Toonen 2019), white-dwarf detonation (Arcavi et al. 2016; McBrien et al. 2019), and tidal disrup-

tion of a star by a black hole (Strubbe & Quataert 2009; Kremer et al. 2021). Arcavi et al. (2016) noted that their objects had light curves very similar to that of SN 2011kl (Greiner et al. 2015), the unusual SN accompanying ultra-long gamma-ray burst (GRB) 111209A (Gendre et al. 2013; Stratta et al. 2013; Levan et al. 2014).

Interpretations have remained speculative because the vast majority of survey-sample objects lack spectroscopic observations, due to being identified archivally and having a short duration. The few spectra obtained were primarily at peak optical light and appeared featureless (Drout et al. 2014; Pursiainen et al. 2018).

In the last few years, the improved grasp of optical surveys (Bellm 2016; Ofek & Ben-Ami 2020) has enabled several short-duration transients to be discovered shortly after explosion and studied with detailed spectroscopy, including AT 2018cow (Prentice et al. 2018; Perley et al. 2019), the Type Ic-BL SN 2018gep (Ho et al. 2019a; Pritchard et al. 2020), the Type Ib ultra-stripped candidate SN 2019dge (Yao et al. 2020), the candidate white-dwarf detonation SN 2019bkc (Chen et al. 2020; Prentice et al. 2020), and the new class of Type Icn SNe (Gal-Yam et al. 2021; Bruch et al. 2019; Gal-Yam 2021; Perley 2021; Perley et al. 2021a). Furthermore, as part of the Zwicky Transient Facility (Bellm et al. 2019a; Graham et al. 2019) Bright Transient Survey (ZTF BTS; Fremling et al. 2020), spectral classifications are available for 14 short-duration events (including AT 2018cow), which include SNe of Type II, Type IIb, and Type Ibn (Perley et al. 2020b).

From individual events and the ZTF BTS sample, it is clear that short-duration optical transients exhibit significant spectroscopic diversity, and that at least some can be spectroscopically classified as SNe. However, the ZTF BTS is based on 3-day cadence light curves and spectroscopic classifications are only obtained uniformly for $m \lesssim 18.5$ mag transients. For rare rapidly evolving events, it is important to search higher cadence data down to the ZTF depth limit (20.5 mag). Here we present a systematically selected sample of day-

timescale[1], short-duration ($1.5 < t_{1/2} < 12$ d) optical transients from 2.5 years of ZTF data. We identify 42 events with well-sampled g- and r-band light curves, of which 30 have redshift measurements and 22 have spectroscopic classifications.

This is one of the largest samples of rapidly evolving transients to-date, and the first that includes spectroscopic classifications. Our light curves significantly improve upon the cadence of previous survey samples. The spectra enable us to show that most events can be classified as SNe, and to divide the loose term of "rapidly evolving transient" into several subgroups for the first time: subluminous He-rich events (predominantly Type IIb SNe), luminous interacting events (predominantly Type Ibn SNe), and very short-duration luminous radio-loud events (including AT 2018cow.) Our work supports the idea that CSM interaction and shock-cooling emission play a key role in powering the light curves of these events.

In Section 2 we present our selection criteria and apply them to the ZTF alert database to identify a sample of events. We also identify a comparison sample by applying similar criteria to the literature. We perform a combined analysis of the ZTF and literature objects in Section 3, and identify several distinct subtypes. We discuss the properties of the host galaxies in Section 4 and the event rates in Section 5. We discuss the implications of our work for the progenitors in Section 6, and summarize in Section 7.

Throughout the paper we assume a flat ΛCDM cosmology with $H_0 = 67.7 \, \mathrm{km \, s^{-1} \, Mpc^{-1}}$ and $\Omega_M = 0.307$ (Planck Collaboration et al. 2016). Times are presented in UTC, and magnitudes are given in AB. The optical photometry and spectroscopy will be made public through WISeREP, the Weizmann Interactive Supernova Data Repository (Yaron & Gal-Yam 2012).

2. OBSERVATIONS AND SELECTION CRITERIA

2.1. *ZTF*

The ZTF custom mosaic camera (Dekany et al. 2020) is mounted on the 48-inch Samuel Oschin Telescope (P48) at Palomar Observatory. As summarized in Bellm et al. (2019b), observing time for ZTF Phase I was divided between public (40%), partnership (40%), and Caltech surveys (20%). Three custom filters are used (g_{ZTF}, r_{ZTF}, and i_{ZTF}; hereafter g, r, and i; Dekany et al. 2020) and images reach a typical dark-time limiting magnitude of $r \sim 20.5$ mag.

Images are processed and reference-subtracted by the IPAC ZTF pipeline (Masci et al. 2019) using the Zackay et al. (2016) image-subtraction algorithm. Every 5-σ point-source detection is saved as an "alert." Alerts are distributed in Avro format (Patterson et al. 2019) and can be filtered based on a machine learning real-bogus metric (Mahabal et al. 2019; Duev et al. 2019); host-galaxy characteristics, including a star-galaxy classifier (Tachibana & Miller 2018); and light-curve properties. During the time period relevant for this paper (ZTF Phase I) the collaboration used a web-based system called the GROWTH marshal (Kasliwal et al. 2019) to identify, monitor, and coordinate follow-up observations for transients of interest.

Although we use observations from all programs, the most useful surveys for discovering rapidly evolving extragalactic transients are the high-cadence partnership survey (HC), which covered $2500 \, \mathrm{deg}^2$ with six visits per night (three in r and three in g); the ZTF Uniform Depth Survey (ZUDS[2]), which covered $2500 \, \mathrm{deg}^2$ with six visits per night ($2r$, $2g$, and $2i$); the one-day cadence Caltech survey (1DC), which covered $3000 \, \mathrm{deg}^2$ with $1r$ and $1g$ visit per night; and one-day cadence observations for shadowing the Transiting Exoplanet Survey Satellite (TESS; Ricker et al. 2014) fields. A small subset of our events were exclusively observed in the public survey ($15{,}000 \, \mathrm{deg}^2$, one r- and one g-band observation every three nights). The effective number of field-nights is described in the next section.

2.2. *Sample Selection*

We searched data from ZTF Phase I, i.e., obtained from March 2018 through October 2020. We used `ztfquery` (Rigault 2018) to identify fields in the primary grid with $E(B - V) < 0.3$ mag at the central field coordinate, and only searched field-nights that had at least one observation in the same field within the preceding and subsequent five nights. This left a total of 127,487 field nights.

For each of the 127,487 field-nights, we searched for transients fulfilling the criteria laid out in Table 1. We performed the search with the following steps:

1. We applied basic cuts to remove artifacts and stellar phenomena. We kept sources with a real-bogus score `rb` > 0.5 (Mahabal et al. 2019) and a deep learning score `braai` > 0.8 (Duev et al. 2019). The `braai` score corresponds to a false positive rate of 0.7% and a false negative rate of 3% (Duev et al. 2019). We removed sources within 2″ of a coun-

---

Table 1. Steps for selecting rapidly evolving transients. Details on each step are provided in the text.

Step	Criteria	# Candidates
1	Real, positive subtractions. Basic cuts to remove stars.	2.5M
2	Candidate has ≥ 3 alerts	651,920
3	ZTF light curve has short duration	19,715
4	Light curve well-sampled	6,059
5	Fast-rising in g or r	1,779
6	Passed manual inspection & forced photometry	40

terpart with a star-galaxy score greater than 0.76 (Tachibana & Miller 2018), and sources within $15''$ of a bright ($r < 15\,\mathrm{mag}$) star. We removed sources that arose from negative subtractions. This left $\sim 2.5\,\mathrm{M}$ unique sources.

2. We required that each source be detected in at least three alerts, leaving 651,920 sources.

3. To remove flaring and long-duration transients, we required that the time from the first to last detection (including the 30-day history in the alert packets, which uses a lower threshold than issued alerts) is between 1.5 d and 120 d. To exclude the majority of SNe (Fig. 1) and approximately match the selection criteria used in previous work (Drout et al. 2014), we required that the timespan between g-band detections above the half-maximum of the g-band light curve did not exceed 12 d. This left 19,715 sources.

4. Because the goal of this work is to study the observational characteristic of each transient, we require that the light curve be well sampled, i.e., that there is an observation within 5.5 d of peak, before and after, in g band and r band. This left 6,059 sources.

5. We further required the source to be fast-rising: that in either g band or r band it rose 1 mag in the preceding 6.5 d. This left 1,779 sources.

6. We examined each of the 1,779 sources manually, and discarded events with a point-like counterpart[3] (making particular use of the eighth data release of the Legacy Survey; Dey et al. 2019), with repeated flaring behavior, or with spectroscopic classifications indicating that they were stellar outbursts. We used forced photometry (Yao et al. 2019) to confirm a short event duration of

$t_{1/2} \lesssim 12\,\mathrm{d}$ in either g- or r-band. This left 40 sources.

We also added two sources that did not pass our cuts from P48 photometry alone (due to sparse ZTF observations) but did pass when taking observations from other facilities into account: AT 2018cow and SN 2019aajs. The latter is a Type Ibn SN that received extensive follow-up observations.[4]

We group the remaining 42 sources into a *gold sample*, 22 events with a spectroscopic classification; a *silver sample*, 9 events with follow-up observations but no spectroscopic classification; and a *bronze sample*, 11 events with no follow-up data. Several objects have been previously published, including the Type Ibn SN 2018bcc (Karamehmetoglu et al. 2019), the ultra-stripped Type Ib candidate SN 2019dge (Yao et al. 2020), the Type Ic-BL SN 2018gep (Ho et al. 2019a), the Type Ic SN 2020oi (Horesh et al. 2020), and the AT 2018cow analogs (Ho et al. 2020b; Perley et al. 2021b).

The duration-luminosity parameter space of the gold and silver samples is shown in the left panel of Figure 1. In the right panel, we show our sample combined with the BTS. It is immediately apparent that most short-duration events are simply part of a continuum of established SN subtypes extending to longer timescales, which we discuss in more detail in Section 6. In Tables 2, 3, and 4, we provide basic information about each transient. Details of discovery and follow-up for the gold and silver objects are provided in Section A in the Appendix.

Most of the objects in our sample were identified in the HC and 1DC surveys in real time by filters explicitly designed to find rapidly evolving transients (Ho et al. 2020a; Perley et al. 2021b). For the events that were missed by scanners, a common reason was that the event was faint, so significant fading behavior was not

---

[3] Extragalactic transients in compact hosts could accidentally be removed by this step. However, we found it important for removing outbursts from cataclysmic variables.

[4] Two rapidly evolving Type Icn SNe, SN 2019hgp (Bruch et al. 2019; Gal-Yam 2021) and SN 2021csp (Perley et al. 2021a; Perley 2021), do not pass our cuts: SN 2019hgp had too long a duration, and SN 2021csp occurred outside the date range we considered.
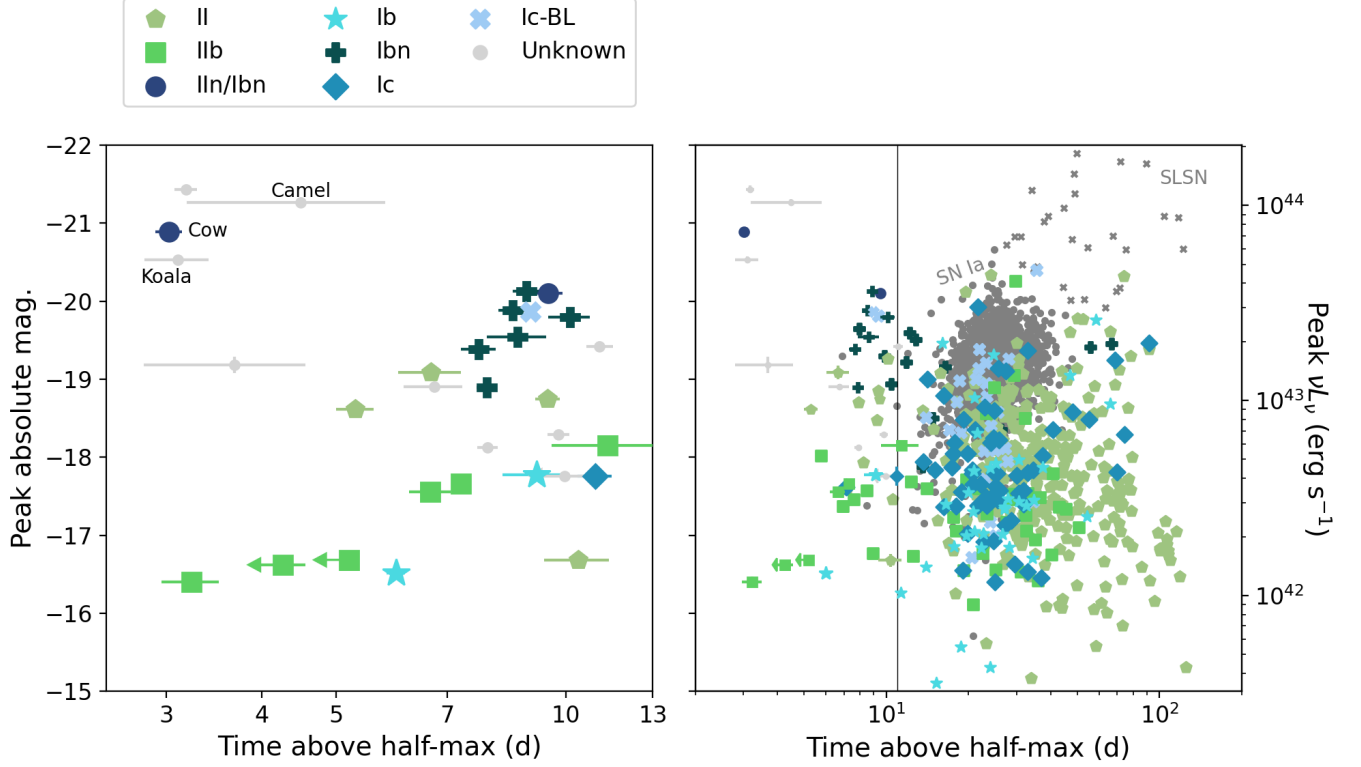
Figure 1. Parameter space of short-duration ($t_{1/2} \lesssim 12$ d) extragalactic transients in ZTF (left panel) in the context of all transients classified as part of the ZTF Bright Transient Survey (right panel; Fremling et al. 2020; Perley et al. 2020b). Measurements are in g band and rest-frame, except for AT 2018cow (we use an o-band detection from ATLAS during the rise) and SN 2018bcc (we use the r-band rise time.) The vertical line in the right panel indicates $t_{1/2} = 12$ d. Events with radio behavior similar to AT 2018cow ("the Cow"), nicknamed the "Koala" (ZTF18abvkwla; AT 2018lug) and the "Camel" (ZTF20acigmel; AT 2020xnd) lie in a distinctly short-duration, high-luminosity part of parameter space. However, it is clear that the majority of what have been dubbed short-duration, rapidly evolving, or fast and blue transients in the literature are simply the extreme of a continuum of established classes of supernovae.

resolved; in other words, there was a detection followed by a non-detection that did not result in an alert. Because of this, we implemented a new scanning routine in October 2020, in which we run forced photometry for all events in the HC and 1DC fields from the previous week. This resulted in the discovery of several events that would otherwise have been missed by the real-time fast-transient filters (e.g., SN 2020xlt and SN 2020rsc). This forced photometry search is now part of the scanning routine, as described in Perley et al. (2021b).

We apply similar selection criteria ($t_{1/2} \lesssim 12$ d, observed a few days before and after peak) to identify a comparison sample from the literature, listed in Table 5. We measured the duration in as close to rest-frame g-band as possible, to account for variations in redshift. In Figure 2 we show the distribution of the comparison sample in timescale-luminosity space with the ZTF sample in the background. Figure 2 shows that our ZTF sample has a similar distribution of timescales and luminosities to events in the literature, although with ZTF

we have identified several very short-duration subluminous transients that do not appear to have been detected by previous surveys. These particularly fast and subluminous objects will be presented in more detail in a separate paper by Fremling et al.

Most of the comparison-sample transients are unclassified, with a few exceptions: Type Ibn SNe (Pastorello et al. 2015; Hosseinzadeh et al. 2017), the Type IIn PTF09uj (Ofek et al. 2010), the Type Ic-BL SN iPTF16asu (Whitesides et al. 2017), and the Type Ic SNe SN 2018kzr (McBrien et al. 2019) and SN 2019bkc (Chen et al. 2020; Prentice et al. 2020). Because we require a short overall duration, events with a fast rise but slow decay (such as most events in Arcavi et al. (2016)) do not meet our criteria. We discuss the limitations of this overall-duration approach in Section 6.

2.3. Optical Photometry
2.3.1. ZTF

Table 2. Gold Sample

ZTF Name	R.A. (J2000)	Dec. (J2000)	IAU Name	Peak MJD	Peak Mag	Telescope	Phase[a]	Sp. Type	z	Ref.
ZTF18aakuewf	16:14:22.65	+35:55:04.4	SN 2018bcc	58230.38	17.46 ± 0.04	P200	16	Ibn	0.0636	[1]
ZTF18abcfcoo	16:16:00.22	+22:16:04.8	AT 2018cow	58287.15	13.11 ± 0.05	Gemini	12	IIn/Ibn?[b]	0.0141	[2]
ZTF18abfcmjw	17:36:46.74	+50:32:52.1	SN 2019dge	58583.16	18.4 ± 0.02	P200	14	Ib	0.0213	[3]
ZTF18abukavn	16:43:48.20	+41:02:43.3	SN 2018gep	58374.22	15.91 ± 0.01	Asiago	4	Ic-BL	0.03154	[4]
ZTF18abvkmgw	00:37:26.87	+15:00:51.2	SN 2018ghd	58377.35	18.49 ± 0.03	Keck1	54	Ib	0.03923	
ZTF18abwkrbl	02:16:15.58	+28:35:28.6	SN 2018gjx	58379.44	15.58 ± 0.01	P60	23	IIb	0.00999	[5]
ZTF19aakssbm	16:11:03.55	+74:21:41.3	SN 2019aajs	58542.11	17.16 ± 0.03	LT	2	Ibn	0.0358	
ZTF19aapfmki	14:05:43.56	+09:30:56.6	SN 2019deh	58587.33	17.22 ± 0.02	LT	-2	Ibn	0.05469	[6]
ZTF19abobxik	00:43:43.12	+37:03:38.9	SN 2019myn	58706.45	18.84 ± 0.02	Keck1	19	Ibn	0.1	
ZTF19abuvqgw	19:50:06.37	+66:04:56.5	SN 2019php	58730.3	18.68 ± 0.06	Keck1	20	Ibn	0.087	
ZTF19abyjzvd	16:48:12.90	+48:04:50.0	SN 2019qav	58739.13	18.99 ± 0.06	Keck1	11	IIn/Ibn	0.1353	
ZTF19acayojs	21:22:41.87	+22:52:54.8	SN 2019rii	58757.18	18.75 ± 0.02	P200	2	Ibn	0.1234	
ZTF19accjfgv	08:28:49.30	+75:19:41.0	SN 2019rta	58759.43	17.88 ± 0.02	Keck1	24	IIb	0.027	[7]
ZTF20aaelulu	12:22:54.92	+15:49:25.0	SN 2020oi	58862.48	14.06 ± 0.12	SOAR	-5	Ic	0.0052	[8]
ZTF20aahfqpm	13:06:25.19	+53:28:45.5	SN 2020ano	58871.45	19.06 ± 0.03	Keck1	25	IIb	0.03113	
ZTF20aaxhzhc	13:36:05.01	+28:59:00.1	SN 2020ikq	58971.3	18.27 ± 0.03	NOT	12	IIb	0.042	[9]
ZTF20aayrobw	09:31:13.19	+38:15:14.4	SN 2020jmb	58981.17	18.51 ± 0.03	P200	15	II	0.061	[10]
ZTF20aazchcq	14:41:40.57	+19:20:56.9	SN 2020jji	58979.25	19.5 ± 0.09	P200	16	II	0.03788	
ZTF20abjbgjj	23:50:14.27	+10:07:41.3	SN 2020ntt	59033.45	18.61 ± 0.09	Keck1	10	II	0.074	[11]
ZTF20aburywx	01:19:56.51	+38:11:09.5	SN 2020rsc	59081.47	19.36 ± 0.07	Keck1	25	IIb	0.0313	
ZTF20acigusw	22:50:25.37	+08:50:41.8	SN 2020vyv	59134.23	18.68 ± 0.03	Keck1	1	II	0.062	[12]
ZTF20aclfmwn	08:17:11.29	+64:31:34.7	SN 2020xlt	59141.45	19.59 ± 0.04	GTC	10	IIb	0.0384	

[a] Of spectroscopic classification, given as days past g-band max.

[b] This is a strict spectroscopic definition based on the presence of H and He emission features in the optical spectrum. This object is very different from IIn/Ibn transitional events in the literature, as we explain in the paper.

Peak time and mag refers to g-band light curve.

References—Classification provided by [1] Karamehmetoglu et al. (2019), [2] Perley et al. (2019) [2] Yao et al. (2020), [4] Costantin et al. (2018), [5] Dahiwale & Fremling (2020a), [6] Prentice et al. (2019), [7] Dahiwale & Fremling (2019), [8] Siebert et al. (2020a), [9] Angus (2020), [10] Dahiwale & Fremling (2020b), [11] Perley et al. (2020a), and [12] Siebert et al. (2020b)
.

Table 3. Silver Sample

ZTF Name	R.A. (J2000)	Dec. (J2000)	IAU Name	Peak MJD	Peak Mag	Redshift	Reference
ZTF18abvkwla	02:00:15.19	+16:47:57.3	AT 2018lug	58374.41	19.34 ± 0.05	0.2714	[1]
ZTF19aatoboa	12:25:40.57	+44:44:48.8	AT 2019esf	58609.22	18.84 ± 0.03	0.0758	
ZTF19abfarpa	11:07:09.56	+57:06:03.2	AT 2019kyw	58676.18	18.28 ± 0.04	0.074	
ZTF20aaivtof	02:48:18.49	−09:26:52.8	AT 2020bdh	58875.16	18.6 ± 0.03	0.04106	
ZTF20aakypiu	11:31:13.75	+34:30:00.7	AT 2020bot	58880.45	19.46 ± 0.04	0.197	
ZTF20ababxjv	16:28:39.48	+56:13:40.6	AT 2020kfw	58991.33	19.05 ± 0.03	0.059	
ZTF20abmocba	16:34:38.89	+50:59:26.5	AT 2020aexw	59051.26	19.39 ± 0.03	0.0734	
ZTF20abummyz	16:50:45.92	+30:45:14.9	AT 2020yqt	59080.21	19.17 ± 0.11	0.0986	
ZTF20acigmel	22:20:02.02	−02:50:25.3	AT 2020xnd	59136.21	19.24 ± 0.04	0.2442	[2]

Peak time and mag refers to g-band light curve.

References—[1] Ho et al. (2020b), [2] Perley et al. (2021b)

We performed forced photometry on P48 images for all events using the pipeline developed by F. Masci and R. Laher[5], with the following additional steps:

[5] http://web.ipac.caltech.edu/staff/fmasci/ztf/forcedphot.pdf

1. We removed data taken in bad observing conditions by discarding observations with scisigpix, zpmaginpsci, or zpmaginpscirms exceeding five times the median of that value for the light curve.

Table 4. Bronze Sample

ZTF Name	R.A. (J2000)	Dec. (J2000)	IAU Name	Peak MJD	Peak Mag.
ZTF18aayrkfa	15:34:00.38	+31:59:49.6	AT 2018lwc	58278.26	20.02 ± 0.06
ZTF18abianhw	19:23:40.60	+44:48:30.1	AT 2018lwd	58318.41	19.55 ± 0.05
ZTF19aankdan	11:53:47.14	+44:44:44.8	AT 2019dcm	58572.27	19.09 ± 0.04
ZTF19aapuudk	15:10:03.55	+38:07:11.8	AT 2019aajt	58585.27	19.49 ± 0.05
ZTF19aasexmy	13:31:54.39	+25:44:05.9	AT 2019aaju	58599.33	19.41 ± 0.02
ZTF19abeyvoi	23:50:15.80	+08:07:05.3	AT 2019lbr	58675.45	19.09 ± 0.04
ZTF19abrpfps	18:36:27.30	+45:05:32.0	AT 2019aajv	58720.22	19.48 ± 0.03
ZTF19acaxbjt	23:12:35.94	+09:02:07.9	AT 2019qwx	58754.2	19.03 ± 0.04
ZTF19accxzsc	03:26:14.73	+04:47:26.7	AT 2019scr	58763.42	18.91 ± 0.05
ZTF19acsakuv	06:21:15.36	+53:16:39.5	AT 2019van	58800.55	18.54 ± 0.11
ZTF20aazrcbp	11:02:20.89	+30:51:52.1	AT 2020mlq	58986.21	19.71 ± 0.06

Peak time and mag refers to g-band light curve.
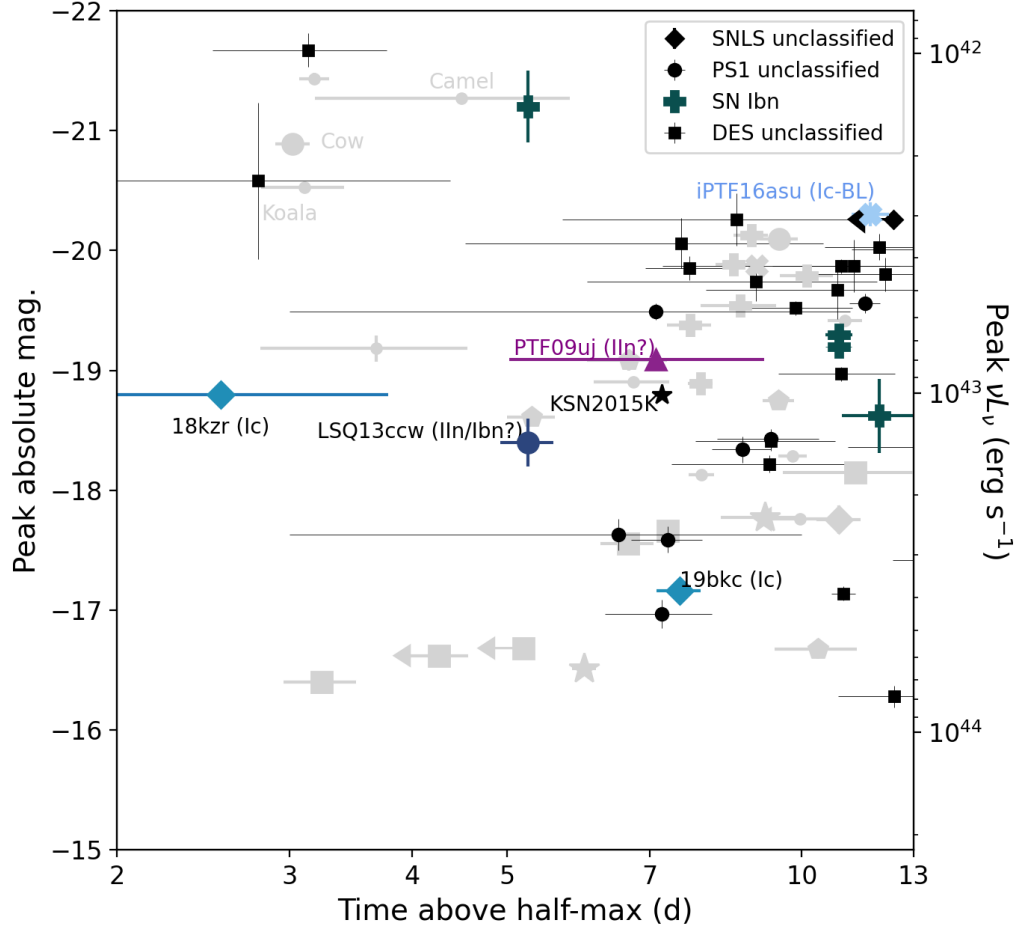
Figure 2. The distribution of duration and luminosity of the literature comparison sample (foreground, in color), with our ZTF sample from Figure 1 in light grey in the background. Comparison-sample objects were obtained from a variety of sources: DES (Pursiainen et al. 2018), PS1 (Drout et al. 2014), SNLS (Arcavi et al. 2016), a sample of Ibn SNe (Hosseinzadeh et al. 2017), and several single-object studies (Whitesides et al. 2017; Ofek et al. 2010; Rest et al. 2018; Pastorello et al. 2015; McBrien et al. 2019; Chen et al. 2020; Prentice et al. 2020). Timescales are shown as close to rest-frame g band as possible. We find that the ZTF and comparison samples cover similar areas of parameter space, but that there are several very short-duration subluminous Type IIb SNe in the ZTF sample that do not seem to have any analogs in the literature.

2. We removed observations with flux values or chisq from the difference image recorded as NaN.

3. Following Yao et al. (2019), we grouped observations by `fcqfID`, a combination of field ID, CCD ID, quadrant ID, and filter ID.

Table 5. Comparison sample of literature transients, most of which are unclassified. Timescales are presented in rest-frame and measured using the light curve that most closely matches rest-frame g band. For the PS1 events, we obtain luminosity and timescale measurements from Table 1 of Drout et al. (2014). For the Type Ibn SNe, we obtain peak magnitudes from Table 4 of Hosseinzadeh et al. (2017) and linearly interpolate the light curves to calculate rise and fade times. We calculate rise and fade times for PTF09uj, KSN2015K, and the DES events (using light curves provided by M. Pursiainen). Values for SNLS04D4ec (Arcavi et al. 2016) and iPTF16asu (Whitesides et al. 2017) are from Ho et al. (2020b). Photometry for SN 2018kzr was obtained from McBrien et al. (2019), and timescales were calculated using g-band as well as one ATLAS o-band upper limit prior to peak. Photometry for SN 2019bkc was obtained from Chen et al. (2020), with a ZTF datapoint added. Luminosity is corrected for Galactic extinction, assuming zero host-galaxy extinction in all cases except for iPTF15ul (see Hosseinzadeh et al. 2017).

Name	Redshift	Type	Filter	$M_{\max}$	$t_{1/2,\mathrm{rise}}$	$t_{1/2,\mathrm{fade}}$	Ref
					(days)	(days)	
SNLS04D4ec	0.593	Unknown	i	-20.26 ± 0.03	< 3.81	8.60 ± 0.43	[1]
PTF09uj	0.065	IIn	r	-19.09 ± 0.04	2.04 ± 0.76	5.05 ± 1.92	[2]
PS1-10ah	0.074	Unknown	g	-17.59 ± 0.11	1.0 ± 0.1	6.3 ± 0.6	[3]
PS1-10bjp	0.113	Unknown	g	-18.34 ± 0.11	1.0 ± 0.1	7.7 ± 0.6	[3]
PS1-11qr	0.324	Unknown	r	-19.56 ± 0.08	2.9 ± 0.1	8.7 ± 0.4	[3]
PS1-12bb	0.101	Unknown	g	-16.97 ± 0.12	< 1.8	6.3 ± 0.3	[3]
PS1-12bv	0.405	Unknown	r	-19.49 ± 0.07	< 2.2	$3–9$	[3]
PS1-12brf	0.275	Unknown	r	-18.43 ± 0.08	< 1.0	8.8 ± 0.6	[3]
PTF12ldy	0.106	Ibn	R	-19.20 ± 0.02	3.34 ± 0.17	7.57 ± 0.29	[4]
PS1-13dwm	0.245	Unknown	r	-17.63 ± 0.13	< 3.0	$3–7$	[3]
LSQ13ccw	0.0603	IIn/Ibn?	g	-18.4 ± 0.2	1.39 ± 0.10	3.86 ± 0.31	[5]
iPTF14aki	0.064	Ibn	R	-19.30 ± 0.03	3.34 ± 0.17	7.58 ± 0.30	[4]
iPTF15akq	0.109	Ibn	R, r	-18.62 ± 0.31	3.13 ± 0.61	8.86 ± 0.80	[4]
iPTF15ul	0.066	Ibn?	g	-21.2 ± 0.3	1.53 ± 0.05	3.72 ± 0.08	[4]
KSN2015K	0.090	Unknown	*Kepler* clear	-18.78	1.15	5.54	[6]
DES15C3lpq	0.61	Unknown	i	-19.8 ± 0.14	$2.65–6.1$	7.73 ± 1.16	[7]
DES16E2pv	0.73	Unknown	i	-20.58 ± 0.65	0.70 ± 0.42	2.05 ± 1.56	[7]
DES15S1fli	0.45	Unknown	r	-20.03 ± 0.11	< 3.39	8.60 ± 1.46	[7]
DES17X3cds	0.49	Unknown	i	-19.52 ± 0.06	$3.2–5.42$	5.60 ± 0.88	[7]
DES15S1fll	0.23	Unknown	r	-18.36 ± 0.06	$4.56–9.28$	6.83 ± 1.16	[7]
DES16C2ggt	0.31	Unknown	r	-18.41 ± 0.08	< 2.93	6.53 ± 1.54	[7]
DES16C1cbd	0.54	Unknown	i	-19.85 ± 0.1	1.78 ± 0.24	5.86 ± 0.64	[7]
DES13X3gmd	0.78	Unknown	i	-19.87 ± 0.22	< 3.75	7.20 ± 4.00	[7]
DES14S2pli	0.35	Unknown	r	-18.97 ± 0.06	< 3.83	7.03 ± 1.53	[7]
DES13X3gms	0.65	Unknown	i	-20.01 ± 0.06	$1.85–6.22$	9.90 ± 1.81	[7]
DES15C3mgq	0.23	Unknown	r	-17.14 ± 0.06	< 2.65	8.41 ± 0.34	[7]
DES17C3gen	0.92	Unknown	z	-20.26 ± 0.22	$1.88–4.02$	5.49 ± 2.51	[7]
DES14C3tnz	0.7	Unknown	i	-19.74 ± 0.16	$2.4–4.46$	5.46 ± 2.61	[7]
DES15E2nqh	0.52	Unknown	i	-19.67 ± 0.24	$3.04–7.34$	5.59 ± 1.90	[7]
DES16S1dxu	0.14	Unknown	g	-16.28 ± 0.09	3.54 ± 0.52	8.83 ± 1.63	[7]
DES17S2fee	0.24	Unknown	r	-18.22 ± 0.07	< 3.27	6.07 ± 1.89	[7]
DES16X3cxn	0.58	Unknown	i	-19.87 ± 0.06	$2.8–5.93$	6.62 ± 0.42	[7]
DES14X3pkl	0.3	Unknown	r	-17.42 ± 0.07	< 4.16	9.17 ± 0.79	[7]
DES16X1eho	0.81	Unknown	z	-21.67 ± 0.14	$1.23–2.41$	1.33 ± 0.23	[7]
DES13X1hav	0.58	Unknown	i	-20.06 ± 0.21	< 1.63	5.84 ± 3.02	[7]
iPTF16asu	0.187	Ic-BL	g	-20.3 ± 0.1	1.14 ± 0.13	10.62 ± 0.55	[8]
SN 2018kzr	0.054	Ic	g	-18.80 ± 0.08	< 2.0	1.6 ± 0.2	[9]
SN 2019bkc	0.0209	Ic	g	-17.16 ± 0.03	5.28 ± 0.38	2.22 ± 0.10	[10,11]

References— [1] Arcavi et al. (2016), [2] Ofek et al. (2010), [3] Drout et al. (2014), [4] Hosseinzadeh et al. (2017), [5] Pastorello et al. (2015), [6] Rest et al. (2018), [7] Pursiainen et al. (2018), [8] Whitesides et al. (2017), [9] McBrien et al. (2019), [10] Prentice et al. (2020), [11] Chen et al. (2020)

4. For each group of `fcqfID`, we checked whether the stack of images used to construct a reference image could overlap with images of the target, by see-ing whether the final reference image was within 15 days of the first ZTF alert issued. If so, we con-

sidered the data to be contaminated by the reference.

5. If the data were contaminated by the reference[6] (as defined in the previous bullet), we checked whether there were sufficient (at least 30) images to subtract a baseline flux value. We obtained images prior to 15 days before the first detection, and after 100 days after the last detection. If there were at least 30 such images, we calculated the median of all the baseline detections, rejected outliers greater than 3 times the median from the median, then recalculated the median, and subtracted that baseline value from the observations. If there were not sufficient baseline measurements, we excluded the observations.

6. Following the Masci & Laher documentation, we validated and rescaled the uncertainties on the flux values.

7. Points with a S/N ratio greater than 3 were regarded as detections, and converted to magnitudes. Points with a lower S/N were regarded as upper limits, and reported as 5-σ.

8. We corrected for Milky Way extinction (Schlafly & Finkbeiner 2011) using the `extinction` package[7] with $R_V = 3.1$ and a Fitzpatrick (1999) extinction law.

When available, we added photometry obtained with other facilities, such as the IO:O on the Liverpool Telescope (LT; Steele et al. 2004) and the Rainbow Camera on the automated 60-inch telescope at Palomar Observatory (P60; Cenko et al. 2006). LT image reduction was provided by the basic IO:O pipeline. P60 and LT image subtraction were performed following Fremling et al. (2016), using PS1 images for $griz$ and SDSS for u band. The final combined light curves are provided in the Appendix, in Table 6. We include all measurements within 5 d of the first alert issued for the source, up to 5 d after the final alert.

Table 6. Full optical light curves

Name	Filter	JD	Flux [uJy]	eFlux [uJy]	Mag	eMag	Tel
...	...	...	...	...			
AT 2018lwc	r	2458275.85	2.353	2.238	21.28	99.0	P48
AT 2018lwc	r	2458275.85	2.353	2.238	21.28	99.0	P48
AT 2018lwc	r	2458276.8	12.35	1.9	21.17	0.17	P48
AT 2018lwc	r	2458276.8	12.35	1.9	21.17	0.17	P48
...	...	...	...	...			

Non-detections are indicated with eMag=99. This table is published in its entirety in the machine-readable format. A portion is shown here for guidance regarding its form and content.

A sample of the resulting light curves for classified events, in some cases binned in time for clarity, is shown in Figure 3. Light curves for all other gold, silver, and bronze sources are provided in the Appendix, in Table 20, Table 21, and Table 22, respectively. For stripped-envelope supernovae and unclassified events, we include a Type Ibc R-band light curve template (shifted to match the peak r-band magnitude) from Drout et al. (2011) for reference. For the Type II and Type IIb SNe, we include the V-band light curve of SN 1993J (Schmidt et al. 1993) for reference.

2.4. *Optical Spectroscopy*

We obtained spectra of the gold- and silver-sample transients and their host galaxies from a variety of telescopes: the Spectral Energy Distribution Machine (SEDM; Blagorodnova et al. 2018; Rigault et al. 2019), the Alhambra Faint Object Spectrograph and Camera (ALFOSC[8]) on the Nordic Optical Telescope (NOT; Djupvik & Andersen 2010), the Double Beam Spectrograph (DBSP; Oke & Gunn 1982) on the 200-inch Hale telescope at Palomar Observatory, the Spectrograph for the Rapid Acquisition of Transients (SPRAT; Piascik et al. 2014) on LT, the Low Resolution Imaging Spectrometer (LRIS; Oke et al. 1995) on the Keck I 10-m telescope, Binospec (Fabricant et al. 2019) on the MMT,

---

[6] In principle a baseline should be subtracted for all events, but it has been found that this correction is very small, only $< 0.1\%$ of transient flux values.

[7] https://github.com/kbarbary/extinction

[8] http://www.not.iac.es/instruments/alfosc/
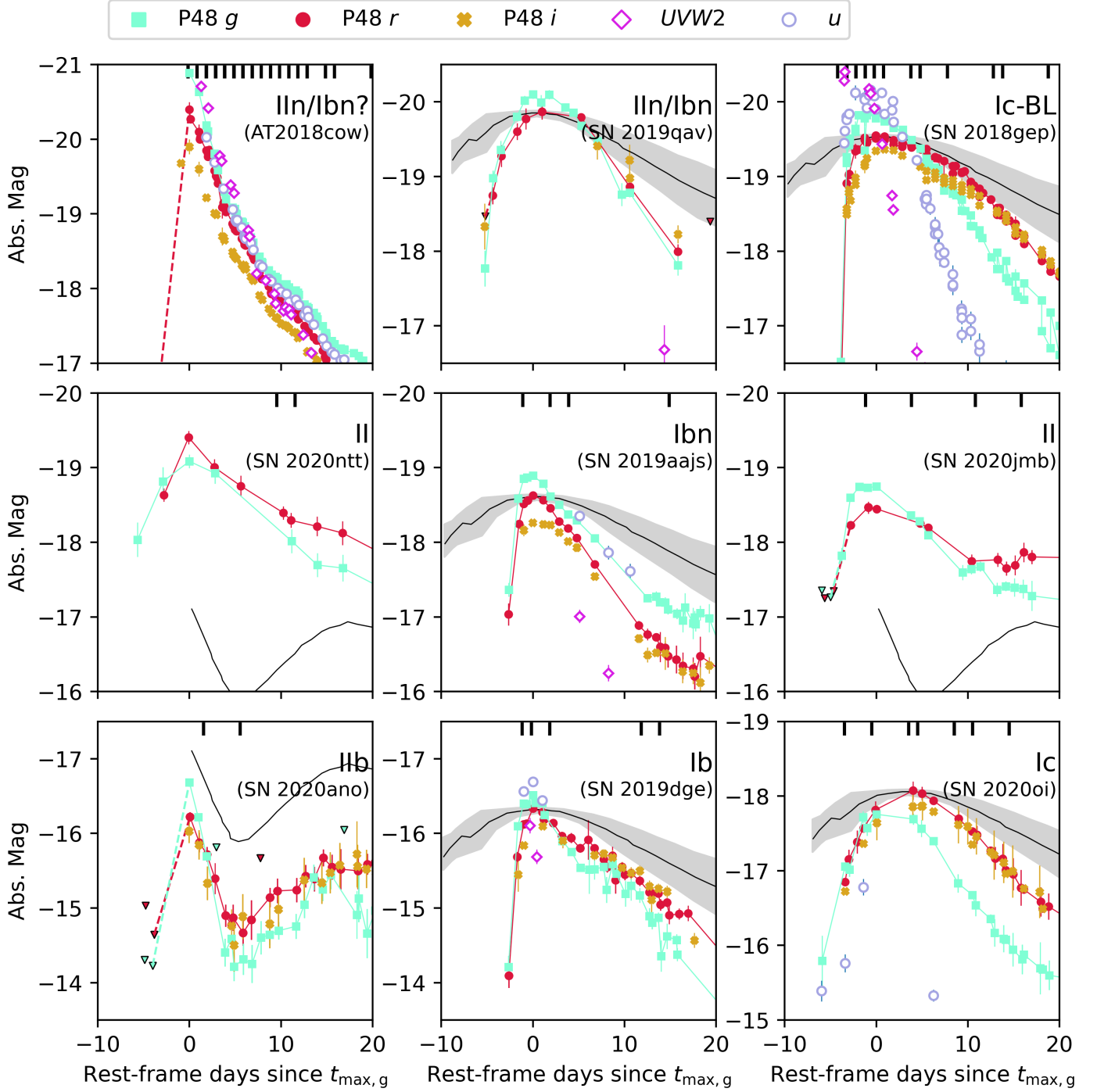
Figure 3. Light curves of rapidly evolving extragalactic transients in our sample, showcasing examples of different spectroscopic classes. Upper limits are indicated with triangles, and dashed lines connect non-detections to detections. Epochs of spectroscopy are indicated with vertical lines along the top of each panel. The contrast in each panel is 4 mag along the y-axis and 30 d along the x-axis. In panels with H-poor SNe we show a Type Ibc light curve template (Drout et al. 2011) for reference, scaled to the peak of the r-band light curve. For the Type II and Type IIb SNe we show the light curve of the Type IIb SN 1993J for reference (Schmidt et al. 1993). The AT 2018cow light curve was obtained directly from Perley et al. (2019).

the Optical System for Imaging and low-Intermediate-Resolution Integrated Spectroscopy (OSIRIS) on the Gran Telescopio Canarias (GTC; Cepa et al. 2000), and the Device Optimized for the LOw RESolution (DO-LORES) on the Telescopio Nazionale Galileo (TNG). The SEDM pipeline is described in Rigault et al. (2019), the SPRAT pipeline is based on the FrodoSpec pipeline (Barnsley et al. 2012), the P200/DBSP pipeline is described in Bellm & Sesar (2016), and the Keck/LRIS pipeline Lpipe is described in Perley (2019).

A log of spectroscopic observations is provided in the Appendix in Table 15.[9] We include several spectra downloaded from the TNS, indicated with references. Epochs of transient spectra are indicated with vertical lines across the top of each light-curve panel in Figures 3, 20, and 21. The sequence of optical spectra for each gold-sample object is shown in the Appendix (Figures 23, 24, 25, and 26).

2.5. UV and X-ray Observations

Of our 22 gold-sample objects, seven were observed with the UV/optical (UVOT; Roming et al. 2005) and X-Ray Telescope (XRT; Burrows et al. 2005) on board the Neil Gehrels *Swift* observatory (Gehrels et al. 2004), three of which are not yet published in the literature. In Table 7 and Table 8 we provide a log of UVOT and XRT observations for the three events.[10] All three were detected by UVOT, but none were detected by XRT.

Table 7. UVOT photometry. Epochs are given with respect to peak of the g-band light curve.

Object Name	Date (JD)	Δt (d)	Filter	AB Mag
SN 2019deh	2458585.0	−2.9	$UVW1$	17.55 ± 0.07
SN 2019deh	2458585.0	−2.9	U	17.28 ± 0.07
SN 2019deh	2458585.0	−2.9	B	17.60 ± 0.09
SN 2019deh	2458585.0	−2.9	$UVW2$	18.41 ± 0.08
SN 2019deh	2458585.0	−2.8	V	17.63 ± 0.15
SN 2019deh	2458585.0	−2.8	$UVM2$	18.01 ± 0.06
SN 2019deh	2458585.7	−2.1	V	17.55 ± 0.15
SN 2019deh	2458585.7	−2.1	$UVM2$	18.06 ± 0.07
SN 2019deh	2458586.0	−1.8	$UVW1$	17.62 ± 0.06
SN 2019deh	2458586.0	−1.8	U	17.27 ± 0.07

Table 7 *continued*

[9] We exclude AT 2018cow, SN 2018gep, SN 2019dge, and SN 2020oi as the details of the spectroscopic observations have been published separately (Perley et al. 2019; Ho et al. 2019a; Yao et al. 2020; Horesh et al. 2020)

[10] The published events are AT 2018cow (Perley et al. 2019; Kuin et al. 2019; Ho et al. 2019b; Margutti et al. 2019), SN 2019dge (Yao et al. 2020), SN 2018gep (Ho et al. 2019a), and SN 2020oi (Horesh et al. 2020).

Table 7 *(continued)*

Object Name	Date (JD)	Δt (d)	Filter	AB Mag
SN 2019deh	2458586.0	−1.8	B	17.34 ± 0.07
SN 2019deh	2458586.0	−1.8	$UVW2$	18.34 ± 0.08
SN 2019qav	2458755.9	16.0	$UVW1$	21.59 ± 0.33
SN 2019qav	2458755.9	16.0	U	21.06 ± 0.49
SN 2019qav	2458755.9	16.0	B	21.64 ± 1.55
SN 2019qav	2458755.9	16.0	$UVW2$	22.41 ± 0.33
SN 2019qav	2458755.9	16.0	V	20.20 ± 0.78
SN 2019qav	2458755.9	16.0	$UVM2$	22.22 ± 0.27
SN 2019aajs	2458547.9	5.3	B	17.93 ± 0.1
SN 2019aajs	2458551.2	8.5	B	18.23 ± 0.12
SN 2019aajs	2458553.6	11.0	B	18.81 ± 0.17
SN 2019aajs	2458569.3	27.0	B	> 20.0
SN 2019aajs	2458575.2	33.0	B	> 20.0
SN 2019aajs	2458547.9	5.3	U	18.04 ± 0.09
SN 2019aajs	2458551.2	8.5	U	18.6 ± 0.1
SN 2019aajs	2458553.6	11.0	U	18.81 ± 0.12
SN 2019aajs	2458569.3	27.0	U	19.81 ± 0.25
SN 2019aajs	2458575.2	33.0	U	19.92 ± 0.22
SN 2019aajs	2458547.9	5.3	$UVM2$	18.71 ± 0.07
SN 2019aajs	2458551.2	8.6	$UVM2$	19.54 ± 0.09
SN 2019aajs	2458553.6	11.0	$UVM2$	20.08 ± 0.12
SN 2019aajs	2458569.3	27.0	$UVM2$	21.06 ± 0.19
SN 2019aajs	2458575.2	33.0	$UVM2$	21.15 ± 0.2
SN 2019aajs	2458547.9	5.3	$UVW1$	18.57 ± 0.08
SN 2019aajs	2458551.2	8.5	$UVW1$	19.33 ± 0.11
SN 2019aajs	2458553.6	11.0	$UVW1$	19.38 ± 0.11
SN 2019aajs	2458569.3	27.0	$UVW1$	20.42 ± 0.19
SN 2019aajs	2458575.2	33.0	$UVW1$	20.8 ± 0.2
SN 2019aajs	2458547.9	5.3	$UVW2$	19.05 ± 0.09
SN 2019aajs	2458551.2	8.6	$UVW2$	19.81 ± 0.11
SN 2019aajs	2458553.6	11.0	$UVW2$	20.24 ± 0.13
SN 2019aajs	2458569.3	27.0	$UVW2$	21.29 ± 0.24
SN 2019aajs	2458575.2	33.0	$UVW2$	21.3 ± 0.2
SN 2019aajs	2458547.9	5.3	V	18.45 ± 0.23
SN 2019aajs	2458551.2	8.6	V	18.37 ± 0.22
SN 2019aajs	2458553.6	11.0	V	18.62 ± 0.25
SN 2019aajs	2458569.3	27.0	V	> 19.0
SN 2019aajs	2458575.2	33.0	V	> 19.0

The brightness in the UVOT filters was measured with UVOT-specific tools in the HEAsoft version 6.26.1. Source counts were extracted from the images using a circular 3″-radius aperture. The background was estimated over a significantly larger area close to the SN position. The count rates were obtained from the images using the *Swift* tool uvotsource. They were converted to magnitudes using the UVOT photometric zero-points (Breeveld et al. 2011) and the UVOT calibration files from September 2020. All magnitudes were transformed into the AB system using Breeveld et al. (2011). If the transient was affected by the host, we made use of archival UVOT observations or obtained templates after the SN faded. XRT data were reduced using the online

Table 8. *Swift* XRT observations. Flux is given as unabsorbed flux. Observations for AT 2018cow, SN 2019dge, SN 2018gep, and SN 2020oi have been published elsewhere (Ho et al. 2019b; Yao et al. 2020; Ho et al. 2019a; Horesh et al. 2020). Conversions from count rate to flux assume a photon index $\Gamma = 2$ and values of n_H are taken from Willingale et al. (2013).

Object Name	Target ID	PI	Start Date	Δt	Count Rate	n_H	Flux	$L_{0.3-10}$ keV
			(UTC)	(d)	(s^{-1})	(cm^{-2})	(erg cm^{-2} s^{-1})	(erg s^{-1})
SN 2019qav	12013	Ho	2019-09-29	16	$< 3.9 \times 10^{-3}$	1.81×10^{20}	$< 1.3 \times 10^{-13}$	$< 6.9 \times 10^{42}$
SN 2020rsc	13670	Ho	2020-08-26	6	$< 6.6 \times 10^{-3}$	6.54×10^{20}	$< 2.7 \times 10^{-13}$	$< 6.5 \times 10^{41}$
SN 2019deh	11193	Perley	2019-03-05	6	$< 5.5 \times 10^{-3}$	3.75×10^{20}	$< 2.1 \times 10^{-13}$	$< 6.7 \times 10^{41}$
SN 2019deh	11193	Perley	2019-03-08	9	$< 4.2 \times 10^{-3}$	3.75×10^{20}	$< 1.6 \times 10^{-13}$	$< 5.1 \times 10^{41}$
SN 2019deh	11193	Perley	2019-03-11	12	$< 5.3 \times 10^{-3}$	3.75×10^{20}	$< 2.0 \times 10^{-13}$	$< 6.3 \times 10^{41}$
SN 2019deh	11193	Perley	2019-03-26	27	$< 4.8 \times 10^{-3}$	3.75×10^{20}	$< 1.8 \times 10^{-13}$	$< 5.7 \times 10^{41}$
SN 2019deh	11193	Perley	2019-04-01	33	$< 3.6 \times 10^{-3}$	3.75×10^{20}	$< 1.3 \times 10^{-13}$	$< 4.1 \times 10^{41}$

tool[11] from the *Swift* team (Evans et al. 2007, 2009), using hydrogen column density values from Willingale et al. (2013).

2.6. *Millimeter and Radio Observations*

Four gold-sample objects have published millimeter and radio observations (Ho et al. 2019b; Margutti et al. 2019; Yao et al. 2020; Ho et al. 2019a; Horesh et al. 2020). We observed an additional four objects obtained with the IRAM Northern Extended Millimeter Array (NOEMA), the Submillimeter Array (SMA), and the Karl G. Jansky Very Large Array (VLA; Perley et al. 2011). Observations are listed in Table 9; all resulted in non-detections.

We observed SN 2019aajs, SN 2019myn, SN 2019qav, and SN 2020rsc with the VLA. Data were calibrated using the automated pipeline available in the Common Astronomy Software Applications (CASA; McMullin et al. 2007) with additional flagging applied manually, then imaged using the CLEAN algorithm (Högbom 1974).

SN 2019qav was observed with NOEMA under conditions of excellent atmospheric stability and transparency. Data calibration and analysis was done within the GILDAS[12] software package using CLIC for calibration and MAPPING for uv-plane analysis and imaging of the data. The absolute flux calibration accuracy is estimated to be better than 10%. The upper limit reported in Table 9 is from combining the two sidebands.

SN 2019aajs was observed with the SMA in the Extended configuration, using all eight antennas, under excellent conditions. Both receivers were tuned to local oscillator (LO) frequency of 225.5 GHz. Data were calibrated in IDL using the Millimeter Interferometer

Reduction (MIR) package then exported for additional analysis and imaging using the *Miriad* package (Sault et al. 1995). No obvious detection was seen in the dirty image, so no CLEANing was attempted.

In addition, we also queried ongoing radio surveys to determine whether any objects had been serendipitously observed. To query the VLA Sky Survey (VLASS; Lacy et al. 2020), which observes at 3 GHz, we used the same approach as Ho et al. (2020b). Twenty-seven of the sources in our sample were observed by VLASS, but none are detected. Table 10 lists the sources, the date they were observed and the associated RMS values.

We also searched for radio counterparts in two surveys that are being undertaken with the Australian Square Kilometre Array Pathfinder (ASKAP; Hotan et al. 2021): the Rapid ASKAP Continuum Survey (RACS: McConnell et al. 2020) and phase one of the Variables And Slow Transients Pilot survey (VAST-P1; Murphy et al. 2013). RACS covers ~ 35000 deg^2 at 888 MHz to a typical RMS noise of $\sim 250\,\mu$Jy, while VAST-P1 targets 113 RACS fields with identical observing parameters, covering ~ 5000 deg^2. There are 12 VAST epochs in total with each field covered at least 5 times, and 7 on average. Nine of the sources in our sample were observed by RACS and none had any associated radio emission. One source (AT 2020bdh) has additional coverage in VAST, and no emission is detected. Tables 11 and 12 list the observation details for sources in RACS and VAST respectively.

2.7. *Host Galaxy Photometry*

We obtained host-galaxy photometry for all transients in the gold and silver samples, listed in Table 13. We retrieved science-ready coadded images from the *Galaxy Evolution Explorer* (*GALEX*) general release 6/7 (Martin et al. 2005), the Sloan Digital Sky Survey data release 9 (SDSS DR9; Ahn et al. 2012), PS-1 Data Release

---

[11] https://www.swift.ac.uk/user_objects/

[12] http://www.iram.fr/IRAMFR/GILDAS

Table 9. Millimeter and radio observations. Upper limit given as 3x the image RMS.

Object Name	Instrument	Program ID (PI)	Start Date	Δt	ν	f_ν	L_ν
			(UTC)	(d)	(Hz)	(μJy)	(erg s^{-1} Hz^{-1})
SN 2019aajs	SMA	2018B-S047 (Ho)	2019-03-21	22	230	< 840	$< 2.7 \times 10^{28}$
SN 2019qav	NOEMA	S19BC (Ho)	2019-09-26	13	90	< 90	$< 4.8 \times 10^{28}$
SN 2019aajs	VLA	18B-242 (Perley)	2019-03-21	22	10	< 15	$< 4.8 \times 10^{26}$
SN 2019myn	VLA	18B-242 (Perley)	2019-08-17 06:38	6	10	< 16	$< 4.3 \times 10^{27}$
SN 2019qav	VLA	20A-374 (Ho)	2019-10-08	25	10	< 18	$< 9.6 \times 10^{27}$
SN 2019qav	VLA	20A-374 (Ho)	2020-03-15	184	10	< 27	$< 1.4 \times 10^{28}$
SN 2020rsc	VLA	20A-374 (Ho)	2020-09-08	19	10	< 15	$< 3.6 \times 10^{26}$

Table 10. Serendipitous observations of short-duration extragalactic transients in ZTF at 3 GHz as part of the VLA Sky Survey.

Name	MJD	Δt [d]	RMS [μJy]
AT 2018lwc	59131	852	201
AT 2018cow	59045	757	160
SN 2019dge	59072	488	156
AT 2018lwd	59074	755	141
SN 2018gep	58607	232	134
SN 2018ghd	59070	692	157
AT 2018lug	58551	176	133
SN 2018gjx	58568	188	171
SN 2019aajs	59094	551	109
AT 2019dcm	58609	36	110
SN 2019deh	58611	23	138
AT 2019aajt	59111	525	140
AT 2019lbr	59090	414	217
AT 2019kyw	59084	407	124
AT 2019aajv	59074	353	143
SN 2019php	59084	353	123
SN 2019qav	59072	332	166
AT 2019qwx	59091	336	161
SN 2019rta	59135	375	175
AT 2019scr	59067	303	162
SN 2020ano	59063	191	139
SN 2020ikq	59109	137	130
AT 2020kfw	59093	101	130
SN 2020ntt	59090	56	151
AT 2020aexw	59072	20	141
AT 2020yqt	59103	22	136

Table 11. Serendipitous observations of short-duration extragalactic transients in ZTF at 888 MHz in the Rapid ASKAP Continuum Survey

Name	MJD	Δt [d]	RMS [μJy]
SN 2018bcc	58595	364	248
AT 2018cow	58596	309	374
SN 2018gep	58595	221	535
SN 2018ghd	58598	221	353
SN 2018gjx	58595	216	257
SN 2019deh	58598	11	248
AT 2018lug	58602	228	332
AT 2018lwc	58596	318	175
AT 2019aajt	58595	10	270

Table 12. Serendipitous observations of AT 2020bdh and AT 2020xnd at 888 MHz in phase one of the VAST Pilot survey

Name	MJD	Δt [d]	RMS [μJy]
AT 2020bdh	59090	215	380

1 (Chambers et al. 2016), the Two Micron All Sky Survey (2MASS; Skrutskie et al. 2006), and preprocessed *WISE* images (Wright et al. 2010) from the unWISE archive (Lang 2014)[13]. The unWISE images are based on the public *WISE* data and include images from the ongoing NEOWISE-Reactivation mission R3 (Mainzer et al. 2014; Meisner et al. 2017). The hosts of two objects (SN 2019php, AT 2020xnd) were too faint, so we retrieved deeper optical images from the DESI Legacy Imaging Surveys (LS; Dey et al. 2019) DR8. We measured the brightness of the host using LAMBDAR[14] (Lambda Adaptive Multi-Band Deblending Algorithm in R; Wright et al. 2016) and the methods described in Schulze et al. (2020). The 2MASS and unWISE photometry were converted from the Vega system to the AB system using the offsets reported by Blanton & Roweis (2007) and Cutri et al. (2013, their Table 3 in Section 4.4h).

[13] http://unwise.me

[14] https://github.com/AngusWright/LAMBDAR

Table 13. Photometry of the host galaxies

Object	Survey/Telescopes/ Instrument	Filter	Brightness (mag)
SN 2018bcc	GALEX	FUV	20.00 ± 0.17
SN 2018bcc	GALEX	NUV	19.90 ± 0.06
SN 2018bcc	SDSS	g	18.53 ± 0.03
SN 2018bcc	SDSS	i	17.96 ± 0.09
SN 2018bcc	SDSS	r	18.24 ± 0.06
SN 2018bcc	SDSS	u	19.55 ± 0.11
SN 2018bcc	SDSS	z	17.93 ± 0.09
SN 2018bcc	WISE	$W1$	18.75 ± 0.14
SN 2018bcc	WISE	$W2$	19.52 ± 0.12

NOTE—All measurements are reported in the AB system and not corrected for reddening. This table is published in its entirety in the machine-readable format. A portion is shown here for guidance regarding its form and content.

In addition to this, we use the UVOT observations of AT 2018cow and SN 2018gep that were obtained after the transients faded. The brightness in the UVOT filters was measured with UVOT-specific tools in the HEAsoft[15] version 6.26.1. Source counts were extracted from the images using large apertures, to measure the total flux of the hosts. The background was estimated from regions close to the SN position. The count rates were obtained from the images using the *Swift* tool uvotsource. They were converted to magnitudes using the UVOT calibration file from September 2020. All magnitudes were transformed into the AB system using Breeveld et al. (2011).

3. ANALYSIS OF THE COMBINED SAMPLE

In this section we present an analysis of the combined sample of 42 ZTF and 38 literature events. We begin with the spectroscopic evolution (Section 3.1) to motivate the classifications that we assigned to the gold-sample transients in Section 2. We then discuss the photometric evolution (Section 3.2) and limits on X-ray, millimeter, and radio emission (Section 3.3).

3.1. *Spectroscopic Evolution*
3.1.1. *Peak-Light Spectra*

One of the challenges in spectroscopically classifying luminous rapidly evolving transients is that the peak-light spectra often appear relatively featureless (Drout et al. 2014; Karamehmetoglu et al. 2019; Perley et al. 2019; Ho et al. 2019a, 2020b; Perley et al. 2021b). Some have weak features from interaction with circumstellar material (CSM), such as PTF09uj (Ofek et al. 2010) and SN 2019dge (Yao et al. 2020), but these have been difficult to discern in the low-S/N spectra often obtained

for events at high redshift (Drout et al. 2014). Furthermore, by the phase at which SN features tend to become most distinguishable (two weeks after peak light; Williamson et al. 2019) a rapidly fading event is difficult to observe. The advantage of a high-cadence and shallow survey like ZTF is that objects are discovered young and relatively nearby, respectively: we were able to obtain spectra within 2–3 days of peak light for many of our 22 gold-sample objects[16], with sufficiently high S/N to discern even weak CSM interaction features, as well as late-time spectra that enabled spectroscopic classifications. For our analysis here, we only consider spectra obtained with instruments other than the SEDM, due to its low resolution ($R \sim 100$); we find that the slightly higher resolution of SPRAT ($R \sim 350$) is capable of discerning narrow lines.

The most common behavior at peak light is a spectrum dominated by a blue continuum, as has been found for previous samples, with weak narrow- to intermediate-width emission features of helium and hydrogen. The events from ZTF and the literature comparison sample that exhibit this behavior are shown in Figure 4.

One object warrants particular note: SN 2019rii has He I $\lambda\lambda3389$, $\lambda\lambda4471$ and $\lambda\lambda5876$ (though neither $\lambda\lambda6678$ nor $\lambda\lambda7065$), with weak narrow emission at $v = 0$, narrow absorption at $v = 900\,\mathrm{km\,s^{-1}}$ for $\lambda\lambda5876$ and $600\,\mathrm{km\,s^{-1}}$ for $\lambda\lambda4471$ and $\lambda\lambda3889$. We tentatively classify it as a Type Ibn on the basis of this spectrum (and do not have a high-quality late-time spectrum of the transient) but note that this classification is not fully secure.

Several objects showed no narrow to intermediate-width emission lines at maximum light, but instead exhibited broad absorption features from high-velocity ($v \gtrsim 0.1c$) material. This was seen in AT 2018cow (Perley et al. 2019), AT 2020xnd (Perley et al. 2021b), and the Type Ic-BL SN 2018gep (Ho et al. 2019a). These are also three of the most luminous objects in our sample, suggesting that high velocities may link the high luminosity of the light curve and the broad features of the spectra.

Broad absorption features were also seen in AT 2020bot, which occupies the same part of luminosity-duration parameter space as the AT 2018cow-like objects (Figure 1). Unlike AT 2018cow, however, AT 2020bot showed a distinct plateau or second peak in the light curve and is located close to an early-type
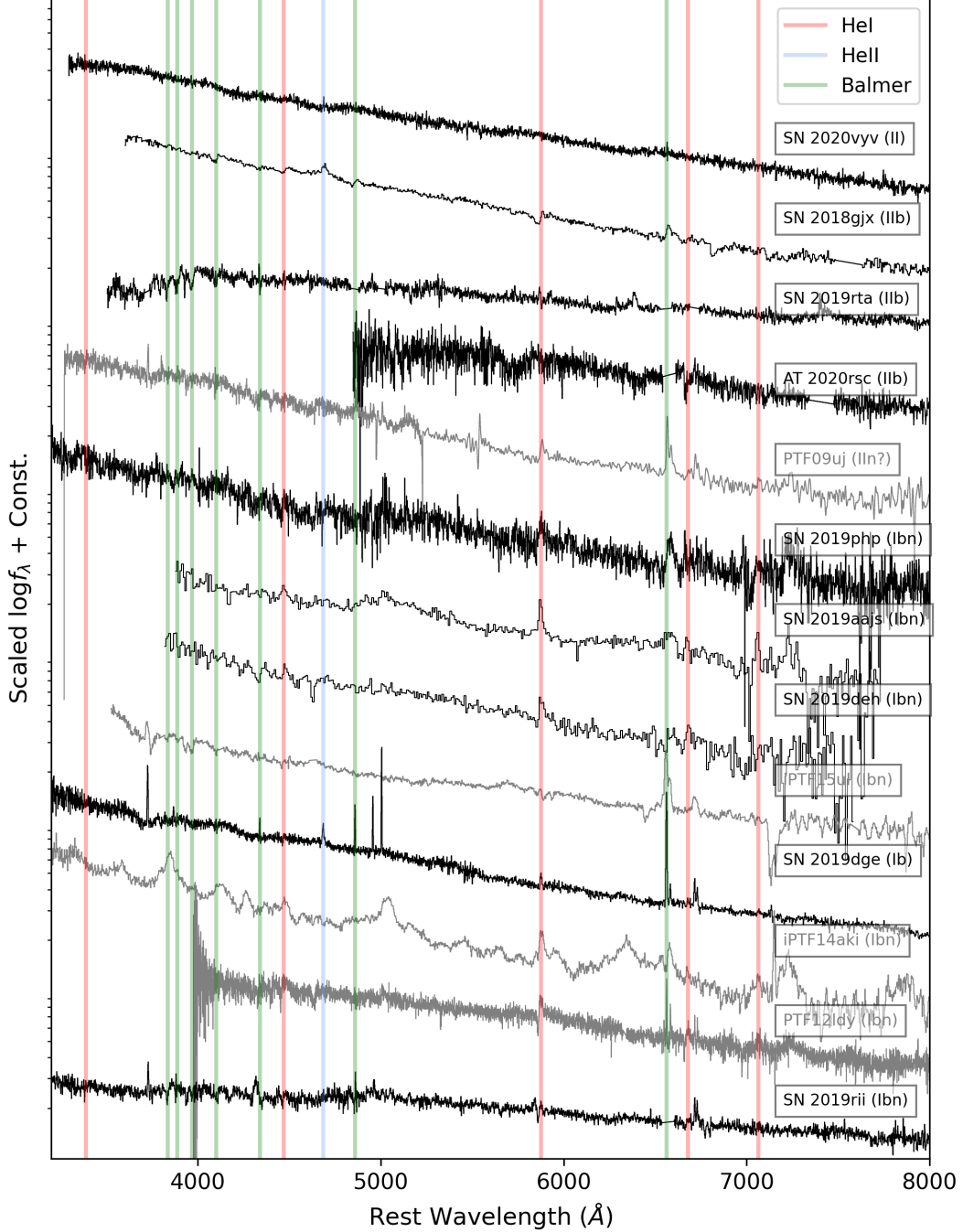
Figure 4. Peak-light spectra of events that show narrow- to intermediate-width features. Events from our ZTF sample are shown in black. The spectra of SN 2018gjx and SN 2020vyv were downloaded from TNS (Gromadzki et al. 2018; Siebert et al. 2020b). Several objects in the comparison sample exhibit very similar behavior and are shown in grey. The comparison-sample spectra were initially presented in Hosseinzadeh et al. (2017) and Ofek et al. (2010).

.

galaxy. A spectrum with GMOS obtained close to peak light, shown in Figure 5, showed broad features somewhat similar to Type Ic-BL SNe at early times. However, a lack of late-time spectra precluded a definitive classification, which is why it is in our silver sample.

Two objects had no discernible features in their peak-light spectra (AT 2018lug and AT 2020jmb). The peak-light spectrum of AT 2018lug (which had luminous radio emission similar to AT 2018cow) had high S/N and was presented in Ho et al. (2020b). The spectrum of
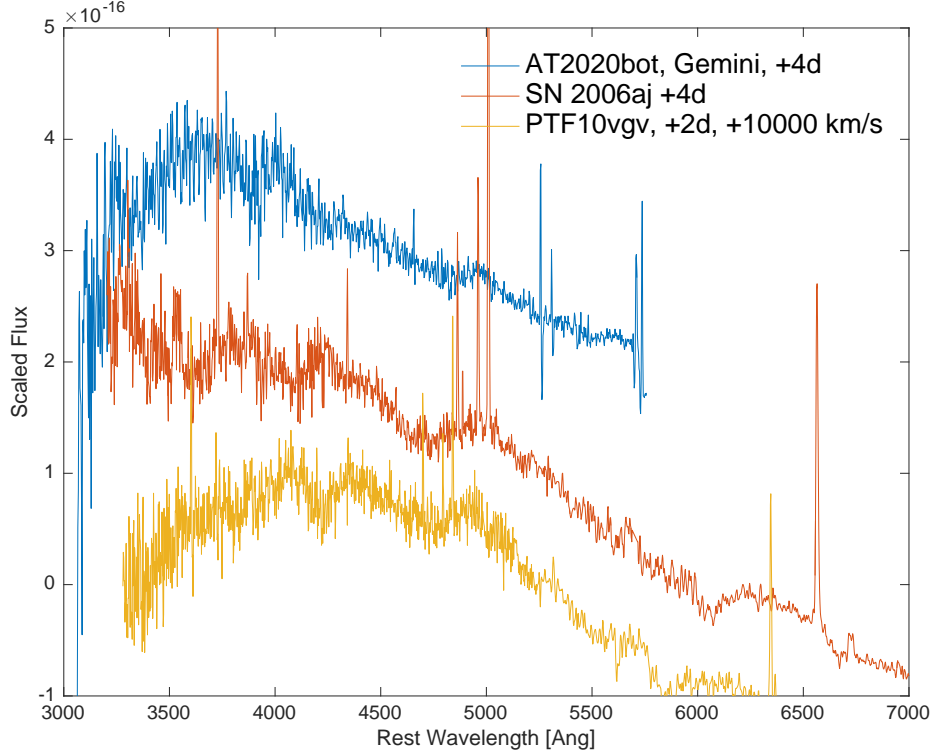
Figure 5. Spectrum of AT 2020bot obtained with GMOS-N close to peak light, compared to early spectra of two Type Ic-BL SNe (Pian et al. 2006; Corsi et al. 2012). The broad features are somewhat similar, although a lack of late-time spectra precluded a definitive classification. Unlike Type Ic-BL SNe, AT 2020bot was located close to an early-type galaxy.

AT 2020jmb was relatively low resolution (obtained with SPRAT) so narrow features cannot be ruled out entirely. We note that AT 2018cow also appeared completely featureless at certain epochs near peak light.

3.1.2. *Spectra After Peak*

Due to a lack of spectra obtained after peak, previous samples of rapidly evolving transients have not been able to conclude whether the objects were hydrogen-rich or hydrogen-poor (Drout et al. 2014; Pursiainen et al. 2018). By 1–3 weeks after peak light the spectra of most of our 22 gold-sample objects began to exhibit nebular features from optically thin ejecta, enabling their spectroscopic classification as SNe. The compositions range from H-rich (Type II/IIb), H-poor (Type Ib), to fully stripped (Type Ic/Ic-BL).

The subluminous events ($M > -18$ mag) most commonly evolve into Type II, Type IIb, and Type Ib SNe, as shown in Figure 6. We note that the distinction between these classes can be subtle when spectroscopic coverage is limited. For example, SN 2020jji and SN 2020jmb have spectra at two weeks after peak light that resemble both Type IIP and Type IIb objects, and we use a Type II classification to be more generic. We

comment on how these objects compare to "typical" members of their classes in Section 6. The full sample of short-duration Type II and Type IIb events will be presented and modeled in a separate paper by Fremling et al.

The luminous ($M < -18$ mag) and somewhat longer duration (> 6 d) events most commonly evolve into Type Ibn SNe. We show the Type Ibn post-peak spectra in Figure 7, together with spectra of the literature comparison sample objects that were also classified as Type Ibn (Pastorello et al. 2015; Hosseinzadeh et al. 2017). Type Ibn SNe are named for the strong and relatively narrow ($\sim 2000\,\mathrm{km\,s^{-1}}$) He I emission lines in their early spectra (Pastorello et al. 2008; Smith et al. 2017; Gal-Yam 2017). We comment on how these objects compare to "typical" Type Ibn SNe in Section 6. The detailed properties of the Type Ibn SNe observed in ZTF will be presented in a separate paper by Kool et al.

Finally, some events have post-peak spectra that remained dominated by a blue continuum with narrow- to intermediate-width emission lines, with no nebular emission from optically thin inner ejecta. In particular, SN 2019qav evolved in a similar fashion to the
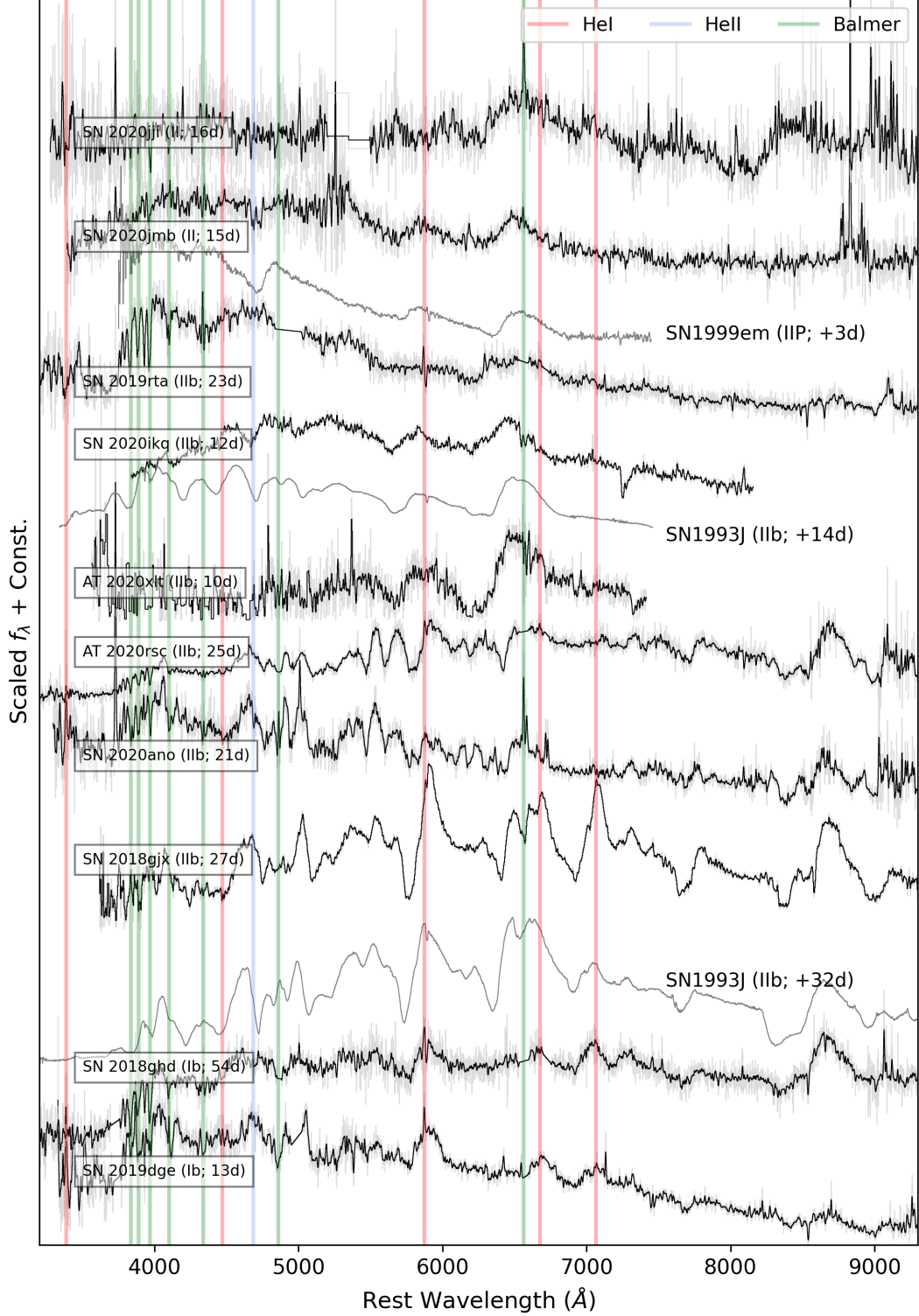
Figure 6. Post-peak spectra of the events in our sample that we classify as Type II, Type IIb, or Type Ib SNe based on their H and He P-Cygni features at late times. For comparison we show spectra of the Type IIP SN 1999em and the Type IIb SN 1993J, all obtained from WISeREP and originally from the UCB SN database (Silverman et al. 2012). For SN 1999em the phase is given with respect to the epoch of peak light reported on WISeREP (31 October 1999). For SN 1993J the phase is given with respect to the peak of the *first* (shock-cooling) peak, 30 March 1993. For the ZTF objects, epochs are given with respect to the maximum of the *g*-band light curve; raw spectra are shown in light grey, with smoothed spectra overlaid in black; and in some cases we have clipped host emission lines for clarity.
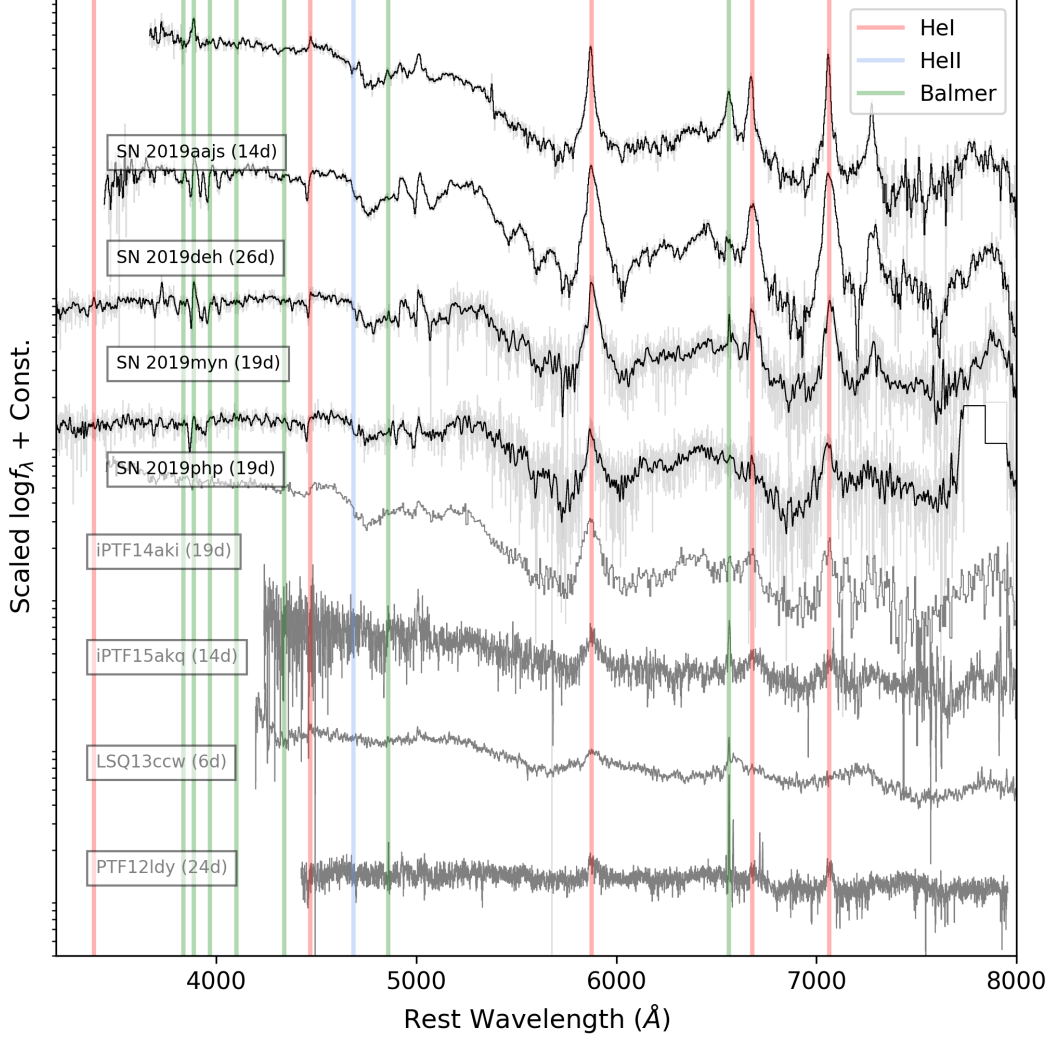
Figure 7. Post-peak spectra of events in our sample which we classify as Type Ibn SNe based on their He P-Cygni features at late times, together with Type Ibn SNe from our literature comparison sample. Literature spectra were obtained from WISeREP and are originally from Hosseinzadeh et al. (2017) and Pastorello et al. (2015).

.

Type IIn/Ibn transition object SN 2005la (Pastorello et al. 2008; Smith et al. 2012), as we show in Figure 8. Similarly, AT 2018cow had He II emission lines that emerged after one week, and Balmer emission lines that emerged one week after that, but never developed P-Cygni features. The only transient in the PS1 sample with a post-peak spectrum, PS1-12bb (+33 d), also had a persistently continuum-dominated spectrum, although weak features would not have been detectable at this low S/N. Drout et al. (2014) noted that a persistent continuum was unusual for rapidly declining SNe.

In conclusion, a picture is emerging in which the spectroscopic evolution of the transient depends on its luminosity, with interacting SNe dominating the most luminous ($M < -18$ mag) events, and Type IIb and Type Ib

dominating the subluminous ($M > -18$ mag) events. Some of the most luminous events have broad absorption features from high velocities, suggesting that the high velocities are related to the high luminosity. With these spectroscopic classes delineated, we now turn to the photometric evolution of the different groups of objects.

3.2. *Photometric Evolution*
3.2.1. *Light-Curve Properties*

In this section we compare the light-curve evolution of the different spectroscopic subtypes delineated in Section 3.1. We start by estimating rise times and fade times in a similar fashion to values reported in the literature. We linearly interpolated the g and r light curves
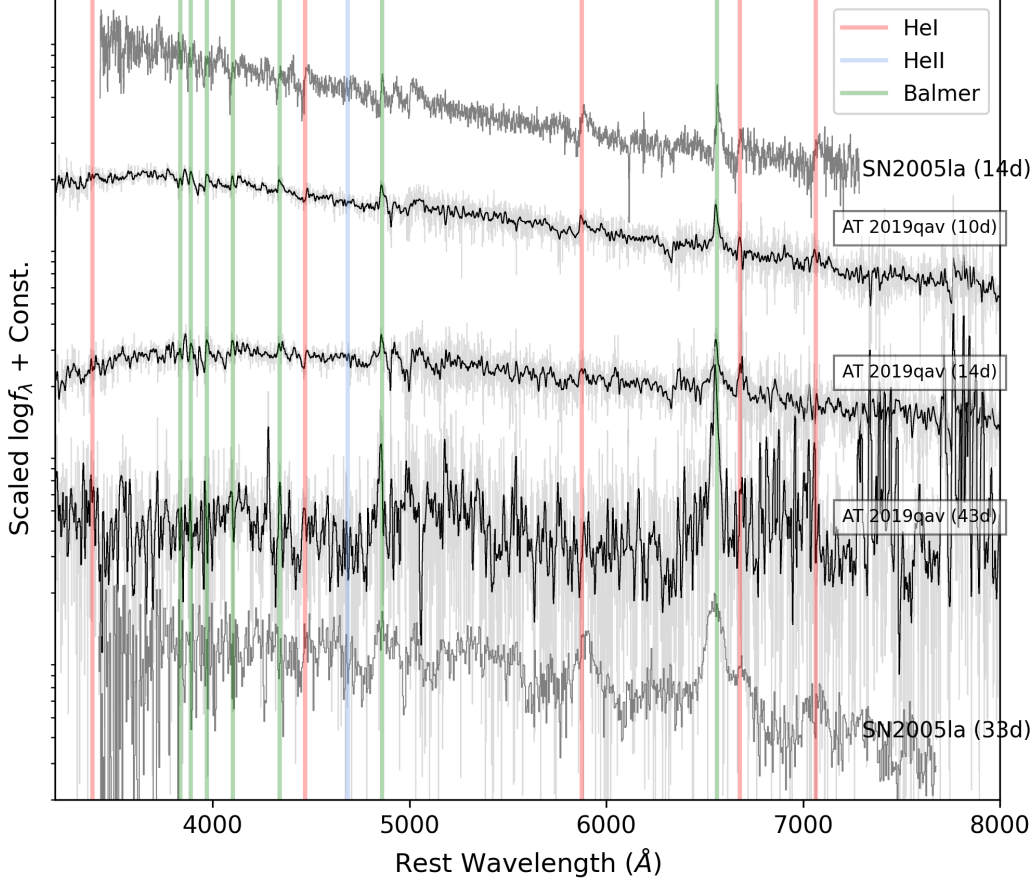
Figure 8. Post-peak evolution of SN 2019qav, which we classify as a Type IIn/Ibn transitional object due to its similarity with SN 2005la. Spectra of SN 2005la were obtained from WiseREP and are originally from Modjaz et al. (2014) and Pastorello et al. (2008).

in flux space to estimate a rise time $t_{1/2,\mathrm{rise}}$ and fade time $t_{1/2,\mathrm{fade}}$ from the half-maximum of the observed peak in each filter individually. For AT 2018cow we use an observation during the rise in the o band from the Asteroid Terrestrial-impact Last Alert System (ATLAS; Tonry et al. 2018b; Smith et al. 2020a). We estimated error bars by performing a Monte Carlo with 600 realizations of the light curve. The measured timescales are provided in Table 14.

As shown in Figures 1, most objects have an overall duration exceeding 5 d. There are two predominant classes of events at the shortest durations: Type IIb events at low luminosities, and events similar to AT 2018cow (in terms of their radio emission) at high luminosities. There is also one unusual, very luminous and fast-evolving unclassified event (AT 2020bot), although unlike AT 2018cow it rose to a plateau or second peak. In addition, SN 2018kzr (McBrien et al. 2019) had an overall very short duration and an intermediate luminosity. Only two objects in the comparison sample

have such short durations: both were from DES, and very luminous. So, it appears that the fast-subluminous Type IIb SNe are a previously unrecognized group of objects, and that—without knowing the redshift of the host galaxy a priori—they represent the primary extragalactic contaminant in the search for events similar to AT 2018cow.

Figure 9 compares the rise time to the fade time of each event. The vast majority of our objects have a slower fade time than rise time, as was found in previous samples (Drout et al. 2014). The exceptions appear to be the two Type Ic events, SN 2018kzr (McBrien et al. 2019) and SN 2019bkc (Chen et al. 2020; Prentice et al. 2020).

In Figure 10 we show the rise time and peak luminosity of each event in our gold and silver samples, as well as of the comparison literature events. We include several Type IIP SNe from the ZTF BTS (Fremling et al. 2020; Perley et al. 2020b) to show that they can also contam-
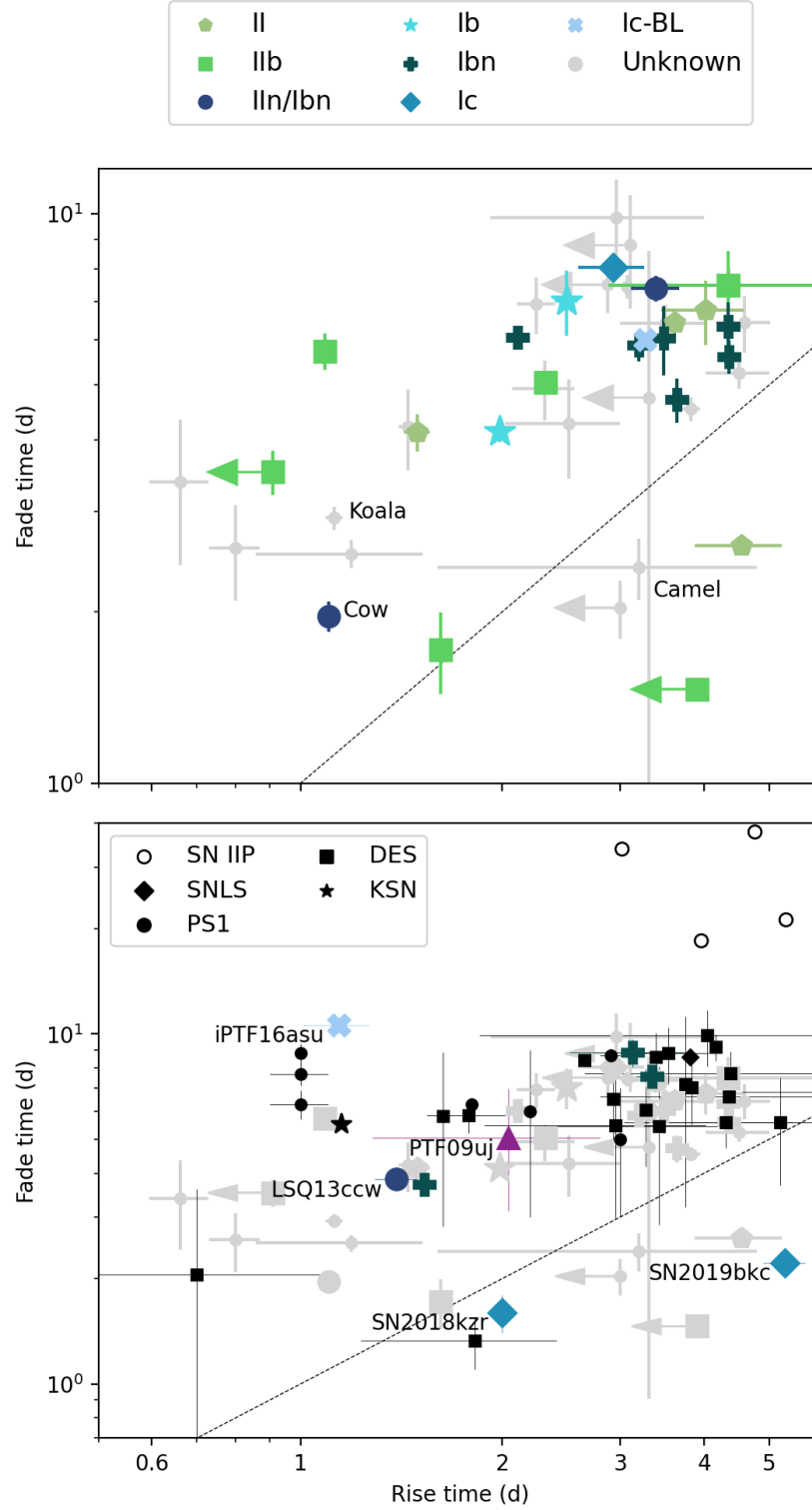
Figure 9. Rise time vs. fade time of short-duration transients in ZTF (top panel), compared to events in the literature (bottom panel). Timescales and luminosities are measured in g band, in the rest-frame, from half-peak to peak. The dashed line in the top panel indicates equal rise and fade times. Consistent with samples of unclassified events in the literature, we find that these events typically have longer fade times than rise times. In addition, Type IIb SNe, AT 2018cow, and the Koala are all distinct in having a rise time and fade time that are both shorter than a few days. We also plot Type IIP SNe with rise times measured from the ZTF BTS (Perley et al. 2020b) to show that they might contaminate the search for short-duration transients when trying to discover them during the rising phase.

Table 14. Light curve properties. A range indicates a rise or fade that was not resolved by detections.

ZTF Name	$m_{\rm g,max}$	$M_{\rm g,max}$	$t_{\rm g,rise}$	$t_{\rm g,fade}$	$m_{\rm r,max}$	$M_{\rm r,max}$	$t_{\rm r,rise}$	$t_{\rm r,fade}$
	(mag)	(mag)	(d)	(d)	(mag)	(mag)	(d)	(d)
ZTF18aakuewf	17.46 ± 0.04	-19.89 ± 0.04	3.20 ± 0.08^{a}	5.87 ± 0.37	17.74 ± 0.03	-19.61 ± 0.03	3.20 ± 0.09	7.84 ± 0.17
ZTF18aayrkfa	20.02 ± 0.06	$-$	$1.92\text{–}4.00$	9.83 ± 1.64	20.26 ± 0.09	$-$	3.47 ± 0.36	10.01 ± 2.76
ZTF18abcfcoo	13.11 ± 0.05	-20.87 ± 0.05	1.10 ± 0.04	1.96 ± 0.12	13.60 ± 0.10	-20.38 ± 0.10	< 5.75	2.56 ± 0.30
ZTF18abfcmjw	18.40 ± 0.02	-16.51 ± 0.02	1.98 ± 0.04	4.14 ± 0.17	18.57 ± 0.01	-16.33 ± 0.01	1.80 ± 0.07	7.68 ± 0.78
ZTF18abianhw	19.55 ± 0.05	$-$	$2.02\text{–}3.00$	4.27 ± 0.85	19.75 ± 0.07	$-$	$2.06\text{–}3.01$	6.29 ± 1.02
ZTF18abukavn	15.91 ± 0.01	-19.87 ± 0.01	3.27 ± 0.02	6.00 ± 0.17	16.23 ± 0.01	-19.55 ± 0.01	3.21 ± 0.05	10.90 ± 0.55
ZTF18abvkmgw	18.49 ± 0.03	-17.73 ± 0.03	2.49 ± 0.10	7.03 ± 0.92	18.58 ± 0.04	-17.64 ± 0.04	2.26 ± 0.16	10.68 ± 4.12
ZTF18abvkwla	19.34 ± 0.05	-21.43 ± 0.05	1.12 ± 0.03	2.92 ± 0.14	19.82 ± 0.06	-20.95 ± 0.06	$1.51\text{–}2.34$	2.75 ± 0.34
ZTF18abwkrbl	15.58 ± 0.01	-17.66 ± 0.01	2.32 ± 0.01	5.05 ± 0.08	15.78 ± 0.01	-17.46 ± 0.01	$1.97\text{–}4.00$	8.22 ± 0.19
ZTF19aakssbm	17.16 ± 0.03	-18.89 ± 0.03	2.11 ± 0.03	6.05 ± 0.24	17.43 ± 0.04	-18.63 ± 0.04	2.01 ± 0.06	5.88 ± 0.22
ZTF19aankdan	19.09 ± 0.04	$-$	$4.02\text{–}5.00$	5.24 ± 0.31	19.17 ± 0.04	$-$	$4.00\text{–}5.04$	7.30 ± 0.40
ZTF19aapfmki	17.22 ± 0.02	-19.79 ± 0.02	4.35 ± 0.07	6.33 ± 0.66	17.43 ± 0.05	-19.58 ± 0.05	5.00 ± 0.15	6.57 ± 0.42
ZTF19aapuudk	19.49 ± 0.05	$-$	1.45 ± 0.04	4.22 ± 0.68	19.75 ± 0.05	$-$	1.36 ± 0.06	5.40 ± 0.47
ZTF19aasexmy	19.41 ± 0.02	$-$	< 3.1	8.80 ± 1.98	19.69 ± 0.06	$-$	< 4.02	15.10 ± 5.15
ZTF19aatoboa	18.84 ± 0.03	-18.90 ± 0.03	2.31 ± 0.24	4.92 ± 0.59	19.20 ± 0.05	-18.54 ± 0.05	1.38 ± 0.09	21.97 ± 7.30
ZTF19abeyvoi	19.09 ± 0.04	$-$	2.25 ± 0.15	6.93 ± 0.78	19.35 ± 0.07	$-$	4.46 ± 0.20	6.52 ± 1.85
ZTF19abfarpa	18.28 ± 0.04	-19.41 ± 0.04	4.35 ± 0.09	7.54 ± 0.47	18.48 ± 0.05	-19.22 ± 0.05	4.26 ± 0.14	> 2.6
ZTF19abobxik	18.84 ± 0.02	-19.54 ± 0.02	3.48 ± 0.06	6.04 ± 0.84	18.91 ± 0.03	-19.47 ± 0.03	3.45 ± 0.15	5.45 ± 0.68
ZTF19abrpfps	19.48 ± 0.03	$-$	0.80 ± 0.07	2.58 ± 0.50	19.86 ± 0.08	$-$	0.78 ± 0.12	1.77 ± 0.62
ZTF19abuvqgw	18.68 ± 0.06	-19.38 ± 0.06	3.64 ± 0.11	4.72 ± 0.42	18.92 ± 0.04	-19.14 ± 0.04	3.21 ± 0.17	5.98 ± 0.28
ZTF19abyjzvd	18.99 ± 0.06	-20.13 ± 0.06	3.39 ± 0.28	7.38 ± 0.38	19.22 ± 0.10	-19.90 ± 0.10	4.51 ± 0.39	8.21 ± 0.42
ZTF19acaxbjt	19.03 ± 0.04	$-$	$3.00\text{–}4.00$	6.41 ± 0.51	19.29 ± 0.08	$-$	$2.91\text{–}4.00$	8.87 ± 2.83
ZTF19acayojs	18.75 ± 0.02	-20.13 ± 0.02	4.36 ± 0.16	5.61 ± 0.38	18.89 ± 0.03	-19.98 ± 0.03	3.96 ± 0.96	5.37 ± 1.61
ZTF19accjfgv	17.88 ± 0.02	-17.55 ± 0.02	1.09 ± 0.03	5.74 ± 0.43	17.98 ± 0.03	-17.45 ± 0.03	1.20 ± 0.04	8.99 ± 1.09
ZTF19accxzsc	18.91 ± 0.05	$-$	< 3.0	2.03 ± 0.24	19.48 ± 0.13	$-$	$13.94\text{–}5.92$	1.20 ± 1.51
ZTF19acsakuv	18.54 ± 0.11	$-$	< 3.31	4.75 ± 3.85	18.75 ± 0.18	$-$	1.36 ± 0.23	8.01 ± 1.93
ZTF20aaelulu	14.06 ± 0.12	-17.76 ± 0.12	2.92 ± 0.33	8.05 ± 0.46	13.74 ± 0.12	-18.07 ± 0.12	6.07 ± 0.39	7.41 ± 0.76
ZTF20aahfqpm	19.06 ± 0.03	-16.68 ± 0.03	< 3.9	1.46 ± 0.07	19.52 ± 0.06	-16.22 ± 0.06	< 3.91	2.02 ± 0.79
ZTF20aaivtof	18.60 ± 0.03	-17.76 ± 0.03	< 2.87	7.5 ± 0.81	18.74 ± 0.06	-17.62 ± 0.06	< 2.85	9.03 ± 2.21
ZTF20aakypiu	19.46 ± 0.04	-20.53 ± 0.04	1.19 ± 0.33	2.53 ± 0.14	19.54 ± 0.17	-20.45 ± 0.17	3.38 ± 0.30	0.55 ± 0.24
ZTF20aaxhzhc	18.27 ± 0.03	-18.15 ± 0.03	$2.88\text{–}5.80$	7.47 ± 1.11	18.51 ± 0.05	-17.90 ± 0.05	$2.73\text{–}5.67$	27.88 ± 2.11
ZTF20aayrobw	18.51 ± 0.03	-18.75 ± 0.03	3.61 ± 0.07	6.44 ± 0.37	18.78 ± 0.03	-18.47 ± 0.03	$1.92\text{–}3.78$	11.98 ± 1.87
ZTF20aazchcq	19.50 ± 0.09	-16.68 ± 0.09	4.02 ± 0.56	6.76 ± 0.88	18.89 ± 0.17	-17.29 ± 0.17	3.13 ± 0.53	10.55 ± 1.00
ZTF20aazrcbp	19.71 ± 0.06	$-$	4.59 ± 0.42	6.44 ± 0.74	19.75 ± 0.06	$-$	3.71 ± 0.28	14.61 ± 2.53
ZTF20ababxjv	19.05 ± 0.03	-18.13 ± 0.03	3.83 ± 0.12	4.54 ± 0.22	19.25 ± 0.04	-17.93 ± 0.04	3.67 ± 0.20	6.76 ± 0.33
ZTF20abjbgjj	18.61 ± 0.09	-19.08 ± 0.09	4.55 ± 0.67	> 2.61	18.29 ± 0.09	-19.40 ± 0.09	2.87 ± 0.57	6.93 ± 1.69
ZTF20abmocba	19.39 ± 0.03	-18.29 ± 0.03	3.07 ± 0.04	7.44 ± 0.35	19.59 ± 0.05	-18.08 ± 0.05	2.87 ± 0.10	9.30 ± 0.95
ZTF20abummyz	19.17 ± 0.11	-19.18 ± 0.11	0.66 ± 0.07	3.38 ± 0.96	19.44 ± 0.09	-18.91 ± 0.09	1.36 ± 0.12	5.58 ± 0.83
ZTF20aburywx	19.36 ± 0.07	-16.4 ± 0.07	1.62 ± 0.04	1.72 ± 0.28	19.36 ± 0.11	-16.4 ± 0.11	0.5 ± 0.26	2.75 ± 1.53
ZTF20acigmel	19.24 ± 0.04	-21.27 ± 0.04	$1.60\text{–}4.81$	2.39 ± 0.30	19.54 ± 0.06	-20.97 ± 0.06	$0.88\text{–}3.26$	3.60 ± 0.18
ZTF20acigusw	18.68 ± 0.03	-18.61 ± 0.03	1.49 ± 0.07	4.13 ± 0.31	18.98 ± 0.05	-18.31 ± 0.05	2.08 ± 0.13	8.21 ± 1.24
ZTF20aclfmwn	19.59 ± 0.04	-16.07 ± 0.04	< 0.91	3.52 ± 0.31	19.61 ± 0.07	-16.05 ± 0.07	$2.06\text{–}2.87$	4.58 ± 0.39

^{a} Based on r-band points

inate the search for fast-evolving transients during the rise phase.

3.2.2. *Light Curve Comparison*

The similarity in the distribution of luminosity and timescale between the ZTF events and objects in the literature raises the possibility that the low-redshift classified objects in our sample could be used to try and classify events at higher redshift. In Figure 11 we show an example of how this could be done, by selecting the most similar ZTF light curve for various events in the literature. The Type IIn PTF 09uj (Ofek et al. 2010), suggested to be shock breakout in CSM, has a similar light-curve morphology to a Type II in our sample, SN 2020ntt, while KSN2015K has a similar light-curve morphology to SN 2018gep—in particular, their very fast rises support their interpretation as due to shock breakout (Rest et al. 2018; Ho et al. 2019a).

In Figure 11 we also show each gold sample transient from Drout et al. (2014), all of which are unclassified, together with a similar light curve from our ZTF sample. Given the similarity of the light curves, and the predominance of certain spectral types in different luminosity regimes, it seems likely that the PS1 objects are dominated by Type IIb SNe at the faint end (e.g., PS1-10ah and PS1-12bb) and Type Ibn SNe at the bright end (e.g., PS1-11qr). We also show the light curve of a luminous rapidly evolving DES transient, which as discussed in Ho et al. (2020b) is one of the few transients in the literature that resembles AT 2018cow.

3.2.3. *Color and Blackbody Evolution*

We calculate the $g - r$ color on nights where observations were acquired in both filters (not correcting for host reddening) and show the evolution of this color as a function of time since g-band max in Figure 12, separating the objects into different spectroscopic subtypes. As in previous samples (Drout et al. 2014), most transients are blue ($-0.2\,\mathrm{mag} > g - r > -0.4\,\mathrm{mag}$ in the rest-frame) at maximum light and redden with time. There are exceptions, however, most notably the Type Ibn SNe and events with persistent interaction-dominated spectra (AT 2018cow and SN 2019qav).

A steady $g - r$ color was one of the distinguishing features of AT 2018cow, and reflected a constant effective temperature T_{eff}, unlike most SNe that cool with time and have expanding photospheric radii R_{ph}. Similar behavior was seen in the Type Ibn SN 2018bcc

(Karamehmetoglu et al. 2019).[17] In Figure 13 we show the estimated T_{eff} and R_{ph} for objects in our sample with multi-band photometry (three or more filters), at two epochs: the first close to peak g-band light, and the second 10–20 d later. For each epoch, we fit a blackbody to photometry obtained during the same night.

As shown in Figure 13, the typical behavior is to have T_{eff} of a few $\times 10^4$ K at peak light, and to cool over time, with an R_{ph} that starts between 10^{14} cm and 10^{15} cm and expands with time. The exceptions are the events with a near-constant $g - r$ color, AT 2018cow and the Type Ibn SNe. DES16X1eho also exhibits this behavior, and is also one of the few events in the fast-luminous part of parameter space occupied by AT 2018cow. Shrinking blackbody radii and near-constant temperature have been observed in interacting SNe like Type IIn (Taddia et al. 2013); in that context, it has been argued to arise by clumps, exposing more material as the optical depth drops (Smith et al. 2008). There are Type IIn SNe that show expanding radii, attributed to asymmetric CSM (Soumagnac et al. 2019).

3.3. *Limits on X-ray and Radio Emission*

There is considerable interest in understanding to what extent AT 2018cow is part of a continuum that extends into other parts of the fast-transient parameter space, and to what extent it is a distinct class. In the literature AT 2018cow is often generically described as a rapidly evolving transient or fast blue optical transient ("FBOT") and grouped together with the other objects. Its photometric evolution (fast rise, high peak luminosity) and spectroscopic behavior (persistent narrow lines; Perley et al. 2019; Margutti et al. 2019) most closely resembles interacting SNe (Fox & Smith 2019). In this section we discuss another distinguishing characteristic of AT 2018cow—luminous X-ray, millimeter, and radio emission—and to what extent similar behavior can be ruled out in other parts of the parameter space of Figure 1.

In Figure 14 we show the millimeter and radio upper limits presented in Section 2.6 compared to the light curve of AT 2018cow. The only events with similar millimeter and radio behavior—AT 2020xnd and AT 2018lug—also have very similar optical light curves to AT 2018cow. SN 2019qav (Type IIn/Ibn) also had a high luminosity and spectra persistently dominated by interaction; yet X-ray, millimeter, and radio observa-

---

[17] Type Ibn SNe can also become dominated by an iron pseudo-continuum in the blue at late times, which shows up as a very blue $g - r$ color even though presumably they have very little flux in the UV.
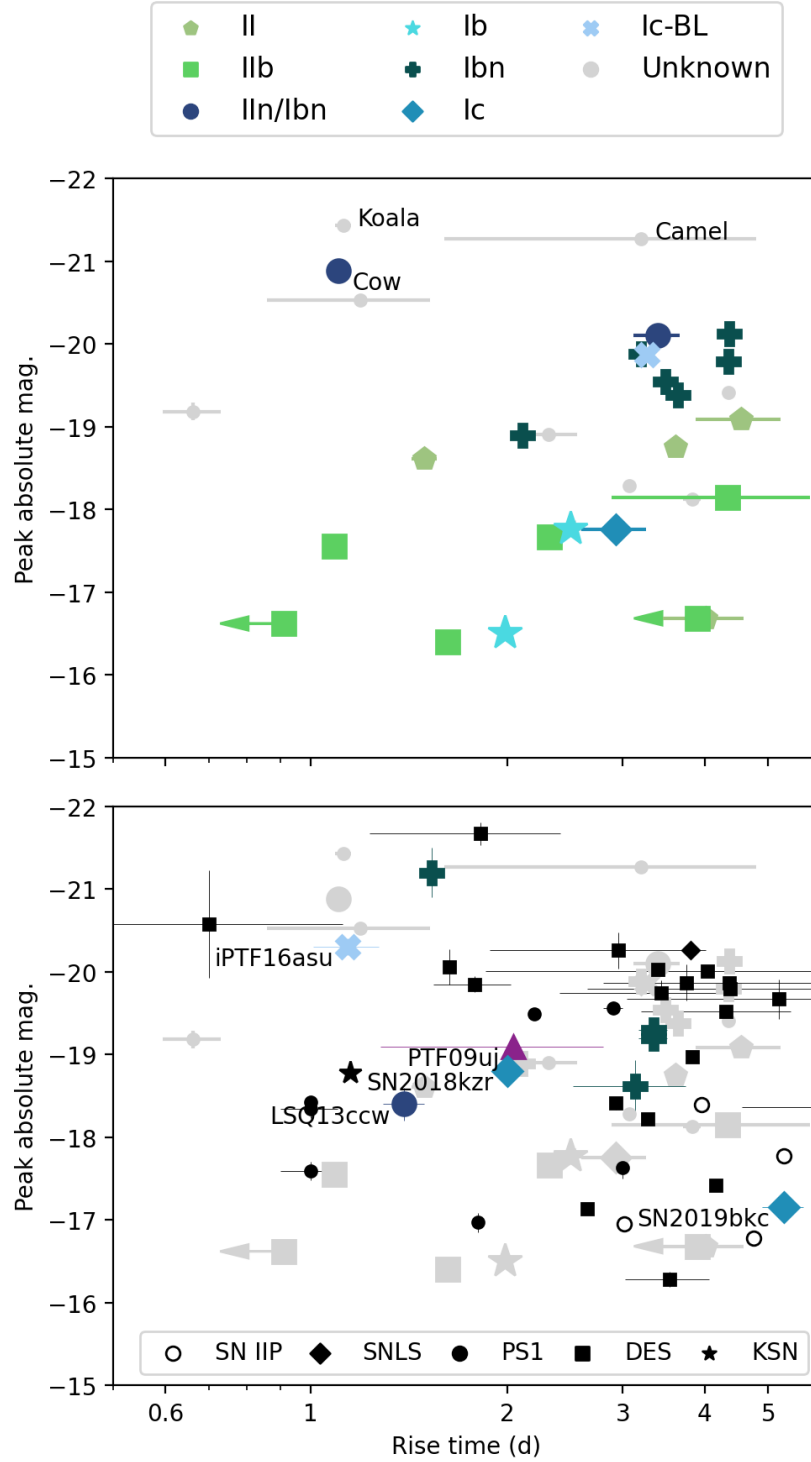
Figure 10. Rise time vs. peak luminosity of the events in our ZTF sample (top panel) and our comparison sample from the literature (bottom panel). Timescales and luminosities are measured in g band, in the rest-frame, from half-peak to peak. In the bottom panel, we include a few Type IIP SNe with timescales measured from the ZTF BTS (Perley et al. 2020b) to show that they lie in an overlapping region of rise time-luminosity parameter space.
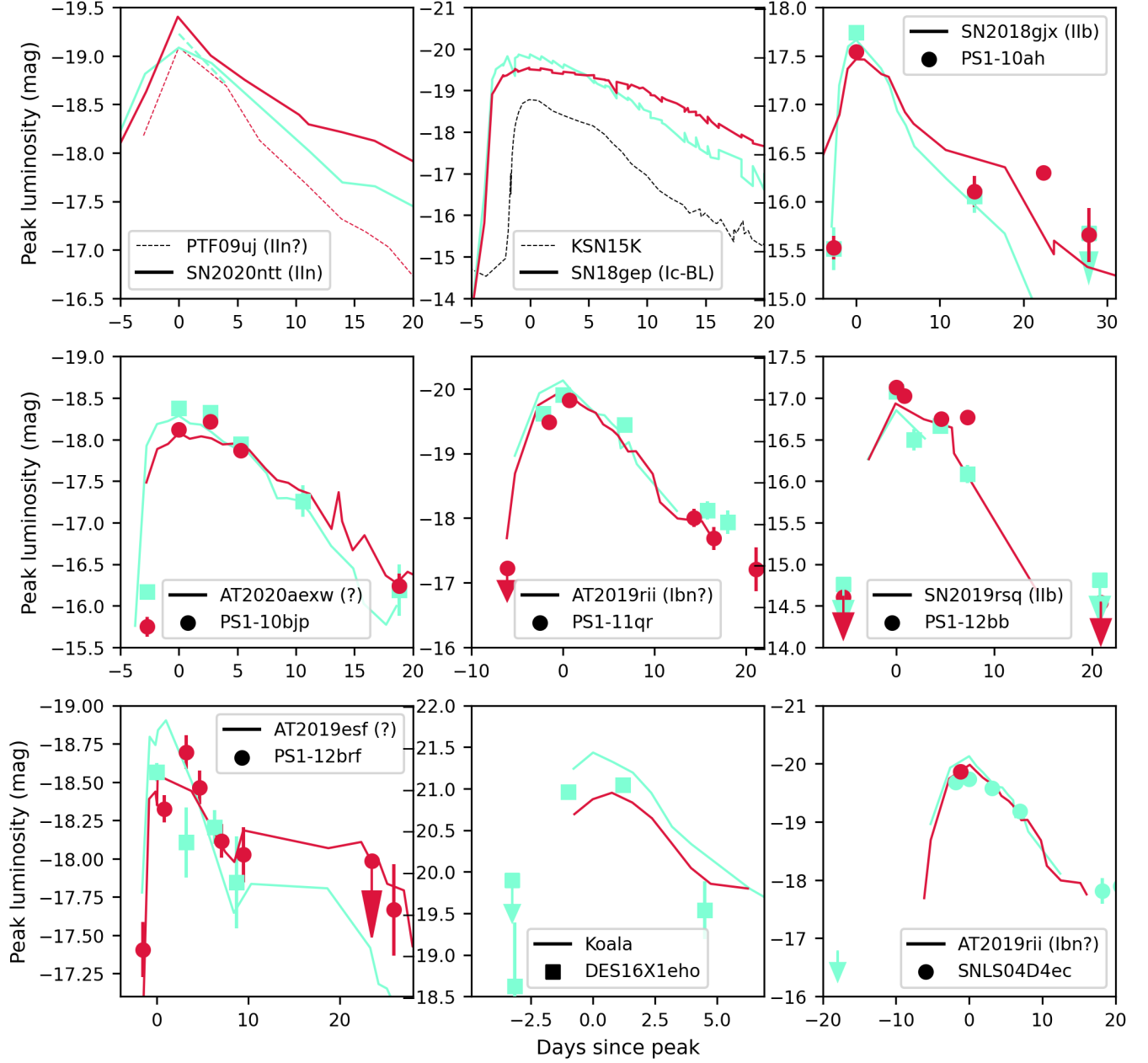
Figure 11. Unclassified short-duration transients from the literature, together with events from ZTF that have similar light curves. The light curves of PS1 events are from Drout et al. (2014). The light curve of DES16X1eho is from M. Pursiainen, private communication. The light curve of KSN2015K is from Rest et al. (2018). Literature light curves were taken to be as close to g (shown in cyan) and r (shown in red) band in the rest-frame as possible.
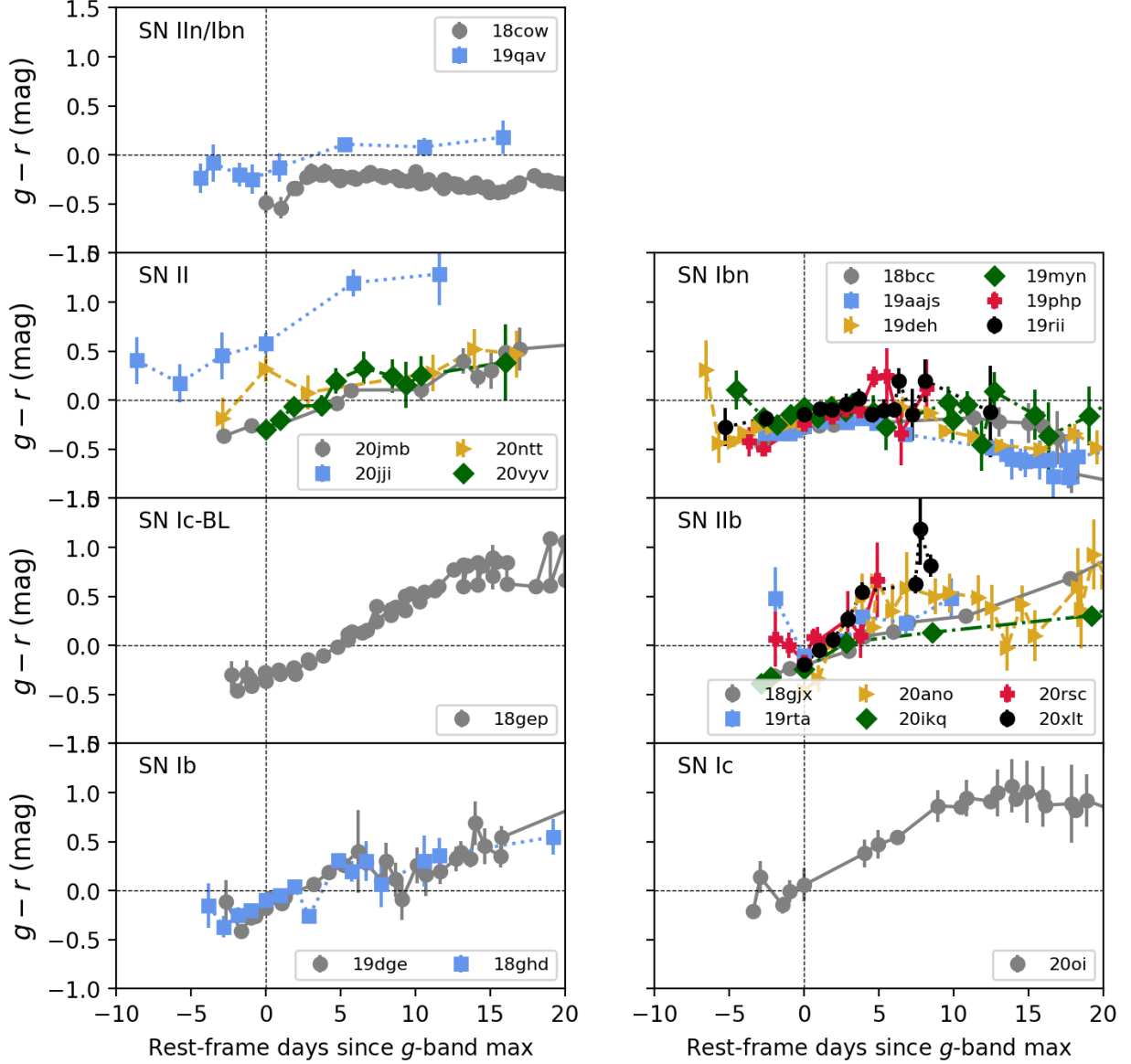
Figure 12. Color evolution for the 22 gold-sample events. Most have blue colors ($g - r < 0$ mag) near the peak of the g-band light curve, then redden after peak. There are exceptions, however, most notably AT 2018cow and Type Ibn SNe.

tions rule out emission similar to that of AT 2018cow. SN 2020rsc (Type IIb) had a light curve similar to AT 2018cow in its duration (albeit significantly less luminous), yet we can also rule out emission similar to AT 2018cow by orders of magnitude. Finally, SN 2019deh was a rapidly evolving and luminous Type Ibn SN that remained persistently blue, with a relatively constant effective temperature—millimeter and radio observations also resulted in non-detections, ruling out emission similar to AT 2018cow by orders of magnitude.

To our knowledge, only two Type Ibn SNe have X-ray detections, and both were nearby: SN 2006jc (Immler

et al. 2008) and SN 2010al (Ofek et al. 2013). Although these two events had a similar late-time luminosity to that of AT 2018cow ($\sim 10^{40}$ erg s^{-1}), the early-time luminosity was orders of magnitude smaller. SN 2006jc took 100 d to rise to peak luminosity in X-rays, whereas AT 2018cow rose to peak light in X-rays within three days.

So, although we cannot rule out AT2018cow-like X-ray, millimeter, and radio emission for all of the events in our sample, it appears that neither a high luminosity, nor persistent interaction, nor a constant blue color, is predictive of this behavior. Such emission is only seen in events that also have a rapidly fading light curve. This
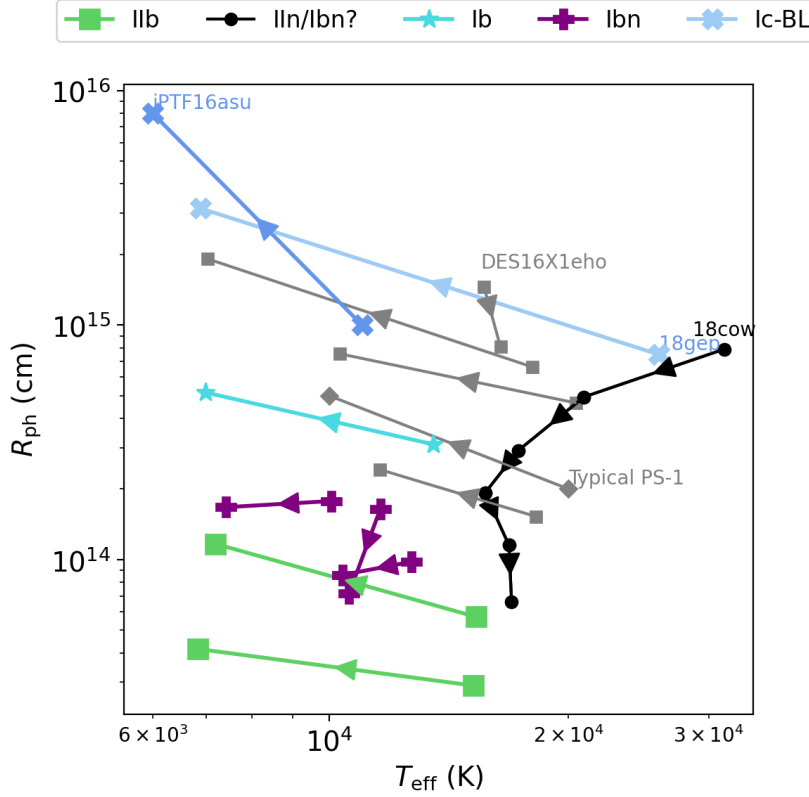
Figure 13. Photospheric evolution of events in our sample with multi-band photometry, together with comparison objects. We show best-fit parameters at two epochs: the first at the peak of the g-band light curve, the second 10–20 d later. Most objects expand and cool with time, and the exceptions include AT 2018cow, the Type Ibn SNe, and DES16X1eho. For some events we take values directly from the literature: AT 2018cow (Perley et al. 2019), SN 2018gep (Ho et al. 2019a), SN 2019dge (Yao et al. 2020), the DES objects (Pursiainen et al. 2018), the PS-1 typical behavior (Drout et al. 2014), and iPTF16asu (Whitesides et al. 2017).

supports the idea that these objects are a distinct class, and that a single term is too vague for a part of parameter space that includes events as diverse as AT 2018cow, subluminous Type IIb SNe with shock-cooling peaks, and the well-established class of Type Ibn SNe. We suggest that the Type IIb SNe and Type Ibn SNe be referred to by their spectroscopic type, as they are likely part of a continuum of properties rather than a distinct class (as we discuss in Section 6).

4. HOST GALAXIES

In this section we present the host-galaxy properties of the objects in our sample. In the Appendix we describe the modeling procedure, and provide a table of the fit parameters (Table 16) as well as the host properties (Table 17).

Figure 15 shows the B-band luminosities of the hosts of the gold and silver objects, which span $M_B \approx -12.7$ mag to $M_B \approx -21.8$ mag. The distribution is similar to that of regular CC SNe, which we illustrate with contours encircling 68, 90 and 95% of the

PTF+iPTF CC SN sample (Schulze et al. 2020), which includes 888 objects spanning all major CC SN classes.

One noteworthy object is the Type Ibn SN 2019php. We detect a $g \sim 25.5 \pm 0.3$ mag object approximately $1''$ South-East of the transient position in Legacy Survey images. If this is indeed the host, its luminosity is $M_B \sim -12.7$ mag. Such faint galaxies are very rare but not unheard of for CC SN host galaxies (e.g., Gutiérrez et al. 2018; Schulze et al. 2020). If the marginally detected object is an image artefact, the SN 2019php host galaxy would be even fainter and pushing into the regime of the faintest and least-massive star-forming galaxies (McConnachie 2012). It could also point to an extremely low-surface brightness galaxy (e.g., van Dokkum et al. 2015).

Figure 16 shows the host properties in the mass-SFR plane. The hosts are located along the so-called main sequence of star-forming galaxies (indicated by the grey shaded region; based on Eq. 5 in Elbaz et al. 2007). A small minority of objects occurred in galaxies that lie above the galaxy main sequence and are experiencing a
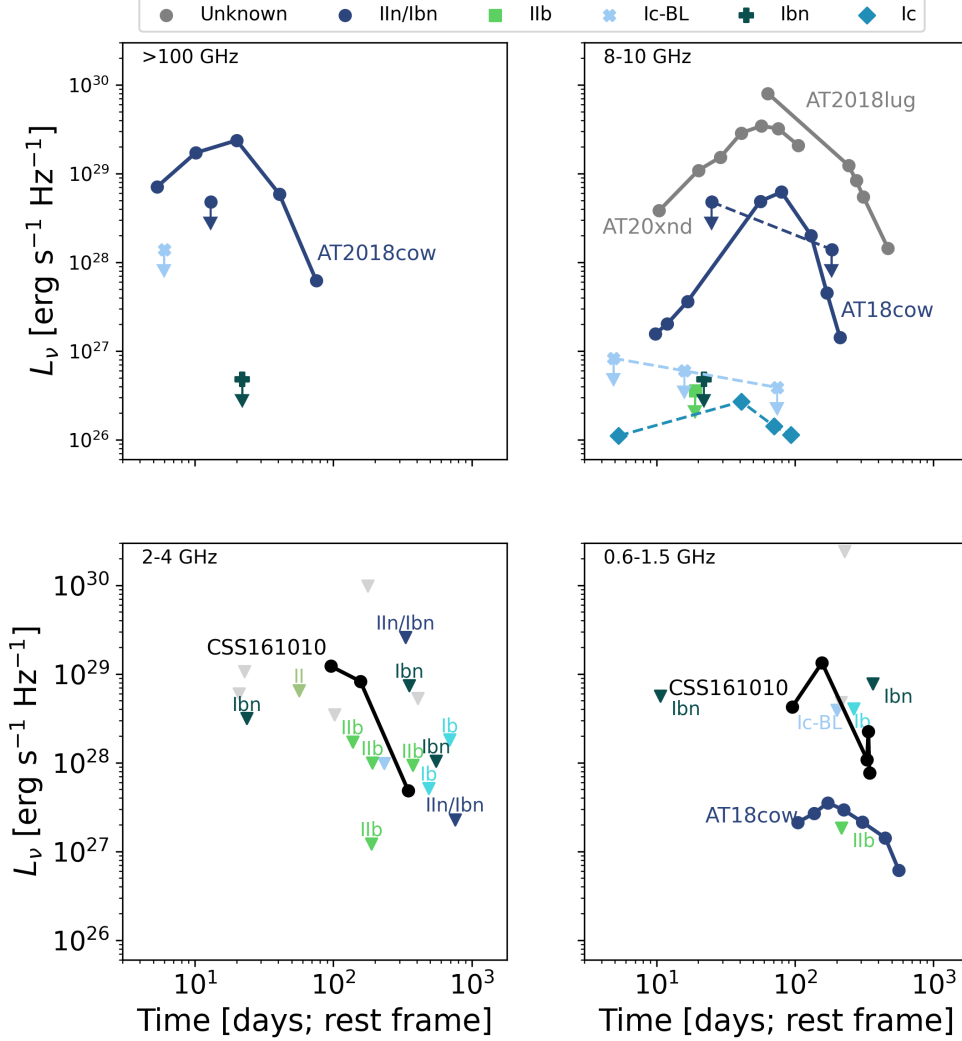
Figure 14. Millimeter and radio observations of short-duration extragalactic transients. The CSS161010 light curves are from Coppejans et al. (2020). The light curves of AT 2018cow, AT 2018lug, SN 2018gep (Ic-BL) at 10 GHz were taken from the literature (Ho et al. 2019a; Margutti et al. 2019; Bietenholz et al. 2020; Ho et al. 2020b; Coppejans et al. 2020). The 10 GHz light curve of AT 2020xnd is Ho et al. in prep. The 0.75 GHz light curve of AT 2018cow is from Nayana & Chandra (2021). Additional observations at > 100 GHz and 8–10 GHz are from this work. Limits at 2–4 GHz are from VLASS. Limits at 888 MHz are from the RACS and VAST (see text). In the bottom-right panel, the positions of the Ic-BL and Ib markers have been shifted slightly for clarity. The only objects with robust detections of luminous ($> 10^{28}\,\mathrm{erg\,s^{-1}\,Hz^{-1}}$) millimeter and radio emission appear to be the shortest-duration, highest-luminosity, fastest fading optical transients: AT 2018cow, AT 2018lug, and AT 2020xnd.

starburst. This phenomenon is not exclusive to a particular spectroscopic subtype. Our results are similar to Wiseman et al. (2020) who studied the hosts of rapidly evolving transients between $z = 0.2$ and $z = 0.85$. As in Figure 15, we overlay the 68, 90 and 95% contours of the PTF CC SN host sample. The hosts of regular CC SNe occupy the same parameter space, including the starburst regime (e.g, Taggart & Perley 2021).

An outstanding object is AT 2020bot. It exploded ≈ 10 kpc from the center of an early-type galaxy. The GalaxyZoo Project classified the host morphology as el-

liptical (Lintott et al. 2008, 2011). The SDSS spectrum shows no emission lines. Such an environment is extreme for any type of transient originating from the explosion of a massive star, but it is not unheard of for CC SNe (Sanders et al. 2013; Irani et al. 2019; Hosseinzadeh et al. 2019, Irani in prep.; Schulze in prep.). We discuss the implications in Section 6.

5. RATE ESTIMATE

There have been a variety of efforts to estimate the rates of rapidly evolving transients, which have typically
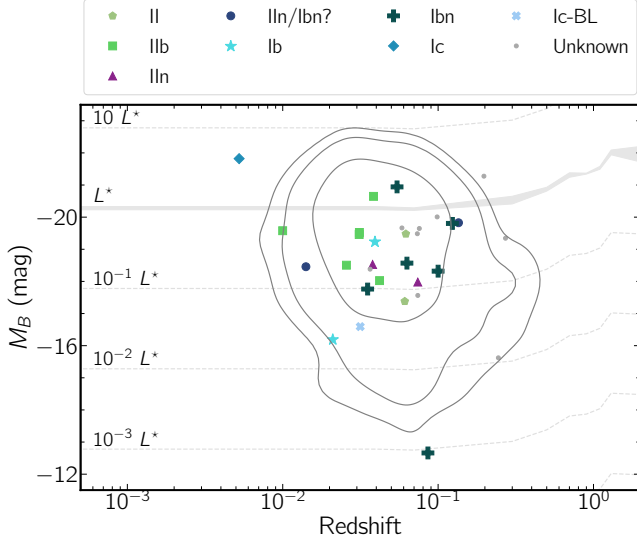
Figure 15. The absolute B magnitude of the host galaxies for our gold and silver-sample objects as a function of redshift. Our events are found in the least-luminous ($10^{-3}\ L^\star$) to the most luminous star-forming galaxies ($\lesssim 10^{-3}\ L^\star$) ($L^\star$ is the characteristic luminosity of the B-band luminosity function of star-forming). Most hosts have luminosities of 10^{-2} to a few $L^\star$, similar to regular CC SNe (indicated by the contours encircling 68, 90 and 95% of the PTF+iPTF CC SN sample). We indicate the $L^\star$ presented in Faber et al. (2007) and multiples of it in gray.

Figure 16. Host galaxies for our events in the mass-SFR plane. Almost all exploded in star-forming galaxies. This is illustrated by their location with respect to the main sequence of star-forming galaxies (grey shaded region). The only exception is AT 2020bot, which exploded ~ 10 kpc from the center of an elliptical galaxy. Moreover, the overwhelming majority of hosts have also properties consistent with those of CC SNe from the PTF+iPTF surveys (grey contours indicate the region encircling 68, 90 and 95% of the sample).

had one of two goals: measure the overall rate as a clue to the underlying physical mechanism (Drout et al. 2014; Pursiainen et al. 2018), or measure the rate of events similar to AT 2018cow (Ho et al. 2020b; Coppejans et al. 2020). Drout et al. (2014) estimated a remarkably high rate of 4–7% of the CC SN rate for events spanning the full range of $-16 > M > -20$ mag, implying that the mechanism producing fast-luminous light curves, perhaps CSM interaction (and therefore end-of-life mass-loss in massive stars) was very common. Motivated by the high luminosity of AT 2018cow-like objects, Coppejans et al. (2020) estimated a rate for only the brightest ($M < -19$ mag) events and found 1–2%. For events with light curves identical to AT 2018cow, they found a rate of $< 0.4\%$ of the (local) CC SN rate.

Because we have spectroscopic classifications across the full range of duration-luminosity parameter space, we are well positioned to address both of these questions. To answer the first question, we construct a luminosity function for our events. Figure 17 shows the distribution of peak g-band absolute magnitudes of our ZTF objects. To apply a volume correction, we divide the number of counts in each bin by the volume out to which the events in that bin would be detectable. Our luminosity function is similar to that constructed using the DES

sample (Pursiainen et al. 2018), and we conclude that the subluminous events dominate the total rate. From our classifications, we can go a step further and suggest that the rate is dominated by short-duration Type II and Type IIb SNe.

Next, we address the rate of events similar to AT 2018cow. Our classifications and additional data at radio, X-ray, and mm bands (§3.3) provide physical motivation for only considering the shortest-duration (3 d) and most luminous ($M = -21$ mag) events. We estimate the rate using two systematic ZTF classification efforts: the volume-limited survey and the magnitude-limited survey.

The Census of the Local Universe (CLU; De et al. 2020) aims to classify all transients down to $r = 20.0$ mag within 200 Mpc, using data from all survey streams. Over the timescale of our search, CLU classified 429 CC SNe brighter than $M = -16$ mag within 150 Mpc. At this distance AT 2018cow would peak at 16 mag and remain over the $r = 20$ mag threshold for over two weeks, so CLU can be expected to be reasonably complete. The primary limitation is the use of a galaxy redshift catalog (Cook et al. 2019), so we caution that our rate is only valid for the types of galaxies well represented in this catalog. Given the detection of a
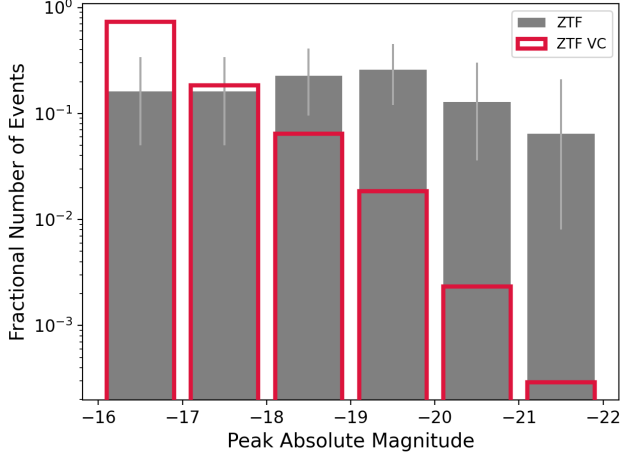
Figure 17. Luminosity function for the rapidly evolving transients in our gold and silver samples. We find that the volumetric rate is dominated by the subluminous events, albeit with large uncertainties on the absolute rate. Error bars are from counting statistics only and represent the 95% confidence interval.

single AT 2018cow-like object (AT 2018cow itself), and accounting for the fact that half of CC SNe are fainter than $M = -16$ mag (Li et al. 2011; Perley et al. 2020b), we find a rate of 0.1% the CC SN rate, with a 95% confidence interval from binomial counting statistics of [0.003%, 0.6%]. In absolute terms, this corresponds to a volumetric rate of $70\,\mathrm{yr}^{-1}\,\mathrm{Gpc}^{-3}$.

We can also estimate the rate using the Bright Transient Survey (BTS; Fremling et al. 2020; Perley et al. 2020b), which aims to classify all transients down to $r = 18.5$ mag in the public survey $(15{,}000\,\mathrm{deg}^2)$. We consider a volume of 250 Mpc, out to which BTS should be quite complete for events like AT 2018cow. Using the BTS Survey Explorer[18], and applying a quality cut, we find that there were 68 CC SNe classified in this volume brighter than $M = -18.5$ mag , and AT 2018cow itself. Correcting for the SN luminosity function (1–3% are fainter than this; Perley et al. 2020b) we find a rate of 0.01% with a 95% confidence interval of [0.0004%, 0.08%].

To be conservative, we take the lower limit from the BTS and the upper limit from CLU, and estimate that the rate is 10^{-5} to 10^{-3} of the CC SN rate, or 0.7–$70\,\mathrm{yr}^{-1}\,\mathrm{Gpc}^{-3}$.

6. DISCUSSION

We have delineated several spectroscopic subtypes of rapidly evolving transients, summarized in a cartoon in

[18] https://sites.astro.caltech.edu/ztf/bts/explorer.php
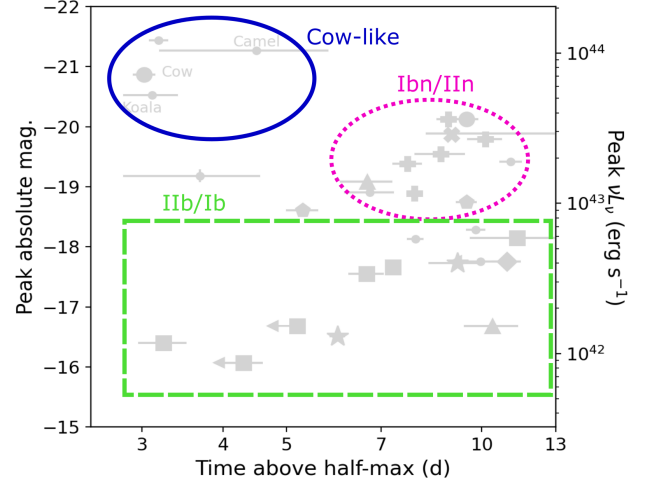
Figure 18. Cartoon illustrating the three predominant subgroups of transients we delineate with our sample.

Figure 18. In this section we discuss the implications of our findings for the progenitors and the powering mechanism for the optical light curves, referring to our summary figure (Figure 19) as a guide.

First, the progenitors are predominantly massive-star explosions, and most events fall into established SN spectroscopic classes. At the subluminous ($M > -18.5$ mag) end, the most common subtype is Type IIb SNe. The light curve durations, luminosities, and colors are all reminiscent of the shock-cooling peaks seen in double-peaked Type IIb SNe such as SN 1993J (Schmidt et al. 1993), SN 2016gkg (Bersten et al. 2018), and ZTF18aalrxas (Fremling et al. 2019), all included in Figure 19. In fact, we see a distinct second peak in SN 2020ano, which is significantly less luminous than the first peak. By analogy, it seems reasonable to conclude that shock-cooling emission plays a key role in powering our events. We suggest that Type IIb SNe simply have a range of relative brightness of the shock-cooling peak and nickel-powered peak, and these so-called "rapid transients" simply reflect cases where the former is significantly brighter than the latter. This could arise from material at particularly large radii (CSM), events with very low nickel masses, or both; we defer modeling our objects to a forthcoming paper by Fremling et al.

Early shock-cooling peaks have also been seen in Type Ic-BL SNe, with (Campana et al. 2006) and without (Ho et al. 2020c) gamma-ray bursts; in Type Ic SNe, argued to be an ultra-stripped SN (De et al. 2018) or simply arising from enhanced pre-SN mass-loss (Taddia et al. 2016); in a Type Ib SNe with an X-ray flash (Modjaz et al. 2006); and in several Type IIb SNe, the subtype in which this phenomenon is most well-established
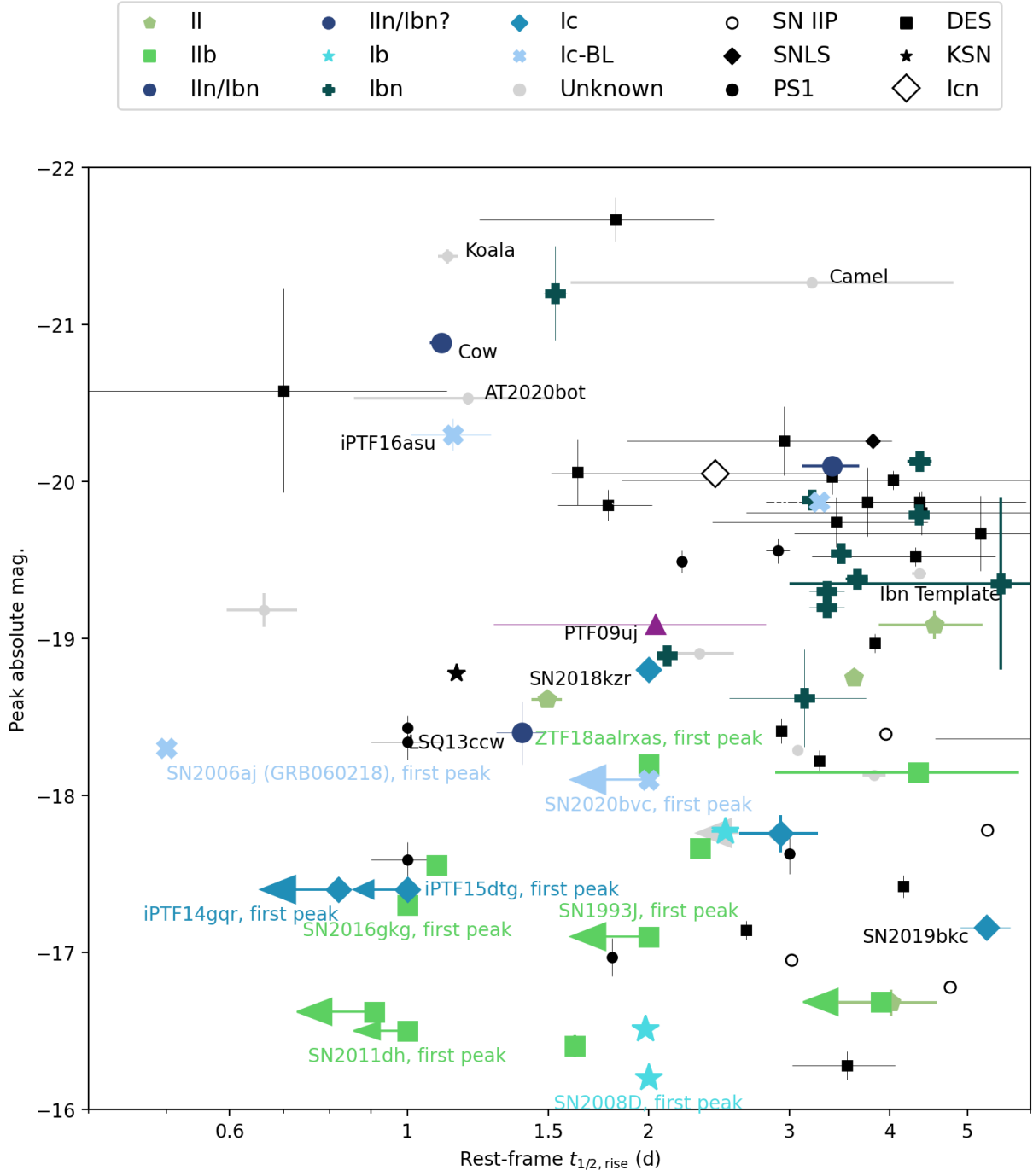
Figure 19. The rise time vs. peak luminosity of the ZTF objects in our sample, the literature comparison events that meet our criteria, and several additional events from the literature that do not strictly meet our search criteria due to a second peak of comparable luminosity but which are clearly related phenomena. We include two Type Ic-BL SNe with shock-cooling peaks, SN 2006aj (Campana et al. 2006) and SN 2020bvc (Ho et al. 2020c). We include three Type IIb SNe with shock-cooling peaks: SN 2016gkg (Bersten et al. 2018), ZTF18aalrxas (Fremling et al. 2019), and SN 1993J (Schmidt et al. 1993). We include the double-peaked Type Ic SN iPTF14gqr, argued to be an ultra-stripped SN (De et al. 2018). Finally, we include the Type Icn SN 2021csp (Perley et al. 2021a). Measurements are in the rest-frame and as close to g-band as possible.

(Schmidt et al. 1993; Arcavi et al. 2011; Bersten et al. 2018; Fremling et al. 2019). We show the first peak of several classes of stripped-envelope SNe in Figure 19.

Fast-rising events with luminosities $-20 < M_g < -18.5$ mag events are dominated by interacting SNe, particularly those of Type Ibn. In Figure 19 we include the rise time and peak luminosity of the Ibn light curve template from Hosseinzadeh et al. (2017). We have no reason to believe that our events are significantly different from the general Type Ibn population: the connection of Type Ibn SNe to fast-evolving transients has already been pointed out (Karamehmetoglu et al. 2019; Fox & Smith 2019), and as discussed in Karamehmetoglu et al. (2019) the rise time of most Type Ibn SNe has not been well sampled, so their true duration is relatively uncertain. Type Ibn light curves are generally thought to be powered by CSM interaction, with material much more extended than that involved in the shock-cooling peaks we have discussed previously.

At the highest luminosities ($M < -20$ mag) lie the radio-loud events AT 2018cow (the Cow), AT 2020xnd (the Camel), and AT 2018lug (the Koala). In the shock-interaction picture, a fast rise time and high peak luminosity arise from a fast shock speed—i.e., a significant amount of energy is coupled to ejecta traveling at high velocities. This is likely a distinguishing characteristic of the AT 2018cow-like events, as well as some of the other most luminous events, like the Type Ic-BL SNe 2018gep and iPTF16asu. Indeed, these events are the only objects that show very broad absorption features in their optical spectra.

However, despite sharing several characteristics with other events—a high luminosity, a fast rise, persistent interaction and blue colors—it appears that only the Cow-like events, the fastest-fading most luminous transients, are accompanied by luminous millimeter, X-ray, and radio emission. One possible explanation is that these events are engine-powered, as has been suggested (Perley et al. 2019; Ho et al. 2019b; Margutti et al. 2019). We conclude that a distinct physical mechanism is at work in the Cow-like events, setting them apart from the other events in Figure 19.

One event in our sample is particularly puzzling. As discussed in Section 4, AT 2020bot is luminous and rapidly evolving but located near an early-type galaxy. The host-galaxy spectrum shows no sign of star formation, and there is no visible dwarf galaxy in deep imaging. It is possible that some of the white-dwarf progenitor models invoked for AT 2018cow (e.g., accretion-induced collapse; Metzger et al. 2009; Lyutikov & Toonen 2019) may be applicable here.

In conclusion, it is clear that the use of a catch-all term for this diverse part of parameter space is not physically meaningful. A cut on a transient's overall duration can be a useful way to identify unusual events, but most of the time it simply selects the extreme of a continuum of properties in established SN subtypes, particularly shock-cooling peaks in Type IIb SNe and fast rise times in Type Ibn SNe. Based on Figure 19, we suggest that cuts based on fast rise times and the presence of early shock-cooling peaks, agnostic to the later evolution of the SN, is the way forward.

The general physical phenomenon probed here is SNe interacting with extended material. In some cases this could be part of the star, as in regular Type IIb events, resulting in brief subluminous shock-cooling peaks. In other cases this could be extended CSM, resulting in longer-lived and more luminous shock-cooling peaks. For even more extended CSM, the interaction can be longer-lived, giving rise to traditional interacting classes. Depending on the nickel mass and ejecta mass, there may or may not be a prominent second peak; depending on the CSM properties, the second peak may or may not be blended in with the first.

7. SUMMARY

We present the first systematically selected sample of day-timescale, short-duration ($t_{1/2} < 12$ d) extragalactic optical transients with spectroscopic classifications. The objects in our sample are very similar to unclassified events in the literature in terms of their photometric evolution (Section 3.2), host-galaxy properties (Section 4), and continuum-dominated spectra at peak light (Section 3.1). By several weeks after peak light, the objects typically redden in color, with declining blackbody temperatures and expanding radii, and develop spectra classifiable as traditional classes of CC SNe.

Our work shows that the dominant physical mechanism among short-duration luminous transients (Figure 18) is shock-interaction with extended material. Subluminous ($M > -18.5$ mag) transients dominate the high rates previously quoted in the literature, likely powered by shock-cooling emission, and the most common type is Type IIb SNe. Events similar to AT 2018cow—with fast rise times, fast fade times, and luminous X-ray and radio emission—are very rare, under 0.1% of the CC SN rate.

Our Figure 19 suggests how to move forward. A major limitation of our work is the arbitrary selection criterion of $t_{1/2} < 12$ d. Future work should focus on the first few days of SN light curves: whether there is shock-cooling emission or a fast rise due to radiative CSM breakout, agnostic to the strength of a second light-

curve peak. Our searches routinely discover SNe via the shock-cooling emission that occurs within the first few days across a wide range of SN progenitors. Ultimately, this early emission is hot and blue and best-observed in the UV. These kinds of objects will therefore be prime targets for wide-field UV time-domain surveys.

Facilities: Hale, Swift, EVLA, VLA, Liverpool:2m, PO:1.2m, PO:1.5m, NOT, GTC, Sloan, AAVSO, ASKAP, Keck:1, IRAM:NOEMA, SMA, MMT, TNG, ASKAP, GALEX, PS1, CTIO:2MASS, FLWO:2MASS, WISE, NEOWISE, Blanco

Software: CASA (McMullin et al. 2007), astropy (Astropy Collaboration et al. 2013, 2018), matplotlib (Hunter 2007), scipy (Virtanen et al. 2020), ztfquery (Rigault 2018), extinction, penquins

APPENDIX

A. DETAILS OF INDIVIDUAL EVENTS

Here we provide details on the discovery and follow-up of the 22 gold and 9 silver events in our sample that have not yet been published elsewhere (Karamehmetoglu et al. 2019; Prentice et al. 2018; Perley et al. 2019; Ho et al. 2019a; Yao et al. 2020; Ho et al. 2020b; Perley et al. 2021b; Horesh et al. 2020).

A.1. *SN 2018ghd / ZTF18abvkmgw / ATLAS18vew*

SN 2018ghd was detected by ATLAS (Tonry et al. 2018b; Smith et al. 2020a) on 2018 September 14 and reported to TNS the same day (Tonry et al. 2018a). It was first detected in ZTF data as ZTF18abvkmgw on 2018 September 12 as part of the Caltech 1DC survey at $g = 20.48 \pm 0.22$ mag, and saved by an alert-stream scanner on September 13 as part of a filter for rapidly evolving transients. It was in a galaxy with an SDSS spectrum and known redshift of $z = 0.0385$. On September 15 it was saved by the CLU filter, and by the public BTS survey on September 16. As part of CLU and BTS, it received a series of SEDM spectra, with the first obtained on September 14. These spectra were not definitive for classification. It was classified as a Type II SN based on an SEDM spectrum on September 21 (Fremling et al. 2018), then reclassified as a Type Ib SN with an LRIS spectrum on November 10.

A.2. *SN 2018gjx / ZTF18abwkrbl / ATLAS18vis / Gaia18csc / kait-18ao / PS19do / PSP18C*

SN 2018gjx was discovered by the Xingming Observatory Sky Survey (XOSS) as PSP18C on 2018 September 15, and reported to TNS on September 16 (Zhang et al. 2018). The source was coincident with NGC 865 ($z = 0.00999$). The first ZTF detection was also on 2018 September 15, at $g = 17.91 \pm 0.06$ mag as part of the Caltech 1DC survey. The source was saved by alert-stream scanners on 2018 September 17 as part of the infant SN and CLU programs, and an SEDM spectrum was triggered which showed flash features; an SEDM spectrum obtained the next day showed that the features had disappeared. It was also saved as part of BTS on September 17, as it exceeded the 19th magnitude threshold in an image obtained as part of the public survey ($r = 16.16 \pm 0.04$ mag).

ePESSTO (Smartt et al. 2015) classified the source as SN II based on a September 18 spectrum obtained with the ESO Faint Object Spectrograph and Camera (EFOSC2) on the 3.6m New Technology Telescope (NTT) at La Silla (Gromadzki et al. 2018). Based on an October 12 SEDM spectrum the classification was revised to SN IIb (Dahiwale & Fremling 2020a).

A.3. *SN 2019aajs / ZTF19aakssbm*

SN 2019aajs was discovered by ZTF on 2019 Feb 25 at $r = 19.10 \pm 0.17$ mag in an image obtained as part of the high-cadence partnership survey. It was saved on Feb 26 as part of a search for rapidly evolving transients, because it rose 1.5 mag in 1 day. This led to an extensive sequence of follow-up observations, including imaging, spectroscopy, millimeter, and radio. The object was classified as a Type Ibn SN using an LT spectrum taken on 2019 Mar 02.

A.4. *SN 2019deh / ZTF19aapfmki / ATLAS19gez / PS19aaq*

SN 2019deh was first detected in a ZTF public-survey image on 2019 Apr 07 at $r = 20.75 \pm 0.28$ mag, and again the same night as part of the 1DC survey. It was reported to the TNS on Apr 10 (Nordin et al. 2019a) by the alert management, photometry, and evaluation of light curves (AMPEL) system (Nordin et al. 2019e; Soumagnac & Ofek 2018). It was classified as a Type Ibn SN by SPRAT using a spectrum obtained on 2019 Apr 12 (Prentice et al. 2019).

A.5. *AT 2019esf / ZTF19aatoboa / PS19afa*

AT 2019esf was discovered by ZTF in an image obtained on 2019 May 3 at $g = 19.97 \pm 0.16$ mag as part of the public survey, and detected the next night as part of both the high-cadence and 1DC surveys. It was saved on May 4 by

filters for infant supernovae and fast transients. As part of the rapidly evolving transients program it received an LT spectrum at peak light that did not show distinct features. It was uploaded to TNS by AMPEL on May 6 (Nordin et al. 2019b). The host galaxy redshift was measured with a Keck spectrum on 2020 Feb 17.

A.6. *AT 2019kyw / ZTF19abfarpa*

AT 2019kyw was discovered by ZTF (Fremling 2019), first detected at $g = 20.18 \pm 0.31$ mag in an image obtained on 2019 Jul 6 as part of the public survey. It was saved as part of BTS, infant supernovae, and CLU, and received an inconclusive SEDM spectrum on July 9 as part of routine classification efforts. It received additional DBSP spectra on Aug 1 and Aug 9 that led to a redshift measurement but no conclusion about the transient itself.

A.7. *SN 2019myn / ZTF19abobxik / PS19eop*

SN 2019myn was discovered by ZTF (Nordin et al. 2019c), first detected at $g = 21.24 \pm 0.31$ mag in an image obtained on 2019 Aug 05 as part of the high-cadence partnership survey. It was saved by a filter for rapidly evolving transients on Aug 11, and SEDM and LT were triggered for spectroscopy and imaging. Given the rapid evolution, the VLA was triggered and the observation took place on Aug 17. An LRIS spectrum on Aug 31 led to the Type Ibn classification. The source will be included in a Type Ibn sample paper by Kool et al.

A.8. *SN 2019php / ZTF19abuvqgw / ATLAS19ufu*

SN 2019php was discovered by ATLAS on September 2 and reported to TNS that day (Tonry et al. 2019). The first ZTF detection was on 2019 Aug 31 as part of the public survey, and passed the AMPEL filter (Nordin et al. 2019e). It was detected the next night (September 1) as part of the Caltech 1DC Survey and passed a filter for fast transients. As part of the fast-transient program, it received a spectrum with DBSP on September 9 that was relatively featureless. It received an additional spectrum on September 23 with LRIS that led to the Type Ibn classification.

A.9. *SN 2019qav / ZTF19abyjzvd / PS19fbn*

SN 2019qav was discovered by Pan-STARRS1 (Chambers et al. 2016) on September 11 and reported to TNS on September 12 (Chambers et al. 2019). The first ZTF detection was at $r = 20.31 \pm 0.24$ mag on 2019 September 8 as part of the partnership high-cadence survey. It was saved on September 12 by the infant SN filter, and SEDM was triggered for a spectrum. On September 14 it was recognized that the rise was unusually fast. An LRIS spectrum on September 24 showed H and He features and led to the measurement of $z = 0.137$. Given the unusual spectrum, it was thought that this might be an analog to AT 2018cow, and as a result a variety of facilities were triggered: Swift, NOEMA, and the VLA. We obtained a spectrum of the host galaxy with LRIS on 2021 Apr 14, leading to a more precise redshift ($z = 0.1353$) from strong starforming emission lines.

A.10. *SN 2019rii / ZTF19acayojs / ATLAS19wqu*

SN 2019rii was first identified in the ZTF public stream by ALeRCE broker (Förster et al. 2020), and reported to TNS on September 28. The first ZTF detection was on 2019 September 25 at $g = 20.30 \pm 0.21$ mag as part of the high-cadence partnership survey. It was saved on October 2 as part of a filter for rapidly evolving transients. It was observed the same night with DBSP, leading to the redshift measurement of $z = 0.1234$ from narrow emission lines from the host galaxy. An additional spectrum was obtained on October 26 with LRIS, which showed distinct He I lines. Given the He features and rapid evolution it was tentatively classified as a Type Ibn.

A.11. *SN 2019rta / ZTF19accjfgv*

SN 2019rta was first detected on 2019 October 3 at $g = 17.96 \pm 0.07$ mag in the public survey, and reported to TNS by AMPEL (Nordin et al. 2019e) the same day (Nordin et al. 2019d). The source was saved on October 3 as part of the BTS, and SEDM was triggered for a spectrum. It was saved again on October 05 as part of CLU, and a spectrum was obtained with DBSP that night that showed a blue continuum and strong emission lines from the host galaxy. A final spectrum was obtained with LRIS on October 27 that led to the Type IIb classification (Dahiwale & Fremling 2019).

A.12. *SN 2020ano / ZTF20aahfqpm*

SN 2020ano was first detected on 2020 Jan 23 at $i = 19.93 \pm 0.21$ mag in an image obtained as part of the ZTF Uniform Depth Survey (ZUDS). It was also detected in a public image, and reported to TNS the same day by ALeRCE (Forster

et al. 2020a). It was saved by the AmpelRapid filter, and SEDM was triggered. The spectrum showed primarily a blue continuum. It was also saved that day by a filter for fast transients.

The next day (Jan 24) it was saved by scanners as part of the CLU experiment due to its proximity to a galaxy at $z = 0.0311$. By this day, it was clear that it was fading quickly. From the blue colors and rapid behavior, it was thought to perhaps be a foreground CV. A GMOS spectrum was obtained on Jan 29, and by Jan 31 it was clear from ZUDS photometry that it was rising again in all three filters—this became clear in the regular alerts by Feb 6. An LRIS spectrum obtained on Feb 18 showed a good match to SN1993J, leading to the Type IIb classification.

A.13. AT 2020bdh / ZTF20aaivtof / ATLAS20elz

AT 2020bdh was discovered by ALeRCE on 2020 Jan 27 using the ZTF public stream and reported to TNS the same day (Forster et al. 2020b). The magnitude at discovery was $g = 18.69 \pm 0.07$ mag. It was also detected the next night as part of the 1DC survey. It was saved on Jan 29 as part of CLU, on Feb 2 as part of a search for rapidly evolving transients, and on Feb 3 as part of the BTS. SEDM was triggered but observations were not successful. A broad H-alpha feature was noted in a report to TNS (Smith et al. 2020b) from an ePESSTO spectrum obtained on Feb 13. A spectrum was obtained on Feb 25 with DBSP by ZTF as part of routine classification, which led to a redshift measurement but not a definitive classification. The spectrum also tentatively showed a broad emission feature around H-alpha.

A.14. AT 2020bot / ZTF20aakypiu / PS20va

AT 2020bot was discovered by ZTF at $r = 20.41 \pm 0.24$ mag in an image obtained as part of ZUDS on 2020 Jan 30. On Feb 1 it passed the infant SN filter. Its proximity to an SDSS galaxy of known redshift ($z = 0.197$) implied a very high luminosity; together with the fast rise, this led us to initiate follow-up observations, including LT and P60 imaging. DBSP and GMOS spectra were not conclusive, although the GMOS spectrum was noted to have broad features somewhat similar to young Ic-BL SNe. Attempts at follow-up spectroscopy with DBSP and Keck were not successful.

A.15. SN 2020ikq / ATLAS20lfu / ZTF20aaxhzhc / PS20ctw

SN 2020ikq was discovered by ATLAS on 2020 April 28 and reported to the TNS the same day (Tonry et al. 2020). The first ZTF detection was on April 29 at $g = 18.42 \pm 0.08$ mag in public-survey data. It was saved the same day by a scanner as part of the BTS and CLU surveys. SN 2020ikq was classified as a Type IIb SN by the NOT on 2020 May 15 (Angus 2020).

A.16. SN 2020jmb / ZTF20aayrobw / ATLAS20lwn

SN 2020jmb was first detected on 2020 May 08 at $g = 19.52 \pm 0.21$ mag in the Caltech one-day cadence survey. The source was saved by alert-stream scanners on 2020 May 10 as part of a search for rapidly evolving transients, and separately as part of the CLU experiment due to its proximity to a galaxy at $z = 0.032$ (the transient later proved unassociated). It was reported to TNS as part of CLU (De 2020a). The source was saved as part of BTS on 2020 May 11, when it exceeded the 19th magnitude threshold in an image obtained as part of the public survey ($g = 18.56 \pm 0.07$ mag). A spectrum was obtained with the SEDM on 2020 May 11 under the CLU program, which showed no distinct features. Additional spectra were obtained with the LT on May 16 and the SEDM on May 23, neither of which showed distinct features. Finally, a spectrum was obtained on May 27 with DBSP on the P200 for the rapidly evolving transients program, which showed a prominent Hα feature and narrow emission lines from the host galaxy consistent with $z = 0.061$, leading to the classification as a Type II SN (Dahiwale & Fremling 2020b).

A.17. SN 2020jji / ZTF20aazchcq / ATLAS20mfw / PS20czx

SN 2020jji was first detected in the ZTF public survey on 2020 May 1 at $r = 20.53 \pm 0.30$ mag. It was saved on May 10 as part of the AMPEL and CLU filters, and reported to TNS that day (De 2020b). It received a follow-up spectrum by the SEDM that night, which was inconclusive. On May 16 it was saved by a scanner as part of the fast transients program, and received a DBSP spectrum as part of that effort. The DBSP spectrum showed a Type IIn classification.

A.18. AT 2020kfw / ZTF20ababxjv / ATLAS20nfg

AT 2020kfw was first detected by ZTF on 2020 May 17 at $r = 20.53 \pm 0.20$ mag in an image obtained as part of the public survey, and reported to TNS by ALeRCE (Forster et al. 2020c). It was detected later that night in the 1DC

survey. On May 23 it had peaked and started fading, and as a result passed a filter for fast transients. The resulting DBSP spectrum was of low quality and not conclusive.

A.19. *SN 2020ntt / ZTF20abjbgjj / PS20gvm*

SN2020ntt was first detected on 2020 Jun 24 at $r = 20.56 \pm 0.28$ mag in the public survey. It was saved on Jun 30 by AMPEL, and reported to TNS the same day (Nordin et al. 2020). It was saved again on July 3 by the BTS survey. SEDM and LT spectra were obtained as part of BTS. The LT spectrum on July 13 led to the Type IIn classification and measurement of $z = 0.074$ (Perley et al. 2020a). Further inspection as part of this paper reclassified it as Type II.

A.20. *AT 2020aexw / ZTF20abmocba*

AT 2020aexw was discovered by ZTF, first detected on 2020 July 18 at $r = 20.52 \pm 0.21$ mag as part of ZUDS. It was saved on July 19 by AMPEL and on July 26 by the rapidly evolving transients program. LT follow-up imaging was acquired. A NOT spectrum was attempted but not successful. A DBSP spectrum was obtained on Aug 12 resulting in a redshift measurement from very strong emission lines.

A.21. *AT 2020yqt / ZTF20abummyz / PS20ksm*

AT 2020yqt was discovered by Pan-STARRS1 on 2020 Aug 22 and reported to TNS on 2020 November 1 (Chambers et al. 2020). It was first detected as part of the ZTF 1DC survey on 2020 Aug 19 at $r = 19.95 \pm 0.17$ mag, and saved by a scanner on Aug 20 as part of a filter for rapidly evolving transients. The host galaxy had an SDSS spectrum which classified it as a starburst, with a redshift $z = 0.09855 \pm 0.00001$. Due to the fast evolution, we triggered a Gemini ToO program (PI: A. Miller) and obtained a spectrum on Aug 25 that was primarily featureless. Subsequent spectra with P200 and LRIS did not show obvious supernova features and were dominated by host-galaxy light.

A.22. *SN 2020rsc / ZTF20aburywx / ATLAS20xxj*

SN 2020rsc was first detected on 2020 Aug 19 as part of the public survey at $g = 19.58 \pm 0.17$ mag, and reported to TNS that day by the ALeRCE broker (Forster et al. 2020d). It was also detected that night as part of the Caltech 1DC survey. It was first saved on 2020 Aug 20 by a filter for rapidly evolving transients. The next day, it was noted that it was already fading, and a Gemini ToO program was triggered. The Gemini spectrum on Aug 22 showed He I at $8000 \, \mathrm{km \, s^{-1}}$. On 2020 Aug 22 the source passed the CLU filter. An additional spectrum with MMT+Binospec was obtained on Aug 24, and a GTC spectrum was obtained on Aug 25. Swift was triggered and observed on Aug 26, and the VLA was triggered on September 2 with the observation taking place on September 9. A final Keck spectrum on September 15 led to the Type IIb classification.

### A.23. *SN2020vyv / ZTF20acigusw / ATLAS20bdhi / PS20kra*

SN 2020vyv was first detected in the ZTF public survey on 2020 October 12 at $r = 19.17 \pm 0.10$ mag. It was saved the same day by AMPEL and the BTS survey, and reported to TNS (Fremling 2020). It was classified as a Type II SN with a Keck/LRIS spectrum on 2020-10-14 (Siebert et al. 2020b).

A.24. *SN 2020xlt / ZTF20aclfmwn*

SN 2020xlt was first detected on 2020 October 19 in public-survey data at $r = 19.93 \pm 0.22$, and was reported to TNS that day by ALeRCE (Forster et al. 2020e). It was also detected that night as part of the Caltech 1DC survey, and the next night as part of the high-cadence partnership survey. It was saved on October 19 as part of AMPEL (Nordin et al. 2019e) and the infant supernova program, and SEDM was triggered: the spectrum was featureless. Despite the proximity to a bright extended galaxy, the redshift was unknown. The transient was noted to be fading on October 22, and on October 26 it passed a filter for rapidly evolving transients, leading to a GTC+OSIRIS spectrum on 2020 October 30 that enabled the redshift measurement of $z = 0.0389$ and the classification as a Type IIb.

B. PHOTOMETRIC EVOLUTION OF INDIVIDUAL EVENTS

Here we provide light curves for the events not shown in the main text.
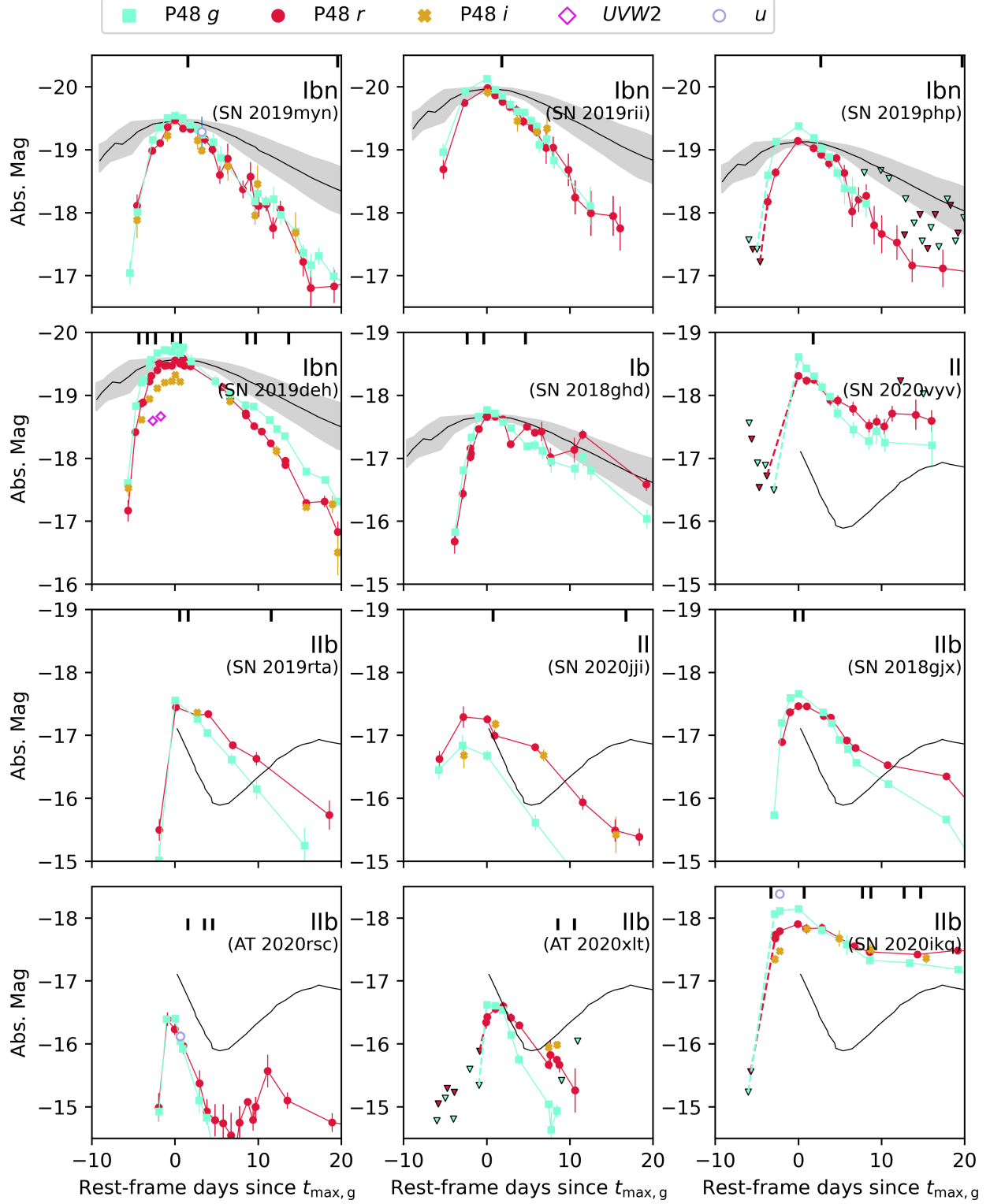
Figure 20. Light curves for gold-sample events whose light curves were not shown in the main text. In panels with H-poor SNe we show the Type Ibc template from Drout et al. (2011) for reference. In the Type II and Type IIb panels we show the V-band light curve of SN 1993J (Schmidt et al. 1993) for reference.
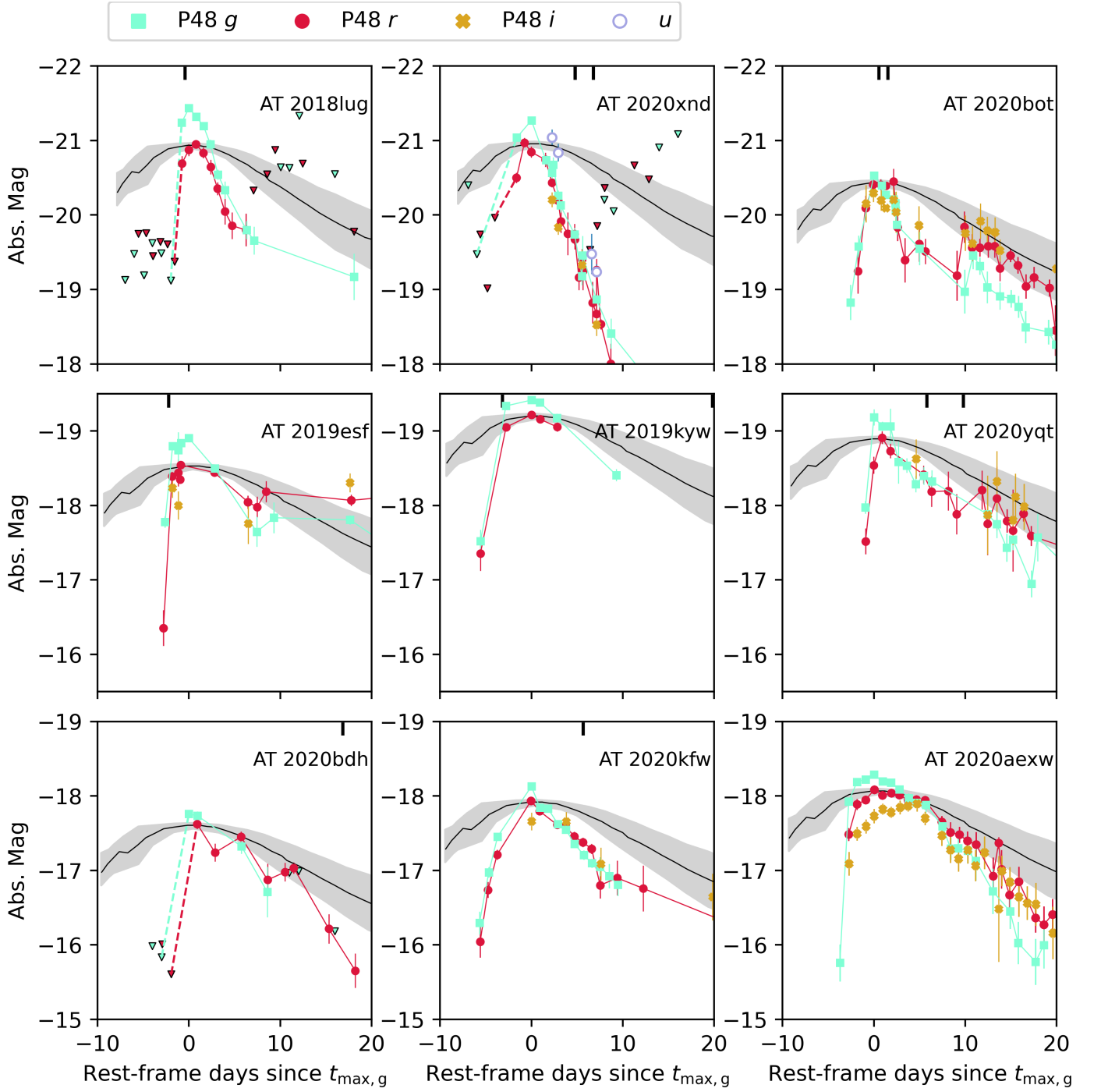
Figure 21. Light curves for the silver sample. For reference, in each panel we show the Type Ibc template from Drout et al. (2011). Upper limits are shown with triangles. Upper limits are connected to detections by dashed lines.
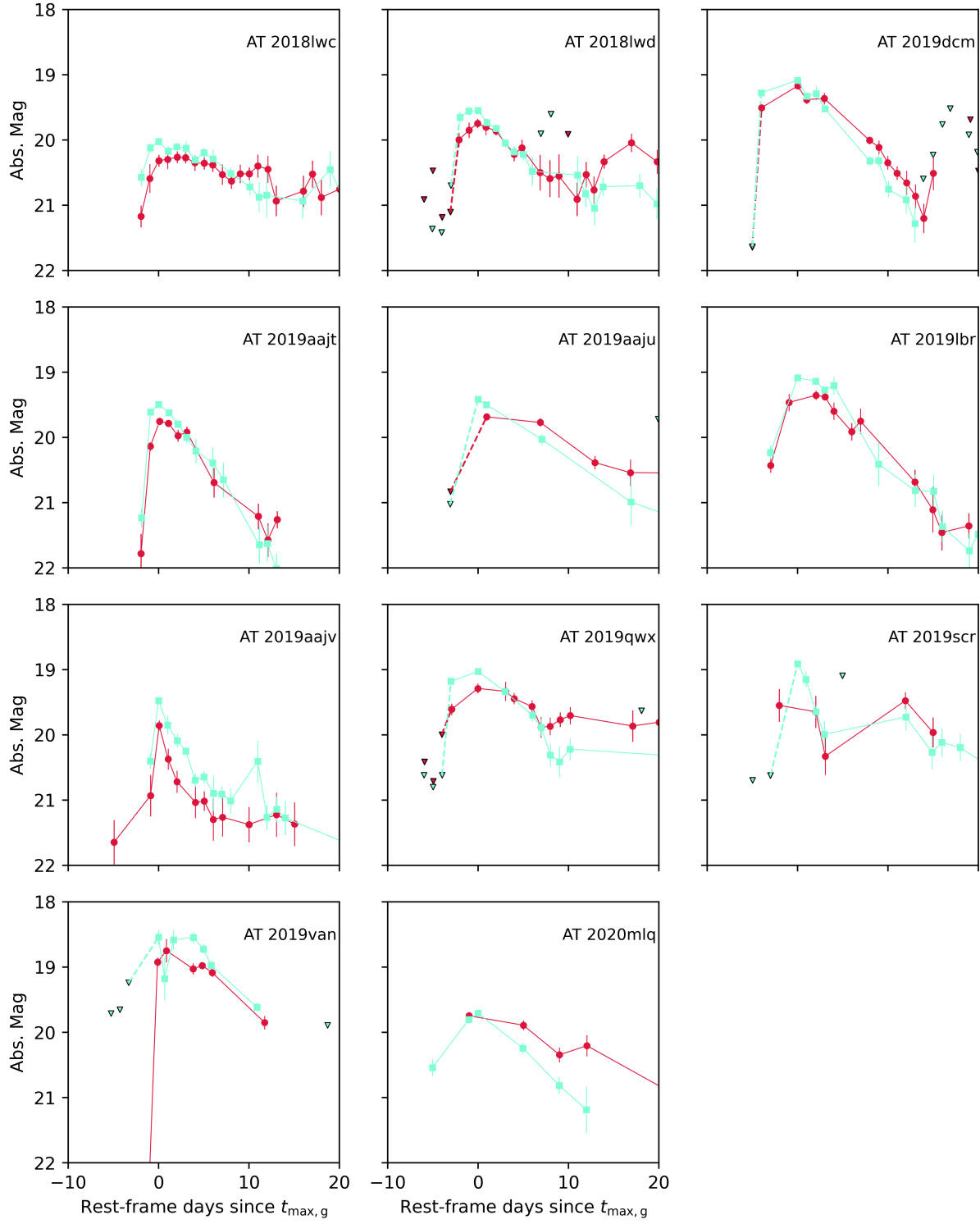
Figure 22. ZTF P48 *g*- and *r*-band light curves for the bronze sample. Upper limits are shown with triangles, and non-detections are connected to detections by dashed lines.

C. LOG OF OPTICAL SPECTRA

Here we provide the full log of optical spectra, some of which were obtained from TNS. We do not report observations for objects with extensive spectroscopic observations previously presented in the literature: AT 2018cow (Perley et al. 2019), SN 2018gep (Ho et al. 2019a), SN 2019dge (Yao et al. 2020), and SN 2020oi.

Table 15. Log of spectroscopic observations of objects presented in this paper. Phase given with respect to the observed maximum of the g-band light curve.

Name	UT Date	Target	Phase	Telescope + Instrument
SN 2018ghd	20180914	Transient	−2	P60+SEDM
SN 2018ghd	20180916	Transient	0	P60+SEDM
SN 2018ghd	20180921	Transient	4	P60+SEDM
SN 2018ghd	20181110	Transient	54	Keck1+LRIS
SN 2018ghd	20190105	Transient	110	Keck1+LRIS
AT 2018lug	20180913	Transient	0	P200+DBSP
AT 2018lug	20190104	Host	112	Keck1+LRIS
SN 2018gjx	20180918	Transient	0	P60+SEDM
SN 2018gjx	20180918	Transient	0	EFOSC2+NTT [1]
SN 2018gjx	20180919	Transient	0	P60+SEDM
SN 2018gjx	20181012	Transient	23	P60+SEDM
SN 2018gjx	20181016	Transient	27	NOT+ALFOSC
SN 2018gjx	20181110	Transient	52	Keck1+LRIS
SN 2018gjx	20181130	Transient	72	TNG+DOLORES
SN 2018gjx	20190105	Transient	108	Keck1+LRIS
SN 2018gjx	20190706	Transient	290	Keck1+LRIS
SN 2019aajs	20190227	Transient	−1	LT+SPRAT
SN 2019aajs	20190302	Transient	1	LT+SPRAT
SN 2019aajs	20190304	Transient	3	NOT+ALFOSC
SN 2019aajs	20190315	Transient	14	NOT+ALFOSC
SN 2019aajs	20190406	Transient	36	Keck1+LRIS
SN 2019deh	20190410	Transient	−4	P60+SEDM
SN 2019deh	20190410	Transient	−4	LT+SPRAT
SN 2019deh	20190411	Transient	−3	LT+SPRAT
SN 2019deh	20190412	Transient	−2	LT+SPRAT
SN 2019deh	20190414	Transient	0	LT+SPRAT
SN 2019deh	20190415	Transient	0	P60+SEDM
SN 2019deh	20190423	Transient	8	NOT+ALFOSC
SN 2019deh	20190423	Transient	8	P60+SEDM
SN 2019deh	20190424	Transient	9	P200+DBSP
SN 2019deh	20190428	Transient	13	P60+SEDM
SN 2019deh	20190511	Transient	26	NOT+ALFOSC
AT 2019esf	20190504	Transient	−2	P60+SEDM
AT 2019esf	20200218	Host	287	Keck1+LRIS
AT 2019kyw	20190709	Transient	−3	P60+SEDM
AT 2019kyw	20190801	Transient	19	P200+DBSP
AT 2019kyw	20190809	Transient	27	P200+DBSP
SN 2019myn	20190813	Transient	1	P60+SEDM
SN 2019myn	20190831	Transient	19	Keck1+LRIS
SN 2019php	20190907	Transient	2	P200+DBSP
SN 2019php	20190924	Transient	19	Keck1+LRIS
SN 2019qav	20190911	Transient	−2	P60+SEDM
SN 2019qav	20190924	Transient	10	Keck1+LRIS
SN 2019qav	20190928	Transient	14	Keck1+LRIS

Table 15 *continued*

Table 15 (continued)

Name	UT Date	Target	Phase	Telescope + Instrument
SN 2019qav	20191027	Transient	43	Keck1+LRIS
SN 2019rii	20191003	Transient	1	P200+DBSP
SN 2019rii	20191027	Transient	25	Keck1+LRIS
SN 2019rta	20191004	Transient	0	P60+SEDM
SN 2019rta	20191005	Transient	1	P200+DBSP
SN 2019rta	20191015	Transient	11	P60+SEDM
SN 2019rta	20191027	Transient	23	Keck1+LRIS
SN 2020ano	20200125	Transient	1	P60+SEDM
SN 2020ano	20200129	Transient	5	Gemini+GMOS
SN 2020ano	20200214	Transient	21	P200+DBSP
SN 2020ano	20200218	Transient	25	Keck1+LRIS
AT 2020bdh	20200213	Transient	16	EFOSC2+NTT [2]
AT 2020bdh	20200226	Transient	29	P200+DBSP
AT 2020bot	20200202	Transient	0	P200+DBSP
AT 2020bot	20200203	Transient	1	Gemini+GMOS
SN 2020ikq	20200429	Transient	−3	P60+SEDM
SN 2020ikq	20200503	Transient	0	P60+SEDM
SN 2020ikq	20200510	Transient	7	LT+SPRAT
SN 2020ikq	20200511	Transient	8	P60+SEDM
SN 2020ikq	20200515	Transient	12	NOT+ALFOSC
SN 2020ikq	20200517	Transient	14	P60+SEDM
SN 2020jmb	20200511	Transient	−1	P60+SEDM
SN 2020jmb	20200516	Transient	3	LT+SPRAT
SN 2020jmb	20200523	Transient	10	P60+SEDM
SN 2020jmb	20200528	Transient	15	P200+DBSP
SN 2020jji	20200511	Transient	0	P60+SEDM
SN 2020jji	20200527	Transient	16	P200+DBSP
AT 2020kfw	20200528	Transient	5	P200+DBSP
SN 2020ntt	20200713	Transient	9	LT+SPRAT
SN 2020ntt	20200715	Transient	11	P60+SEDM
AT 2020aexw	20200812	Host	21	P200+DBSP
AT 2020yqt	20200825	Transient	5	Gemini+GMOS
AT 2020yqt	20200829	Transient	9	P200+DBSP
AT 2020yqt	20200920	Transient	31	Keck1+LRIS
SN 2020rsc	20200822	Transient	−2	Gemini+GMOS
SN 2020rsc	20200824	Transient	0	MMT
SN 2020rsc	20200825	Transient	0	GTC+OSIRIS
SN 2020rsc	20200915	Transient	21	Keck1+LRIS
AT 2020xnd	20201019	Transient	4	Keck1+LRIS
AT 2020xnd	20201021	Transient	6	Keck1+LRIS
SN 2020vyv	20201014	Transient	1	Keck1+LRIS [3]
SN 2020xlt	20201028	Transient	8	P60+SEDM
SN 2020xlt	20201030	Transient	10	GTC+OSIRIS

References—[1] Gromadzki et al. (2018), [2] Smith et al. (2020b), [3] Siebert et al. (2020b)

D. SPECTROSCOPIC EVOLUTION OF INDIVIDUAL EVENTS

In this section we plot the full set of spectra for each object in the gold sample.

E. HOST GALAXY PROPERTIES

In this section we provide additional details and figures for the host-galaxy properties described in Section 4. We model the spectral energy distributions

(SEDs) with the software package CIGALE (Code Investigating GALaxy Evolution; Burgarella et al. 2005; Noll et al. 2009; Boquien et al. 2019). We adopt the Bruzual & Charlot (2003) simple stellar population model to compute the stellar emission and the Chabrier (2003) initial mass function. Furthermore, we assume a linear-exponential star-formation history [functional form $t \times \exp(-t/\tau)$, where t is the age of the SFH episode and τ is the e-folding timescale]. To calculate the neb-
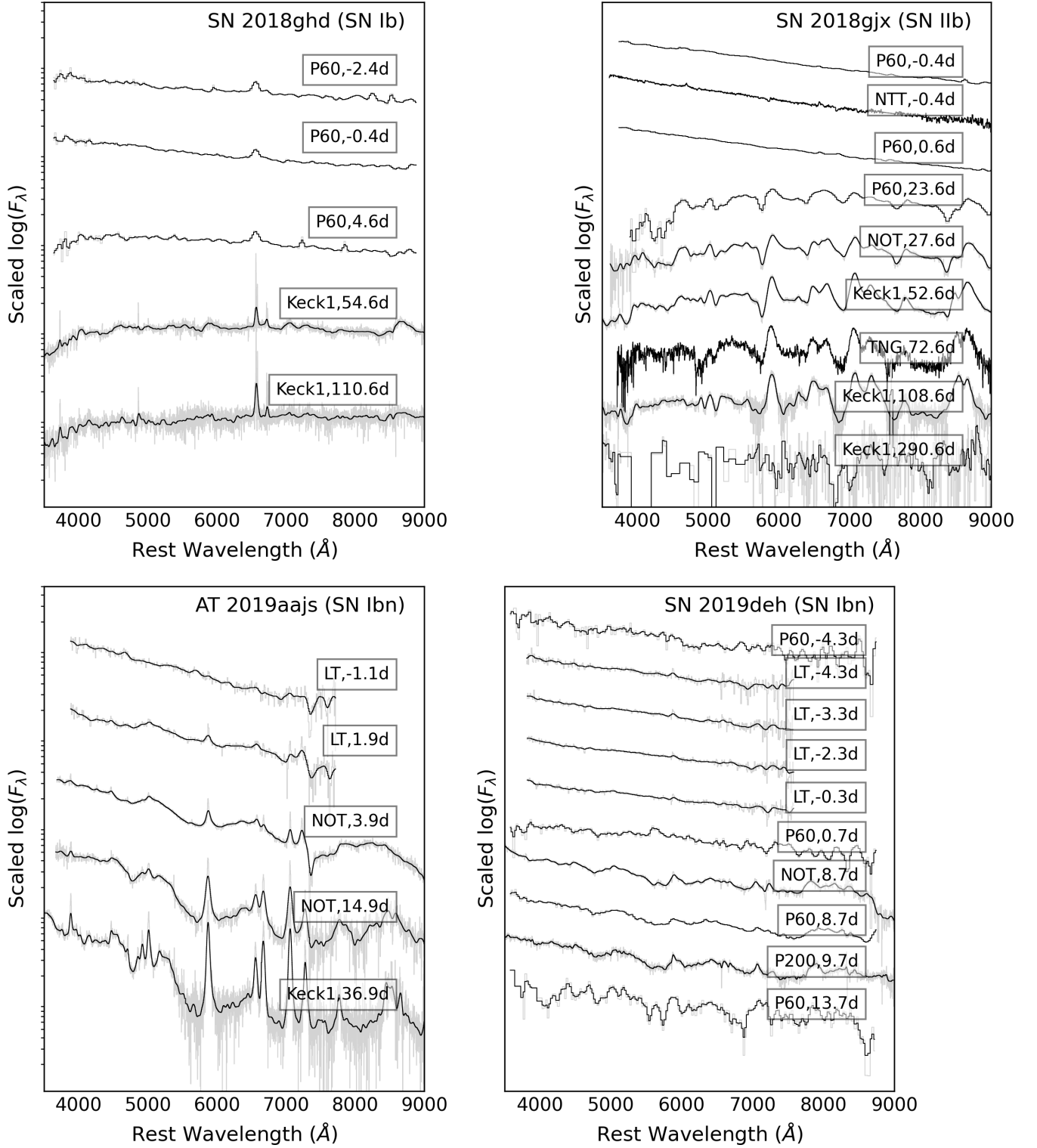
Figure 23. Spectroscopic evolution for gold-sample objects. Raw spectra are shown in light grey, and smoothed spectra are overlaid in black.
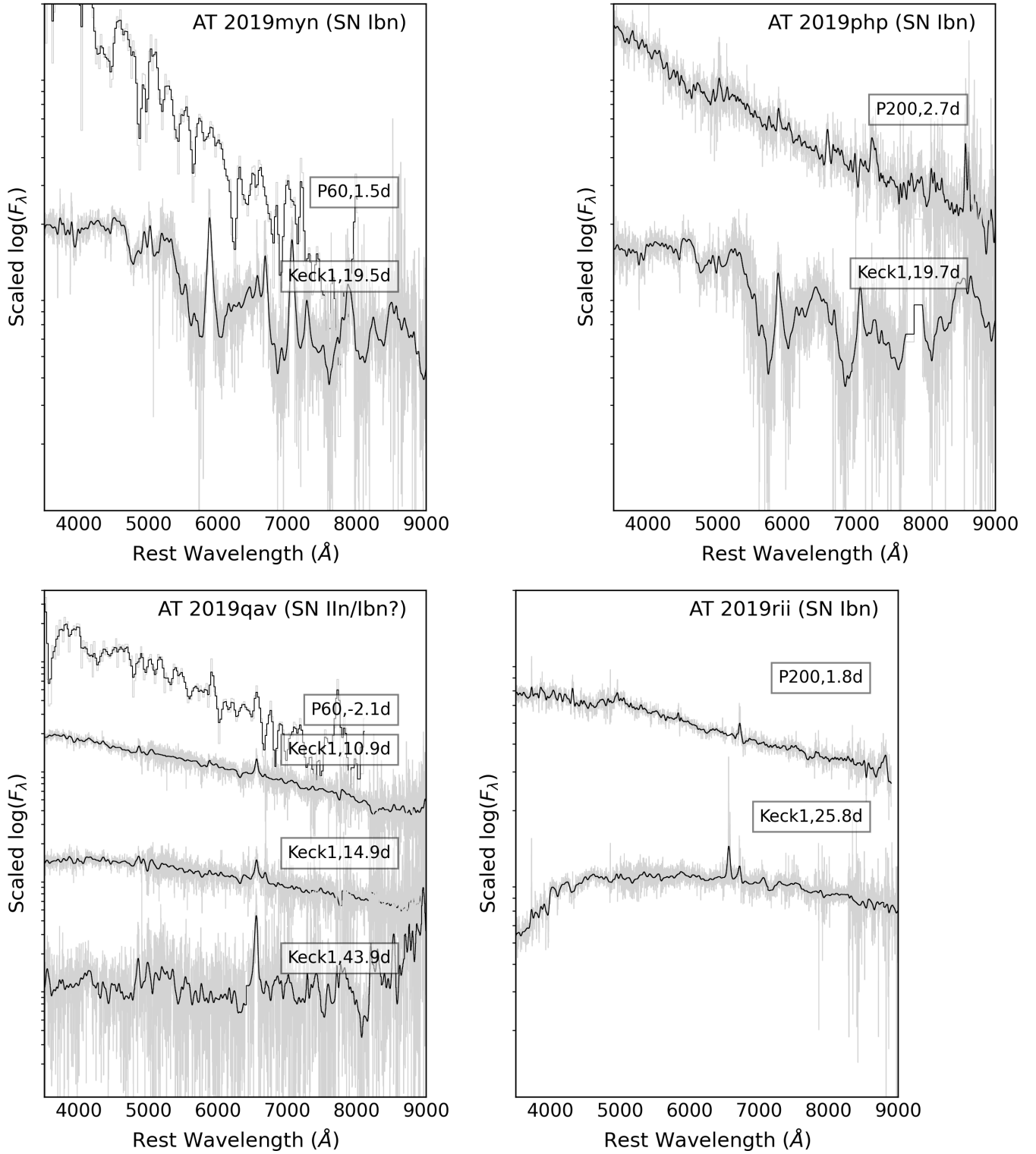
Figure 24. Spectroscopic evolution for gold-sample objects. Raw spectra are shown in light grey, and smoothed spectra are overlaid in black.
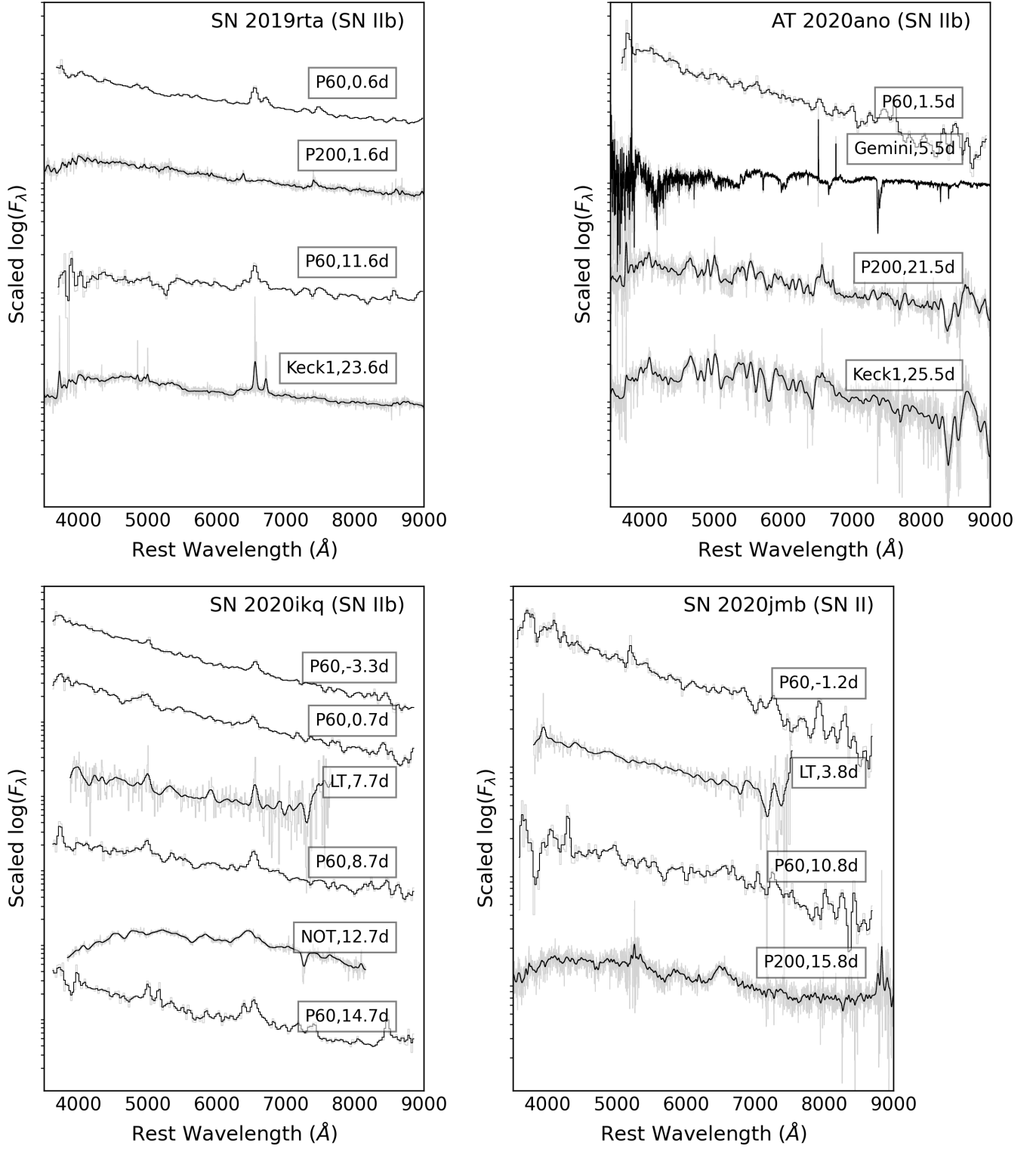
Figure 25. Spectroscopic evolution for gold-sample objects. Raw spectra are shown in light grey, and smoothed spectra are overlaid in black.
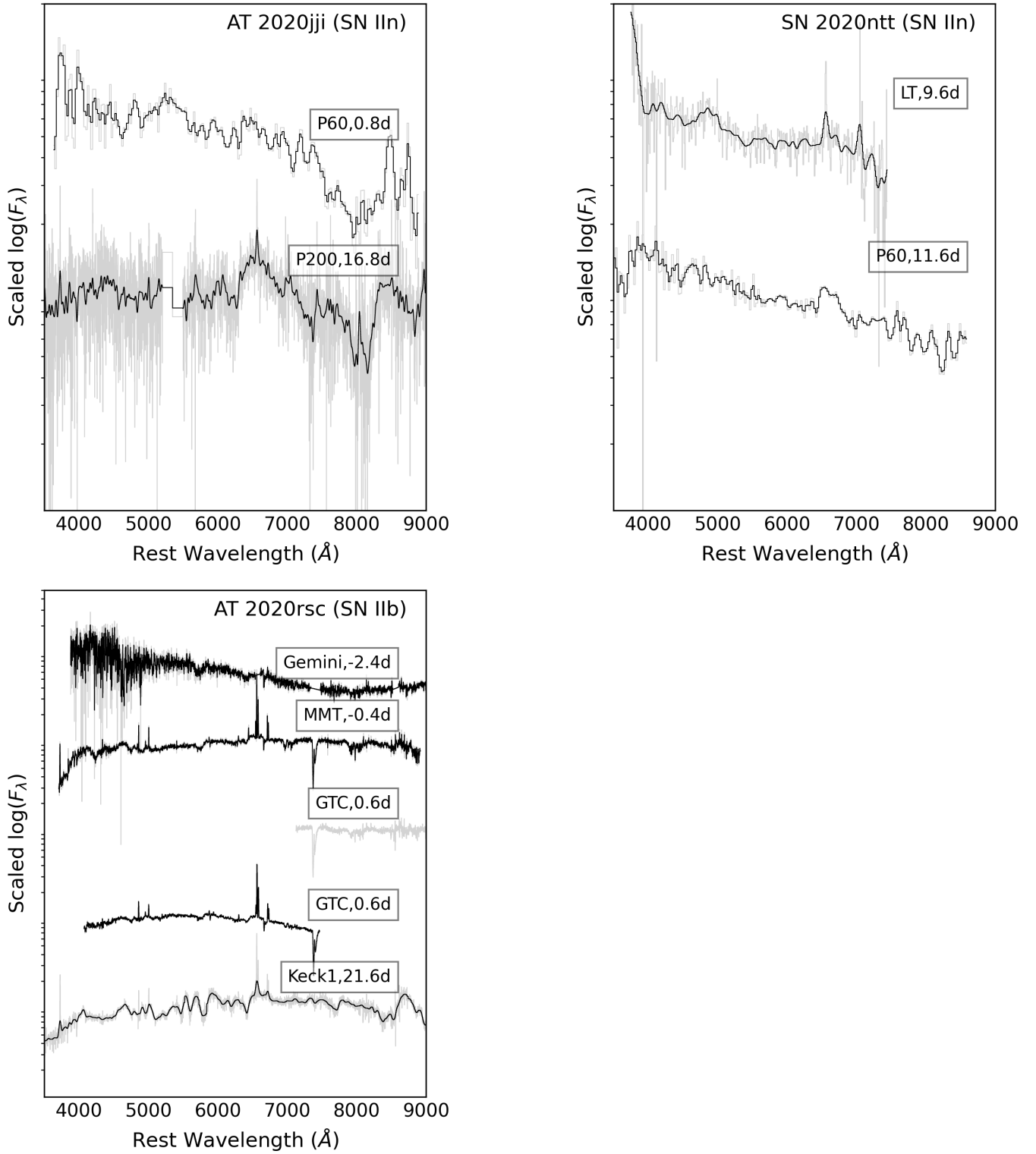
Figure 26. Spectroscopic evolution for gold-sample objects. Raw spectra are shown in light grey, and smoothed spectra are overlaid in black.

ular emission from the ionised gas in H II regions, we fix the CIGALE ionisation parameter log U_{ion} as -2. We use a modified Calzetti et al. (2000) starburst attenuation curve to model the dust attenuation. Dust emission was included via the Dale et al. (2014) dust templates.

More details on the models used can be found in Boquien et al. (2019). We generate 24385536 models and choose the best-fit SED using Bayesian inference. In Figure 27 we show the best-fit SED for the host galaxy of AT 2020yqt as an example.

<div align="center">REFERENCES</div>

Ahn, C. P., Alexandroff, R., Allende Prieto, C., et al. 2012, ApJS, 203, 21, doi: 10.1088/0067-0049/203/2/21

Andreoni, I., Kool, E. C., Sagués Carracedo, A., et al. 2020, ApJ, 904, 155, doi: 10.3847/1538-4357/abbf4c

Angus, C. 2020, Transient Name Server Classification Report, 2020-1392, 1

Arcavi, I., Gal-Yam, A., Yaron, O., et al. 2011, ApJL, 742, L18, doi: 10.1088/2041-8205/742/2/L18

Arcavi, I., Wolf, W. M., Howell, D. A., et al. 2016, ApJ, 819, 35, doi: 10.3847/0004-637X/819/1/35

Astier, P., Guy, J., Regnault, N., et al. 2006, A&A, 447, 31, doi: 10.1051/0004-6361:20054185

Astropy Collaboration, Robitaille, T. P., Tollerud, E. J., et al. 2013, A&A, 558, A33, doi: 10.1051/0004-6361/201322068

Astropy Collaboration, Price-Whelan, A. M., Sipőcz, B. M., et al. 2018, AJ, 156, 123, doi: 10.3847/1538-3881/aabc4f

Barnsley, R. M., Smith, R. J., & Steele, I. A. 2012, Astronomische Nachrichten, 333, 101, doi: 10.1002/asna.201111634

Bellm, E. C. 2016, PASP, 128, 084501, doi: 10.1088/1538-3873/128/966/084501

Bellm, E. C., & Sesar, B. 2016, pyraf-dbsp: Reduction pipeline for the Palomar Double Beam Spectrograph. http://ascl.net/1602.002

Bellm, E. C., Kulkarni, S. R., Graham, M. J., et al. 2019a, PASP, 131, 018002, doi: 10.1088/1538-3873/aaecbe

Bellm, E. C., Kulkarni, S. R., Barlow, T., et al. 2019b, PASP, 131, 068003, doi: 10.1088/1538-3873/ab0c2a

Bersten, M. C., Folatelli, G., García, F., et al. 2018, Nature, 554, 497, doi: 10.1038/nature25151

Bietenholz, M. F., Margutti, R., Coppejans, D., et al. 2020, MNRAS, 491, 4735, doi: 10.1093/mnras/stz3249

Blagorodnova, N., Neill, J. D., Walters, R., et al. 2018, PASP, 130, 035003, doi: 10.1088/1538-3873/aaa53f

Blanton, M. R., & Roweis, S. 2007, AJ, 133, 734, doi: 10.1086/510127

Boquien, M., Burgarella, D., Roehlly, Y., et al. 2019, A&A, 622, A103, doi: 10.1051/0004-6361/201834156

Breeveld, A. A., Landsman, W., Holland, S. T., et al. 2011, in American Institute of Physics Conference Series, Vol. 1358, American Institute of Physics Conference Series, ed. J. E. McEnery, J. L. Racusin, & N. Gehrels, 373–376, doi: 10.1063/1.3621807

Bruch, R., Schulze, S., Yang, Y., et al. 2019, Transient Name Server Discovery Report, 2019-973, 1

Bruzual, G., & Charlot, S. 2003, MNRAS, 344, 1000, doi: 10.1046/j.1365-8711.2003.06897.x

Burgarella, D., Buat, V., & Iglesias-Páramo, J. 2005, MNRAS, 360, 1413, doi: 10.1111/j.1365-2966.2005.09131.x

Burrows, D. N., Hill, J. E., Nousek, J. A., et al. 2005, SSRv, 120, 165, doi: 10.1007/s11214-005-5097-2

Calzetti, D., Armus, L., Bohlin, R. C., et al. 2000, ApJ, 533, 682, doi: 10.1086/308692

Campana, S., Mangano, V., Blustin, A. J., et al. 2006, Nature, 442, 1008, doi: 10.1038/nature04892

Cenko, S. B., Fox, D. B., Moon, D.-S., et al. 2006, PASP, 118, 1396, doi: 10.1086/508366

Cepa, J., Aguiar, M., Escalera, V. G., et al. 2000, in Society of Photo-Optical Instrumentation Engineers (SPIE) Conference Series, Vol. 4008, Optical and IR Telescope Instrumentation and Detectors, ed. M. Iye & A. F. Moorwood, 623–631, doi: 10.1117/12.395520

Chabrier, G. 2003, PASP, 115, 763, doi: 10.1086/376392

Chambers, K. C., Magnier, E. A., Metcalfe, N., et al. 2016, arXiv e-prints, arXiv:1612.05560. https://arxiv.org/abs/1612.05560

Chambers, K. C., Boer, T. D., Bulger, J., et al. 2019, Transient Name Server Discovery Report, 2019-1814, 1

—. 2020, Transient Name Server Discovery Report, 2020-3320, 1

Chen, P., Dong, S., Stritzinger, M. D., et al. 2020, ApJL, 889, L6, doi: 10.3847/2041-8213/ab62a4

Cook, D. O., Kasliwal, M. M., Van Sistine, A., et al. 2019, ApJ, 880, 7, doi: 10.3847/1538-4357/ab2131

Coppejans, D. L., Margutti, R., Terreran, G., et al. 2020, ApJL, 895, L23, doi: 10.3847/2041-8213/ab8cc7

Corsi, A., Ofek, E. O., Gal-Yam, A., et al. 2012, ApJL, 747, L5, doi: 10.1088/2041-8205/747/1/L5

Table 16. The models and fitting parameters used for cigale

Galaxy attributes	Brief description
SFH	SFR $\propto \frac{t}{\tau^2} exp(-t/\tau)$
	$\tau = 250, 500, 1000, 2000, 4000, 6000, 8000$ Myr
	Age $t = 250, 500, 1000, 2000, 4000, 8000, 12000$ Myr
SSPs models	BC03 (Bruzual & Charlot 2003) + Chabrier IMF (Chabrier 2003)
	Stellar metallicity = 0.0004, 0.004, 0.008, 0.02 $Z_\odot$
Dust Attenuation	Modified power law curves (Calzetti et al. 2000) + differential reddening of stars according to age
	$E(B-V)_{\mathrm{young}} = 0.0, 0.2, 0.3, 0.5, 0.8, 1.0, 1.5, 2.0, 3.0$
	$E(B-V)_{\mathrm{old}} = 0.3, 0.50, 1.0$
	UV $-$ bump wavelength = 217.5 nm
	UV $-$ bump amplitude = 0.0, 1.0, 2.0, 3.0
	powerlaw slope = $-0.13, -0.2, -0.5$
Dust emission	Dust templates of Dale et al. (2014) + Energy Balance
	AGN fraction = 0
	alpha = 1.0, 1.5, 2.0, 2.5
Nebular	$\log U_{\mathrm{ion}}$ = -2.0
	emission line width = 300.0 km/s

Costantin, L., Avramova-Bonche, A., Pinter, V., et al. 2018, The Astronomer's Telegram, 12047, 1

Cutri, R. M., Wright, E. L., Conrow, T., et al. 2013, Explanatory Supplement to the AllWISE Data Release Products, Explanatory Supplement to the AllWISE Data Release Products

Dahiwale, A., & Fremling, C. 2019, Transient Name Server Classification Report, 2019-2407, 1

—. 2020a, Transient Name Server Classification Report, 2020-2234, 1

—. 2020b, Transient Name Server Classification Report, 2020-1756, 1

Dale, D. A., Helou, G., Magdis, G. E., et al. 2014, ApJ, 784, 83, doi: 10.1088/0004-637X/784/1/83

De, K. 2020a, Transient Name Server Discovery Report, 2020-1294, 1

—. 2020b, Transient Name Server Discovery Report, 2020-1294, 1

De, K., Kasliwal, M. M., Ofek, E. O., et al. 2018, Science, 362, 201, doi: 10.1126/science.aas8693

De, K., Kasliwal, M. M., Tzanidakis, A., et al. 2020, ApJ, 905, 58, doi: 10.3847/1538-4357/abb45c

Dekany, R., Smith, R. M., Riddle, R., et al. 2020, PASP, 132, 038001, doi: 10.1088/1538-3873/ab4ca2

Dey, A., Schlegel, D. J., Lang, D., et al. 2019, AJ, 157, 168, doi: 10.3847/1538-3881/ab089d

Djupvik, A. A., & Andersen, J. 2010, Astrophysics and Space Science Proceedings, 14, 211, doi: 10.1007/978-3-642-11250-8_21

Drout, M. R., Soderberg, A. M., Gal-Yam, A., et al. 2011, ApJ, 741, 97, doi: 10.1088/0004-637X/741/2/97

Drout, M. R., Chornock, R., Soderberg, A. M., et al. 2014, ApJ, 794, 23, doi: 10.1088/0004-637X/794/1/23

Duev, D. A., Mahabal, A., Masci, F. J., et al. 2019, MNRAS, 489, 3582, doi: 10.1093/mnras/stz2357

Elbaz, D., Daddi, E., Le Borgne, D., et al. 2007, A&A, 468, 33, doi: 10.1051/0004-6361:20077525

Evans, P. A., Beardmore, A. P., Page, K. L., et al. 2007, A&A, 469, 379, doi: 10.1051/0004-6361:20077530

—. 2009, MNRAS, 397, 1177, doi: 10.1111/j.1365-2966.2009.14913.x

Table 17. Summary of the host galaxy SED modelling

Object	χ^2/n.o.f.	M_B (mag)	$\log M/M_\odot$	$\log \mathrm{SFR}/\left(M_\odot\,\mathrm{yr}^{-1}\right)$	$\log \mathrm{Age/yr}$	$E(B-V)$ (mag)
Gold sample						
ZTF18aakuewf	2.10/9	-18.57	$9.47^{+0.15}_{-0.10}$	$-0.48^{+0.09}_{-0.08}$	$9.91^{+0.12}_{-0.19}$	$0.25^{+0.06}_{-0.03}$
ZTF18abcfcoo	56.74/24	-18.46	$9.59^{+0.06}_{-0.13}$	$-0.19^{+0.10}_{-0.13}$	$9.93^{+0.10}_{-0.15}$	$0.25^{+0.07}_{-0.04}$
ZTF18abfcmjw	0.61/14	-16.19	$8.65^{+0.12}_{-0.14}$	$-1.22^{+0.28}_{-0.23}$	$9.89^{+0.13}_{-0.21}$	$0.31^{+0.15}_{-0.08}$
ZTF18abukavn	9.85/19	-16.59	$8.45^{+0.09}_{-0.08}$	$-1.08^{+0.04}_{-0.07}$	$9.81^{+0.18}_{-0.19}$	$0.25^{+0.06}_{-0.03}$
ZTF18abvkmgw	2.09/15	-19.23	$10.30^{+0.12}_{-0.13}$	$0.37^{+0.32}_{-0.20}$	$9.89^{+0.13}_{-0.23}$	$0.58^{+0.43}_{-0.24}$
ZTF18abwkrbl	3.11/16	-19.58	$10.19^{+0.08}_{-0.13}$	$0.42^{+0.15}_{-0.14}$	$9.91^{+0.12}_{-0.21}$	$0.28^{+0.12}_{-0.06}$
ZTF19aakssbm	1.55/9	-17.76	$9.64^{+0.17}_{-0.14}$	$-0.61^{+0.22}_{-0.49}$	$9.94^{+0.09}_{-0.13}$	$0.28^{+0.11}_{-0.06}$
ZTF19aapfmki	5.75/17	-20.94	$10.72^{+0.05}_{-0.07}$	$0.89^{+0.07}_{-0.12}$	$9.95^{+0.09}_{-0.12}$	$0.25^{+0.06}_{-0.03}$
ZTF19abobxik	5.43/14	-18.32	$9.42^{+0.13}_{-0.10}$	$-0.54^{+0.06}_{-0.08}$	$9.90^{+0.13}_{-0.19}$	$0.25^{+0.06}_{-0.03}$
ZTF19abuvqgw	1.27/3	-12.66	$6.51^{+0.56}_{-0.39}$	$-2.21^{+0.37}_{-0.34}$	$8.94^{+0.80}_{-0.38}$	$0.37^{+0.58}_{-0.13}$
ZTF19abyjzvd	14.49/18	-19.83	$9.87^{+0.20}_{-0.16}$	$0.60^{+0.21}_{-0.25}$	$9.66^{+0.22}_{-0.50}$	$0.25^{+0.08}_{-0.04}$
ZTF19acayojs	4.23/10	-19.81	$10.27^{+0.18}_{-0.31}$	$0.67^{+0.37}_{-0.20}$	$9.84^{+0.17}_{-0.63}$	$0.28^{+0.15}_{-0.06}$
ZTF19accjfgv	10.75/11	-18.50	$9.43^{+0.20}_{-0.18}$	$0.01^{+0.29}_{-0.22}$	$9.72^{+0.24}_{-0.55}$	$0.33^{+0.19}_{-0.10}$
ZTF20aaelulu	1.22/10	-21.82	$10.90^{+0.23}_{-0.14}$	$1.46^{+0.22}_{-0.41}$	$9.75^{+0.23}_{-0.52}$	$0.43^{+0.49}_{-0.15}$
ZTF20aahfqpm	0.64/7	-19.52	$9.57^{+0.19}_{-0.21}$	$0.54^{+0.45}_{-0.25}$	$9.23^{+0.55}_{-0.49}$	$0.32^{+0.26}_{-0.09}$
ZTF20aaxhzhc	8.57/16	-18.02	$9.25^{+0.07}_{-0.31}$	$-0.53^{+0.31}_{-0.07}$	$9.91^{+0.12}_{-0.49}$	$0.25^{+0.06}_{-0.03}$
ZTF20aayrobw	5.93/13	-17.38	$8.77^{+0.16}_{-0.15}$	$-0.70^{+0.11}_{-0.09}$	$9.78^{+0.20}_{-0.41}$	$0.26^{+0.08}_{-0.04}$
ZTF20aazchcq	1.00/14	-18.53	$9.49^{+0.20}_{-0.15}$	$-0.24^{+0.19}_{-0.32}$	$9.86^{+0.15}_{-0.21}$	$0.25^{+0.08}_{-0.04}$
ZTF20abjbgjj	4.73/13	-17.98	$9.16^{+0.24}_{-0.22}$	$-0.19^{+0.37}_{-0.33}$	$9.68^{+0.27}_{-0.62}$	$0.34^{+0.26}_{-0.10}$
ZTF20aburywx	9.05/14	-19.46	$10.15^{+0.13}_{-0.14}$	$0.41^{+0.18}_{-0.21}$	$9.88^{+0.14}_{-0.25}$	$0.32^{+0.15}_{-0.09}$
ZTF20acigusw	4.68/18	-19.48	$9.86^{+0.15}_{-0.15}$	$0.46^{+0.20}_{-0.12}$	$9.74^{+0.23}_{-0.50}$	$0.26^{+0.11}_{-0.05}$
ZTF20aclfmwn	6.18/11	-20.65	$10.70^{+0.09}_{-0.12}$	$0.70^{+0.16}_{-0.16}$	$9.93^{+0.10}_{-0.15}$	$0.26^{+0.09}_{-0.04}$
Silver sample						
ZTF18abvkwla	19.49/14	-19.34	$9.32^{+0.16}_{-0.21}$	$0.31^{+0.10}_{-0.10}$	$9.29^{+0.22}_{-0.32}$	$0.25^{+0.06}_{-0.03}$
ZTF19aatoboa	23.53/17	-19.65	$9.91^{+0.18}_{-0.15}$	$0.42^{+0.20}_{-0.16}$	$9.78^{+0.21}_{-0.50}$	$0.29^{+0.11}_{-0.06}$
ZTF19abfarpa	4.10/11	-17.56	$8.76^{+0.18}_{-0.18}$	$-0.64^{+0.33}_{-0.18}$	$9.70^{+0.25}_{-0.56}$	$0.28^{+0.11}_{-0.06}$
ZTF20aaivtof	2.95/11	-18.38	$8.93^{+0.20}_{-0.27}$	$-0.08^{+0.14}_{-0.41}$	$9.22^{+0.64}_{-0.32}$	$0.25^{+0.06}_{-0.03}$
ZTF20aakypiu	10.77/17	-21.28	$11.67^{+0.04}_{-0.12}$	$0.41^{+0.92}_{-0.10}$	$9.78^{+0.09}_{-0.12}$	$0.29^{+0.53}_{-0.07}$
ZTF20ababxjv	2.96/15	-19.66	$10.31^{+0.17}_{-0.22}$	$0.61^{+0.33}_{-0.25}$	$9.84^{+0.17}_{-0.50}$	$0.42^{+0.51}_{-0.16}$
ZTF20abmocba	10.15/16	-19.48	$9.86^{+0.12}_{-0.38}$	$0.18^{+0.36}_{-0.05}$	$9.90^{+0.12}_{-0.66}$	$0.26^{+0.11}_{-0.05}$
ZTF20abummyz	7.74/16	-20.01	$10.04^{+0.17}_{-0.20}$	$0.98^{+0.27}_{-0.26}$	$9.26^{+0.55}_{-0.36}$	$0.42^{+0.48}_{-0.14}$
ZTF20acigmel	4.62/3	-15.62	$7.23^{+0.25}_{-0.19}$	$-1.12^{+0.16}_{-0.15}$	$8.71^{+0.35}_{-0.22}$	$0.27^{+0.11}_{-0.05}$

NOTE—The absolute magnitudes are not corrected for host reddening. The SFRs are corrected for host reddening. The abbreviation 'n.o.f.' stands for number of filters. The 'age' in the last column refers to the age of the stellar population.

Faber, S. M., Willmer, C. N. A., Wolf, C., et al. 2007, ApJ, 665, 265, doi: 10.1086/519294

Fabricant, D., Fata, R., Epps, H., et al. 2019, PASP, 131, 075004, doi: 10.1088/1538-3873/ab1d78

Fitzpatrick, E. L. 1999, PASP, 111, 63, doi: 10.1086/316293

Förster, F., Cabrera-Vives, G., Castillo-Navarrete, E., et al. 2020, arXiv e-prints, arXiv:2008.03303. https://arxiv.org/abs/2008.03303

Forster, F., Pignata, G., Bauer, F. E., et al. 2020a, Transient Name Server Discovery Report, 2020-225, 1

—. 2020b, Transient Name Server Discovery Report, 2020-278, 1

Forster, F., Bauer, F. E., Galbany, L., et al. 2020c, Transient Name Server Discovery Report, 2020-1380, 1

Forster, F., Hernandez-Garcia, L., Munoz-Arancibia, A., et al. 2020d, Transient Name Server Discovery Report, 2020-2542, 1

Forster, F., Bauer, F. E., Munoz-Arancibia, A., et al. 2020e, Transient Name Server Discovery Report, 2020-3172, 1

Fox, O. D., & Smith, N. 2019, MNRAS, 488, 3772, doi: 10.1093/mnras/stz1925

Fremling, C. 2019, Transient Name Server Discovery Report, 2019-1272, 1
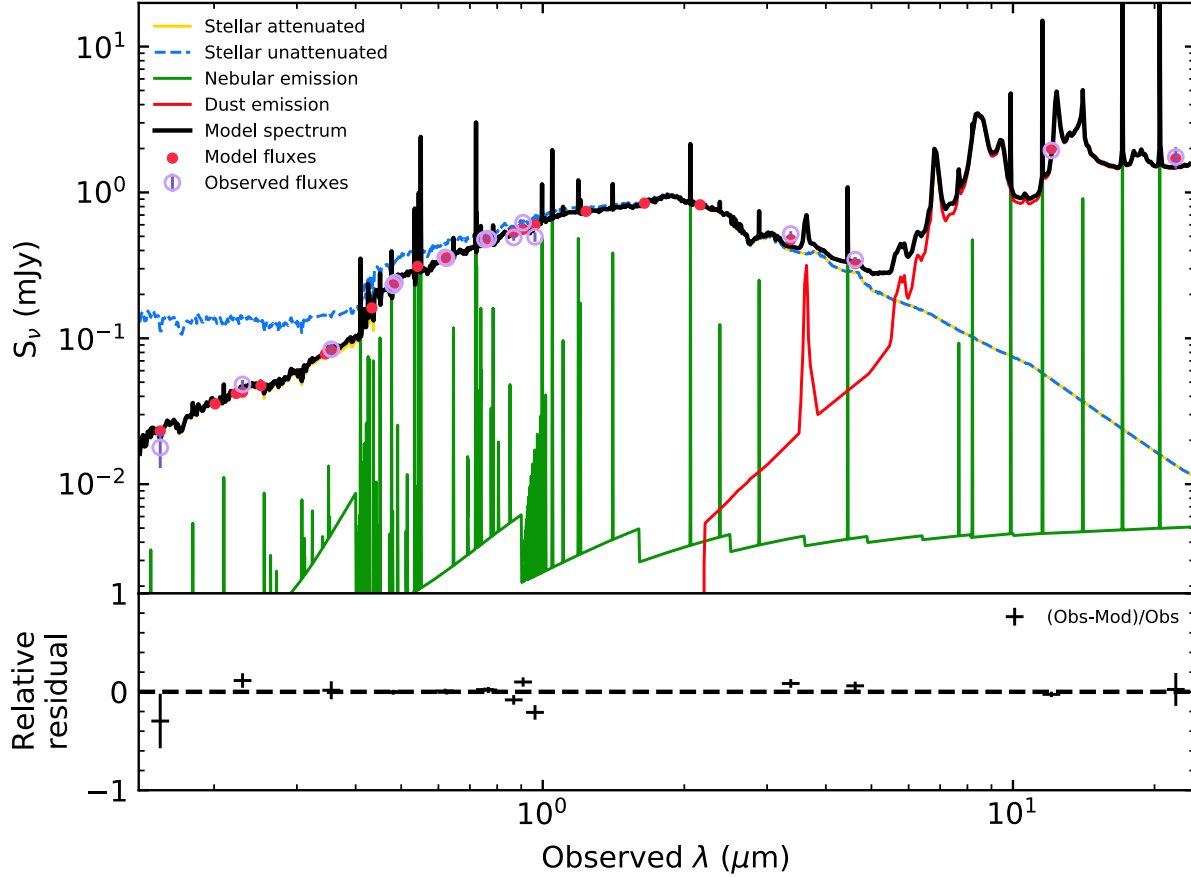
Figure 27. The SED of ZTF20abummyz's host galaxy (empty circles) from the UV to mid-IR. The solid black line shows the best-fitting model of the SED. The SED model consists of a stellar component (yellow curve), a contribution ionised gas, e.g., star-forming regions (green curve) and emission from heated dust (red curve) at $> 30,000$ Å. The photometry predicted by the best-fit model is shown by the red circles. The blue curve represents the stellar component corrected for host attenuation.

—. 2020, Transient Name Server Discovery Report, 2020-3094, 1

Fremling, C., Dugas, A., & Sharma, Y. 2018, Transient Name Server Classification Report, 2018-1567, 1

Fremling, C., Sollerman, J., Taddia, F., et al. 2016, A&A, 593, A68, doi: 10.1051/0004-6361/201628275

Fremling, C., Ko, H., Dugas, A., et al. 2019, ApJL, 878, L5, doi: 10.3847/2041-8213/ab218f

Fremling, C., Miller, A. A., Sharma, Y., et al. 2020, ApJ, 895, 32, doi: 10.3847/1538-4357/ab8943

Gal-Yam, A. 2017, Observational and Physical Classification of Supernovae, ed. A. W. Alsabti & P. Murdin, 195, doi: 10.1007/978-3-319-21846-5_35

—. 2021, Transient Name Server Classification Report, 2021-547, 1

Gal-Yam, A., Yaron, O., Pastorello, A., et al. 2021, Transient Name Server AstroNote, 76, 1

Gehrels, N., Chincarini, G., Giommi, P., et al. 2004, ApJ, 611, 1005, doi: 10.1086/422091

Gendre, B., Stratta, G., Atteia, J. L., et al. 2013, ApJ, 766, 30, doi: 10.1088/0004-637X/766/1/30

Graham, M. J., Kulkarni, S. R., Bellm, E. C., et al. 2019, PASP, 131, 078001, doi: 10.1088/1538-3873/ab006c

Greiner, J., Mazzali, P. A., Kann, D. A., et al. 2015, Nature, 523, 189, doi: 10.1038/nature14579

Gromadzki, M., Wevers, T., Lyman, J., & Yaron, O. 2018, Transient Name Server Classification Report, 2018-1410, 1

Gutiérrez, C. P., Anderson, J. P., Sullivan, M., et al. 2018, MNRAS, 479, 3232, doi: 10.1093/mnras/sty1581

Ho, A. Y. Q., Goldstein, D. A., Schulze, S., et al. 2019a, ApJ, 887, 169, doi: 10.3847/1538-4357/ab55ec

Ho, A. Y. Q., Phinney, E. S., Ravi, V., et al. 2019b, ApJ, 871, 73, doi: 10.3847/1538-4357/aaf473

Ho, A. Y. Q., Perley, D. A., Beniamini, P., et al. 2020a, ApJ, 905, 98, doi: 10.3847/1538-4357/abc34d

Ho, A. Y. Q., Perley, D. A., Kulkarni, S. R., et al. 2020b, ApJ, 895, 49, doi: 10.3847/1538-4357/ab8bcf

Ho, A. Y. Q., Kulkarni, S. R., Perley, D. A., et al. 2020c, ApJ, 902, 86, doi: 10.3847/1538-4357/aba630

Högbom, J. A. 1974, A&AS, 15, 417

Horesh, A., Sfaradi, I., Ergon, M., et al. 2020, ApJ, 903, 132, doi: 10.3847/1538-4357/abbd38

Hosseinzadeh, G., McCully, C., Zabludoff, A. I., et al. 2019, ApJL, 871, L9, doi: 10.3847/2041-8213/aafc61

Hosseinzadeh, G., Arcavi, I., Valenti, S., et al. 2017, ApJ, 836, 158, doi: 10.3847/1538-4357/836/2/158

Hotan, A. W., Bunton, J. D., Chippendale, A. P., et al. 2021, PASA, 38, e009, doi: 10.1017/pasa.2021.1

Howell, S. B., Sobeck, C., Haas, M., et al. 2014, PASP, 126, 398, doi: 10.1086/676406

Hunter, J. D. 2007, Computing in Science and Engineering, 9, 90, doi: 10.1109/MCSE.2007.55

Immler, S., Modjaz, M., Landsman, W., et al. 2008, ApJL, 674, L85, doi: 10.1086/529373

Inserra, C. 2019, Nature Astronomy, 3, 697, doi: 10.1038/s41550-019-0854-4

Irani, I., Schulze, S., Gal-Yam, A., et al. 2019, ApJ, 887, 127, doi: 10.3847/1538-4357/ab505d

Karamehmetoglu, E., Fransson, C., Sollerman, J., et al. 2019, arXiv e-prints, arXiv:1910.06016. https://arxiv.org/abs/1910.06016

Kasen, D., & Bildsten, L. 2010, ApJ, 717, 245, doi: 10.1088/0004-637X/717/1/245

Kasliwal, M. M. 2012, PASA, 29, 482, doi: 10.1071/AS11061

Kasliwal, M. M., Kulkarni, S. R., Gal-Yam, A., et al. 2010, ApJL, 723, L98, doi: 10.1088/2041-8205/723/1/L98

Kasliwal, M. M., Cannella, C., Bagdasaryan, A., et al. 2019, PASP, 131, 038003, doi: 10.1088/1538-3873/aafbc2

Kleiser, I. K. W., Kasen, D., & Duffell, P. C. 2018, MNRAS, 475, 3152, doi: 10.1093/mnras/stx3321

Kremer, K., Lu, W., Piro, A. L., et al. 2021, ApJ, 911, 104, doi: 10.3847/1538-4357/abeb14

Kuin, N. P. M., Wu, K., Oates, S., et al. 2019, MNRAS, 487, 2505, doi: 10.1093/mnras/stz053

Lacy, M., Baum, S. A., Chandler, C. J., et al. 2020, PASP, 132, 035001, doi: 10.1088/1538-3873/ab63eb

Lang, D. 2014, AJ, 147, 108, doi: 10.1088/0004-6256/147/5/108

Law, N. M., Kulkarni, S. R., Dekany, R. G., et al. 2009, PASP, 121, 1395, doi: 10.1086/648598

Levan, A. J., Tanvir, N. R., Starling, R. L. C., et al. 2014, ApJ, 781, 13, doi: 10.1088/0004-637X/781/1/13

Li, W., Chornock, R., Leaman, J., et al. 2011, MNRAS, 412, 1473, doi: 10.1111/j.1365-2966.2011.18162.x

Lintott, C., Schawinski, K., Bamford, S., et al. 2011, MNRAS, 410, 166, doi: 10.1111/j.1365-2966.2010.17432.x

Lintott, C. J., Schawinski, K., Slosar, A., et al. 2008, MNRAS, 389, 1179, doi: 10.1111/j.1365-2966.2008.13689.x

Lyutikov, M., & Toonen, S. 2019, MNRAS, 487, 5618, doi: 10.1093/mnras/stz1640

Mahabal, A., Rebbapragada, U., Walters, R., et al. 2019, PASP, 131, 038002, doi: 10.1088/1538-3873/aaf3fa

Mainzer, A., Bauer, J., Cutri, R. M., et al. 2014, ApJ, 792, 30, doi: 10.1088/0004-637X/792/1/30

Margutti, R., Metzger, B. D., Chornock, R., et al. 2019, ApJ, 872, 18, doi: 10.3847/1538-4357/aafa01

Martin, D. C., Fanson, J., Schiminovich, D., et al. 2005, ApJL, 619, L1, doi: 10.1086/426387

Masci, F. J., Laher, R. R., Rusholme, B., et al. 2019, PASP, 131, 018003, doi: 10.1088/1538-3873/aae8ac

McBrien, O. R., Smartt, S. J., Chen, T.-W., et al. 2019, ApJL, 885, L23, doi: 10.3847/2041-8213/ab4dae

McConnachie, A. W. 2012, AJ, 144, 4, doi: 10.1088/0004-6256/144/1/4

McConnell, D., Hale, C. L., Lenc, E., et al. 2020, PASA, 37, e048, doi: 10.1017/pasa.2020.41

McMullin, J. P., Waters, B., Schiebel, D., Young, W., & Golap, K. 2007, Astronomical Society of the Pacific Conference Series, Vol. 376, CASA Architecture and Applications, ed. R. A. Shaw, F. Hill, & D. J. Bell, 127

Meisner, A. M., Lang, D., & Schlegel, D. J. 2017, AJ, 153, 38, doi: 10.3847/1538-3881/153/1/38

Metzger, B. D., Piro, A. L., Quataert, E., & Thompson, T. A. 2009, arXiv e-prints, arXiv:0908.1127. https://arxiv.org/abs/0908.1127

Modjaz, M., Gutiérrez, C. P., & Arcavi, I. 2019, Nature Astronomy, 3, 717, doi: 10.1038/s41550-019-0856-2

Modjaz, M., Stanek, K. Z., Garnavich, P. M., et al. 2006, ApJL, 645, L21, doi: 10.1086/505906

Modjaz, M., Blondin, S., Kirshner, R. P., et al. 2014, AJ, 147, 99, doi: 10.1088/0004-6256/147/5/99

Moriya, T. J., & Eldridge, J. J. 2016, MNRAS, 461, 2155, doi: 10.1093/mnras/stw1471

Moriya, T. J., Marchant, P., & Blinnikov, S. I. 2020, A&A, 641, L10, doi: 10.1051/0004-6361/202038903

Murphy, T., Chatterjee, S., Kaplan, D. L., et al. 2013, PASA, 30, e006, doi: 10.1017/pasa.2012.006

Nayana, A. J., & Chandra, P. 2021, arXiv e-prints, arXiv:2103.06008. https://arxiv.org/abs/2103.06008

Noll, S., Burgarella, D., Giovannoli, E., et al. 2009, A&A, 507, 1793, doi: 10.1051/0004-6361/200912497

Nordin, J., Brinnel, V., Giomi, M., et al. 2019a, Transient Name Server Discovery Report, 2019-543, 1

—. 2019b, Transient Name Server Discovery Report, 2019-720, 1

—. 2019c, Transient Name Server Discovery Report, 2019-1461, 1

—. 2019d, Transient Name Server Discovery Report, 2019-1984, 1

—. 2020, Transient Name Server Discovery Report, 2020-1997, 1

Nordin, J., Brinnel, V., van Santen, J., et al. 2019e, A&A, 631, A147, doi: 10.1051/0004-6361/201935634

Ofek, E. O., & Ben-Ami, S. 2020, PASP, 132, 125004, doi: 10.1088/1538-3873/abc14c

Ofek, E. O., Rabinak, I., Neill, J. D., et al. 2010, ApJ, 724, 1396, doi: 10.1088/0004-637X/724/2/1396

Ofek, E. O., Fox, D., Cenko, S. B., et al. 2013, ApJ, 763, 42, doi: 10.1088/0004-637X/763/1/42

Oke, J. B., & Gunn, J. E. 1982, PASP, 94, 586, doi: 10.1086/131027

Oke, J. B., Cohen, J. G., Carr, M., et al. 1995, PASP, 107, 375, doi: 10.1086/133562

Pastorello, A., Quimby, R. M., Smartt, S. J., et al. 2008, MNRAS, 389, 131, doi: 10.1111/j.1365-2966.2008.13603.x

Pastorello, A., Hadjiyska, E., Rabinowitz, D., et al. 2015, MNRAS, 449, 1954, doi: 10.1093/mnras/stv335

Patterson, M. T., Bellm, E. C., Rusholme, B., et al. 2019, PASP, 131, 018001, doi: 10.1088/1538-3873/aae904

Perley, D. 2021, Transient Name Server Classification Report, 2021-570, 1

Perley, D., Yao, Y., & Ho, A. 2021a, Transient Name Server Discovery Report, 2021-443, 1

Perley, D. A. 2019, PASP, 131, 084503, doi: 10.1088/1538-3873/ab215d

Perley, D. A., Taggart, K., Dahiwale, A., & Fremling, C. 2020a, Transient Name Server Classification Report, 2020-2127, 1

Perley, D. A., Mazzali, P. A., Yan, L., et al. 2019, MNRAS, 484, 1031, doi: 10.1093/mnras/sty3420

Perley, D. A., Fremling, C., Sollerman, J., et al. 2020b, ApJ, 904, 35, doi: 10.3847/1538-4357/abbd98

Perley, D. A., Ho, A. Y. Q., Yao, Y., et al. 2021b, arXiv e-prints, arXiv:2103.01968. https://arxiv.org/abs/2103.01968

Perley, R. A., Chandler, C. J., Butler, B. J., & Wrobel, J. M. 2011, ApJL, 739, L1, doi: 10.1088/2041-8205/739/1/L1

Pian, E., Mazzali, P. A., Masetti, N., et al. 2006, Nature, 442, 1011, doi: 10.1038/nature05082

Piascik, A. S., Steele, I. A., Bates, S. D., et al. 2014, in Society of Photo-Optical Instrumentation Engineers (SPIE) Conference Series, Vol. 9147, Proc. SPIE, 91478H, doi: 10.1117/12.2055117

Planck Collaboration, Ade, P. A. R., Aghanim, N., et al. 2016, A&A, 594, A13, doi: 10.1051/0004-6361/201525830

Poznanski, D., Chornock, R., Nugent, P. E., et al. 2010, Science, 327, 58, doi: 10.1126/science.1181709

Prentice, S. J., Maguire, K., Skillen, K., Magee, M. R., & Clark, P. 2019, Transient Name Server Classification Report, 2019-567, 1

Prentice, S. J., Maguire, K., Smartt, S. J., et al. 2018, ApJL, 865, L3, doi: 10.3847/2041-8213/aadd90

Prentice, S. J., Maguire, K., Flörs, A., et al. 2020, A&A, 635, A186, doi: 10.1051/0004-6361/201936515

Pritchard, T. A., Bensch, K., Modjaz, M., et al. 2020, arXiv e-prints, arXiv:2008.04321. https://arxiv.org/abs/2008.04321

Pursiainen, M., Childress, M., Smith, M., et al. 2018, MNRAS, 481, 894, doi: 10.1093/mnras/sty2309

Rau, A., Kulkarni, S. R., Law, N. M., et al. 2009, PASP, 121, 1334, doi: 10.1086/605911

Rest, A., Garnavich, P. M., Khatami, D., et al. 2018, Nature Astronomy, 2, 307, doi: 10.1038/s41550-018-0423-2

Ricker, G. R., Winn, J. N., Vanderspek, R., et al. 2014, in Society of Photo-Optical Instrumentation Engineers (SPIE) Conference Series, Vol. 9143, Space Telescopes and Instrumentation 2014: Optical, Infrared, and Millimeter Wave, ed. J. Oschmann, Jacobus M., M. Clampin, G. G. Fazio, & H. A. MacEwen, 914320, doi: 10.1117/12.2063489

Rigault, M. 2018, ztfquery, a python tool to access ZTF data, doi, Zenodo, doi: 10.5281/zenodo.1345222

Rigault, M., Neill, J. D., Blagorodnova, N., et al. 2019, A&A, 627, A115, doi: 10.1051/0004-6361/201935344

Roming, P. W. A., Kennedy, T. E., Mason, K. O., et al. 2005, SSRv, 120, 95, doi: 10.1007/s11214-005-5095-4

Sanders, N. E., Soderberg, A. M., Foley, R. J., et al. 2013, ApJ, 769, 39, doi: 10.1088/0004-637X/769/1/39

Sault, R. J., Teuben, P. J., & Wright, M. C. H. 1995, Astronomical Society of the Pacific Conference Series, Vol. 77, A Retrospective View of MIRIAD, ed. R. A. Shaw, H. E. Payne, & J. J. E. Hayes, 433

Schlafly, E. F., & Finkbeiner, D. P. 2011, ApJ, 737, 103, doi: 10.1088/0004-637X/737/2/103

Schmidt, B. P., Kirshner, R. P., Eastman, R. G., et al. 1993, Nature, 364, 600, doi: 10.1038/364600a0

Schulze, S., Yaron, O., Sollerman, J., et al. 2020, arXiv e-prints, arXiv:2008.05988. https://arxiv.org/abs/2008.05988

Siebert, M. R., Kilpatrick, C. D., Foley, R. J., & Cartier, R. 2020a, Transient Name Server Classification Report, 2020-90, 1

Siebert, M. R., Tinyanont, S., Taggart, K., Dimitriadis, G., & Foley, R. J. 2020b, Transient Name Server Classification Report, 2020-3121, 1

Silverman, J. M., Foley, R. J., Filippenko, A. V., et al. 2012, MNRAS, 425, 1789, doi: 10.1111/j.1365-2966.2012.21270.x

Skrutskie, M. F., Cutri, R. M., Stiening, R., et al. 2006, AJ, 131, 1163, doi: 10.1086/498708

Smartt, S. J., Valenti, S., Fraser, M., et al. 2015, A&A, 579, A40, doi: 10.1051/0004-6361/201425237

Smith, K. W., Smartt, S. J., Young, D. R., et al. 2020a, PASP, 132, 085002, doi: 10.1088/1538-3873/ab936e

Smith, M., Möller, A., Amenouche, M., et al. 2020b, Transient Name Server AstroNote, 39, 1

Smith, N., Chornock, R., Li, W., et al. 2008, ApJ, 686, 467, doi: 10.1086/591021

Smith, N., Mauerhan, J. C., Silverman, J. M., et al. 2012, MNRAS, 426, 1905, doi: 10.1111/j.1365-2966.2012.21849.x

Smith, N., Kilpatrick, C. D., Mauerhan, J. C., et al. 2017, MNRAS, 466, 3021, doi: 10.1093/mnras/stw3204

Soumagnac, M. T., & Ofek, E. O. 2018, PASP, 130, 075002, doi: 10.1088/1538-3873/aac410

Soumagnac, M. T., Ofek, E. O., Gal-yam, A., et al. 2019, ApJ, 872, 141, doi: 10.3847/1538-4357/aafe84

Steele, I. A., Smith, R. J., Rees, P. C., et al. 2004, in Society of Photo-Optical Instrumentation Engineers (SPIE) Conference Series, Vol. 5489, Proc. SPIE, ed. J. Oschmann, Jacobus M., 679–692, doi: 10.1117/12.551456

Stratta, G., Gendre, B., Atteia, J. L., et al. 2013, ApJ, 779, 66, doi: 10.1088/0004-637X/779/1/66

Strubbe, L. E., & Quataert, E. 2009, MNRAS, 400, 2070, doi: 10.1111/j.1365-2966.2009.15599.x

Tachibana, Y., & Miller, A. A. 2018, PASP, 130, 128001, doi: 10.1088/1538-3873/aae3d9

Taddia, F., Stritzinger, M. D., Sollerman, J., et al. 2013, A&A, 555, A10, doi: 10.1051/0004-6361/201321180

Taddia, F., Fremling, C., Sollerman, J., et al. 2016, A&A, 592, A89, doi: 10.1051/0004-6361/201628703

Taggart, K., & Perley, D. A. 2021, MNRAS, 503, 3931, doi: 10.1093/mnras/stab174

Tampo, Y., Tanaka, M., Maeda, K., et al. 2020, ApJ, 894, 27, doi: 10.3847/1538-4357/ab7ccc

Tolstov, A., Nomoto, K., Sorokina, E., et al. 2019, ApJ, 881, 35, doi: 10.3847/1538-4357/ab2876

Tonry, J., Stalder, B., Denneau, L., et al. 2018a, Transient Name Server Discovery Report, 2018-1379, 1

Tonry, J., Denneau, L., Heinze, A., et al. 2019, Transient Name Server Discovery Report, 2019-1694, 1

—. 2020, Transient Name Server Discovery Report, 2020-1158, 1

Tonry, J. L., Denneau, L., Heinze, A. N., et al. 2018b, PASP, 130, 064505, doi: 10.1088/1538-3873/aabadf

van Dokkum, P. G., Abraham, R., Merritt, A., et al. 2015, ApJL, 798, L45, doi: 10.1088/2041-8205/798/2/L45

Virtanen, P., Gommers, R., Oliphant, T. E., et al. 2020, Nature Methods, 17, 261, doi: https://doi.org/10.1038/s41592-019-0686-2

Whitesides, L., Lunnan, R., Kasliwal, M. M., et al. 2017, ApJ, 851, 107, doi: 10.3847/1538-4357/aa99de

Williamson, M., Modjaz, M., & Bianco, F. B. 2019, ApJL, 880, L22, doi: 10.3847/2041-8213/ab2edb

Willingale, R., Starling, R. L. C., Beardmore, A. P., Tanvir, N. R., & O'Brien, P. T. 2013, MNRAS, 431, 394, doi: 10.1093/mnras/stt175

Wiseman, P., Pursiainen, M., Childress, M., et al. 2020, MNRAS, 498, 2575, doi: 10.1093/mnras/staa2474

Woosley, S. E. 2010, ApJL, 719, L204, doi: 10.1088/2041-8205/719/2/L204

Wright, A. H., Robotham, A. S. G., Bourne, N., et al. 2016, MNRAS, 460, 765, doi: 10.1093/mnras/stw832

Wright, E. L., Eisenhardt, P. R. M., Mainzer, A. K., et al. 2010, AJ, 140, 1868, doi: 10.1088/0004-6256/140/6/1868

Yao, Y., Miller, A. A., Kulkarni, S. R., et al. 2019, ApJ, 886, 152, doi: 10.3847/1538-4357/ab4cf5

Yao, Y., De, K., Kasliwal, M. M., et al. 2020, ApJ, 900, 46, doi: 10.3847/1538-4357/abaa3d

Yaron, O., & Gal-Yam, A. 2012, PASP, 124, 668, doi: 10.1086/666656

Zackay, B., Ofek, E. O., & Gal-Yam, A. 2016, ApJ, 830, 27, doi: 10.3847/0004-637X/830/1/27

Zhang, M., Ding, Y., Liu, S., et al. 2018, Transient Name Server Discovery Report, 2018-1393, 1